MINISTRY OF NATIONAL EDUCATION
AND SCIENTIFIC RESEARCH

THE ANNALS OF "DUNAREA DE JOS" UNIVERSITY OF GALATI

Fascicle IX
METALLURGY AND MATERIALS SCIENCE

YEAR XXXIII (XXXVIII)
December 2015, no. 4

ISSN 1453-083X

2015
GALATI UNIVERSITY PRESS

EDITORIAL BOARD

THE ANNALS OF "DUNAREA DE JOS" UNIVERSITY OF GALATI
FASCICLE IX. METALLURGY AND MATERIALS SCIENCE
Nº. 4 - 2015, ISSN 1453 – 083X

Table of Content

THE ANNALS OF "DUNAREA DE JOS" UNIVERSITY OF GALATI
FASCICLE IX. METALLURGY AND MATERIALS SCIENCE
Nº. 4 - 2015, ISSN 1453 – 083X

SURFACE ROUGHNESS AND TOPOGRAPHY OF Ni / MICRO-SiC LAYERS: INFLUENCE OF CURRENT DENSITY ON ELECTRODEPOSITION PROCESS

Alina CIUBOTARIU[1,*], **Lidia BENEA**[1], **Wolfgang SAND**[2]
[1]Dunărea de Jos University of Galati, Faculty of Engineering, Competences Center Interfaces-Tribocorrosion and Electrochemical Systems,47 Domneasca Street, 80008, GALATI, Romania
[2]University of Duisburg Essen, Biofilm Centre, Geibelstraße 41, 47057, Duisburg, Germany
[*]*Corresponding author*
e-mail: alina.ciubotariu@ugal.ro

ABSTRACT

The surface properties are directly responsible for the performance of engineering materials because most of failures such as friction, wear, corrosion and fatigue often take place on the material surface. Electrodeposition technique is of great interest for industrial usage because it produces functional and protective coatings with low cost and easy control. The present work has the purpose to evaluate roughness and to analyze surfaces of Ni / micro-SiC composite layers obtained at different parameters for electrodeposition. The layers were electroplated from a Watts bath with a suspension of SiC particles (mean diameter size of particles 30 μm) by adding 5g/L of particles. Electrodeposition took place at 40 ºC and a current density of 2 A/dm^2 and 4 A/dm^2 for 1h. The suspension bath was stirred by a mechanical stirrer at a constant rotational speed of about 500 rpm. The roughness and topography of the layers were evaluated by atomic force microscopy (AFM) method.

KEYWORDS: electrodeposition, composite layers, atomic force microscopy, topography, roughness

1. Introduction

In the last years, composite layers have been developed quickly because they have many advantages in technology with a good resistance to aggressive working environments and fast processing systems. Embedding different particles into a metal matrix improve the material properties such as surface hardness, corrosion resistance, wear resistance, erosion – corrosion resistance etc. [1-3].

Layers of Ni / SiC composites have been studied because of their high wear resistance and good corrosion properties provided by the ceramic particles embedded in the nickel matrix [4-6].

Electrodeposition is one of the most used techniques for obtaining metallic and non-metallic composite layers. Between 1950-1960, the development of electrodeposited composite coatings expended progressively [7]. During the 1970s and 1980s, researches were focused on the need to produce coatings with enhanced mechanical, corrosion and tribological properties.

The advanced physical properties of composite layers quickly became clear and during the 1990s, new areas such as electrocatalysts and photoelectrocatalysts were considered [8].

To obtain composite layers a metal can be used as a matrix that could embed a dispersed phase with a good adhesion property on a substrate. As dispersed phases to obtain composite layers pure metals particles, ceramic particles or organic particles could be used.

The surface roughness has an important role on the mechanical as well as tribological properties of the composite layers.

The different properties such as wear, friction, corrosion, creep, fatigue failure, heat transmission, electrical conductivity, light reflection and lubricity etc. are affected by the surface roughness that has an important role for composite layers because affects their porosity. Due to higher porosity the corrosion resistance of the composite coating may be reduced. Hence, it is very essential to carry out investigations on the surface roughness and to optimize the bath

process parameters to reduce the surface roughness at the preferred level. Atomic force microscopy (AFM) is a method to see a surface in its full, extremely versatile tool to investigate the three- dimensional morphology of surfaces. The method applies to hard and soft synthetic materials as well as biological structures (tissues, cells, biomolecules), irrespective of opaqueness or conductivity. The 3D object is not perceived in the usual way, that is, by line-of-sight, reflections or shadows. Given that the image is constructed from height numbers, one also can measure peak-to-valley distances, compute standard deviations of height, compile histograms of heights or slopes of hills. These metrics of topography can be directly relevant to the technological performance or biological function, whether in microelectronics (roughness of layers in multilayer deposition processes), tribology (friction and wear on hard disk read heads), polymer-drug coatings (surface contour area impacting drug release), intrabody medical devices (shape of surface in contact with cells, tissues), cellular membranes and surface components (phospholipid bilayer, protein receptors) and much more [10-12].

The paper intends to study the surface topography and roughness of Ni/micro-SiC composite layers compared with pure nickel layers. The samples were obtained at two values of the electrodeposition current densities because the the electrodeposition parameters influence the topography of the surfaces. The topography of the layers was evaluated by the atomic force microscopy method and the values of surface roughness were evaluated by histograms of the tested layers.

2. Experimental

Nickel and Ni / micro-SiC composite layers were electrochemically deposited from a Watts bath with the following composition: 0.90M $NiSO_4x6H_2O$; 0.21M $NiCl_2x6H_2O$; 0.48M H_3BO_3 and additive: SDS (sodium dodecyl sulphate) 0.4 g/L. The pH of the solution was maintained at 4. The suspension was prepared by adding SiC particles with a mean diameter size of 30 μm to the solution to give a concentration of 5 g/L in the nickel plating electrolyte. The electrodeposition took place in the bath at a temperature of 40 ºC and a current density of 2 A/dm^2 and 4 A/dm^2 for 60 minutes. The suspension bath was stirred by a mechanical stirrer at a constant rotational speed of about 500 rpm.

A NanoWizardII atomic force microscope (JPK Instruments, Germany) was used for surface analysis and for evaluating the roughness of the surfaces.

For AFM images, a silicon cantilever CSC37 A (Mikromasch, Estonia) with the following features was used: typical length, 250 μm; width, 35 μm; thickness, 2 μm; resonance frequency, 41 kHz; and nominal force/spring constant, 0.65 N/m. Each AFM image consists of 512 by 512 pixels. AFM images were performed by contact mode in air.

3. Results and discussion

The surface topography of pure nickel layers electrodeposited at a current density of 2A/dm^2 and 4A/dm^2 under atomic force microscope are presented in Figures 1 and 2.

From the AFM images of the tested surfaces for nickel obtained at a low current density, the electrodeposited nickel was observed to consist of pyramidal crystals with pronounced crystallographic polyhedral form with equigrannular structure. A bimodal grain structure of truncated pyramidal type can be observed. A cluster of fine grains is surrounded by relatively large grains. For nickel layers obtained at 4 A/dm^2 the surface topography was changed and it a homogeneous metallic structure with regular pyramidal shape was observed, characteristically for nickel crystallites [13-15].

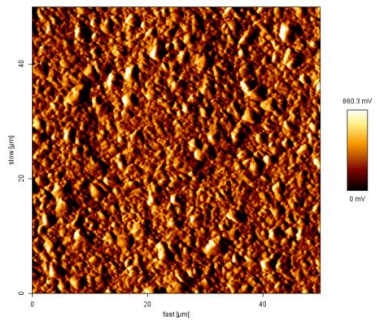

(a)

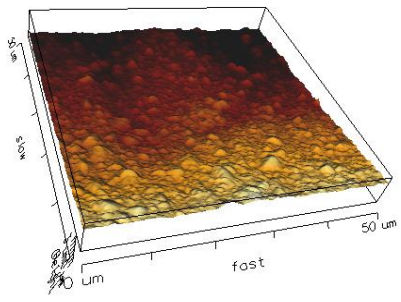

(b)

Fig. 1. *AFM images of pure nickel surface electrodeposited at 2A/dm^2: 2D (a) and 3D (b)*

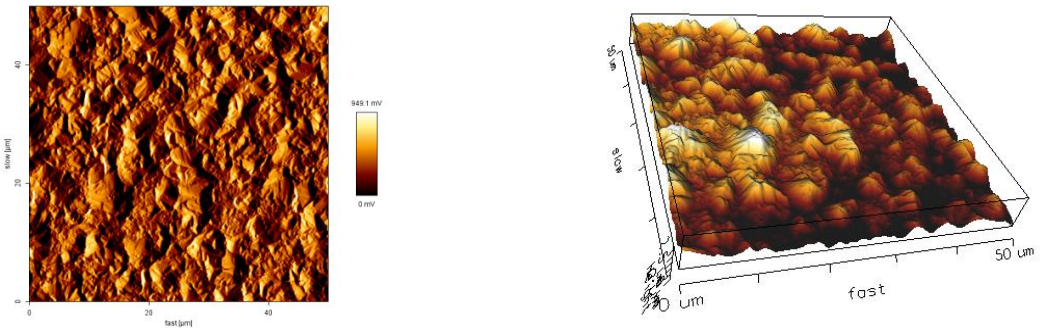

(a) *(b)*

Fig. 2. *AFM images of pure nickel surface electrodeposited at 4A/dm^2: 2D (a) and 3D (b)*

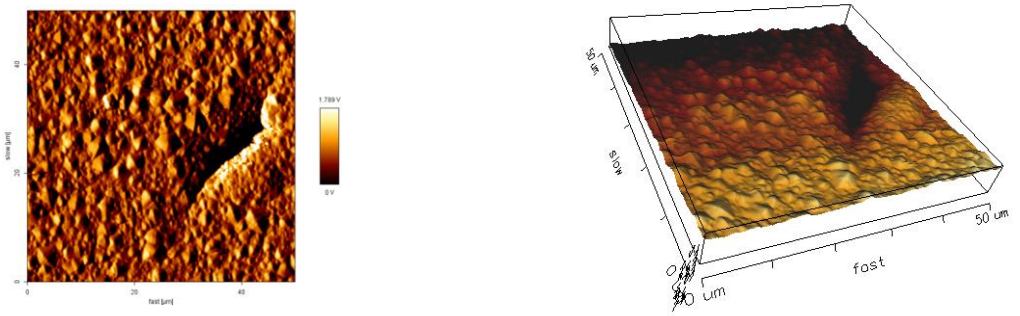

(a) *(b)*

Fig. 3. *AFM images of Ni / micro-SiC surface layers obtained at 2A/dm^2: 2D (a) and 3D (b)*

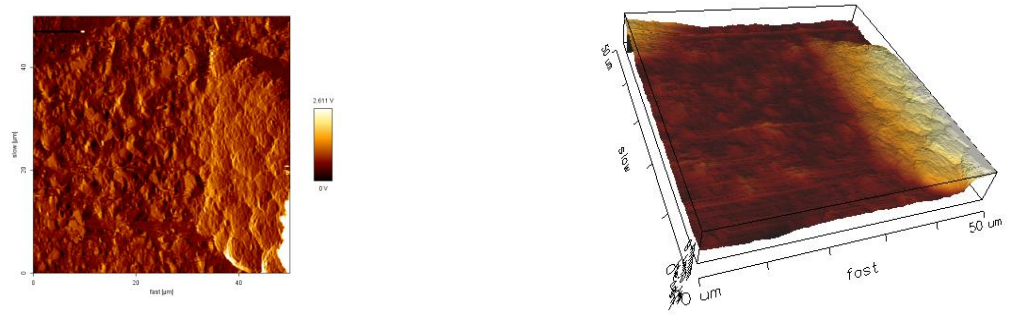

(a) *(b)*

Fig. 4. *AFM images of Ni / micro-SiC surface layers obtained at 4A/dm^2: 2D (a) and 3D (b)*

Figures 3 and 4 represent the 2D and 3D AFM images of Ni / micro-SiC composite layers obtained at 2A/dm^2 (Fig. 3) and 4 A/dm^2 (Fig. 4).

From the AFM images for Ni / micro-SiC composite layers it could be observed that the composite layers are smooth surfaces and it could be observed particles of SiC embedded into Ni matrix.

The particle size of SiC has an important role in the entrapment of SiC in the electrodeposited nickel coatings layers. The micro SiC particles could adsorbe more nickel ions and the Coulombic force is stronger than in case of nano SiC particles. On the other hand, the codeposition of pure nickel compared with SiC particles codeposited into nickel matrix is complex because a lot of factors act simultaneously. These factors include particle-particle interactions and the mobility of particles as a function of size and charge [16].

Comparing the topography of pure nickel layers with composite layers the pure nickel layers can be observed to have a rather regular surface and the composite coatings to have a nodular disturbed

surface structure. Growing nickel crystals was perturbed by the current density used for electrodeposition and the incorporation of SiC macro particles. Fig. 3 and 4 show that the micron-sized particles are codeposited at the borders and the edges of the nickel crystallites and the embedding mechanism can be characterized as inter-crystalline [17, 18]. Fig. 5-8 show the histograms of the scanned surfaces of pure nickel layers and Ni / micro-SiC composite layers.

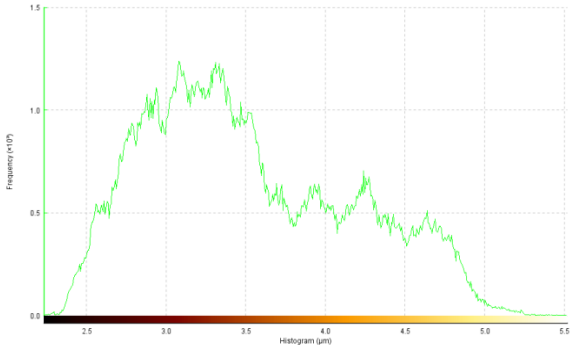

Fig. 5. *Histogram of the scanned surfaces for pure nickel layers obtained at 2A/dm^2*

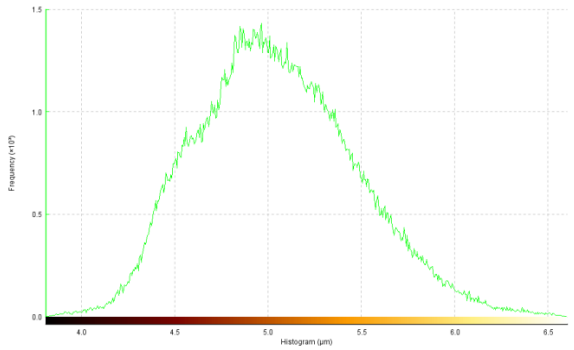

Fig. 6. *Histogram of the scanned surfaces for pure nickel layers obtained at 4A/dm^2*

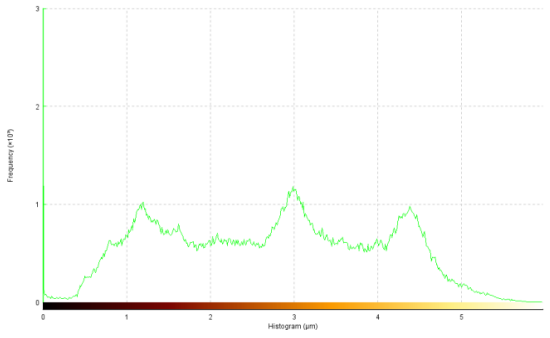

Fig. 7. *Histogram of the scanned surfaces for Ni / micro-SiC composite layers obtained at 2A/dm^2*

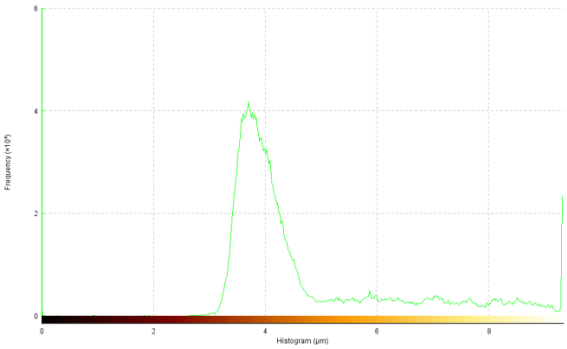

Fig. 8. *Histogram of the scanned surfaces for Ni / micro-SiC composite layers obtained at 4A/dm^2*

The histograms presented in Figures 5-8 were used to estimate the surface roughness of pure nickel and Ni / micro-SiC composite layers.

The surface roughness has an influence on how a real system interacts with the environment and is quantified by the vertical deviations of a real surface from its ideal form. If these deviations are large, the surface is rough; if they are small the surface is smooth.

The roughness can be characterized by several parameters and functions, but the average value is by far the most commonly used. The average roughness is the area between the roughness profile and its mean line, or the integral of the absolute value of the roughness profile height over the evaluation length and is described in equation 1.

$$R_a = \frac{1}{L}\int_L^0 |Z(x)|\,dx \qquad (1)$$

where Z(x) is the function that describes the surface profile analyzed in terms of height (Z) and position (x) of the sample over the evaluation length "L". Thus, the Ra is the arithmetic mean of the absolute values of the height of the surface profile Z(x) [19, 20].

Variations of the surface roughness for pure nickel and Ni / micro-SiC composite layers are shown in Fig. 9.

From the values of average roughness of the surfaces presented in Fig. 9 it could be observed that the roughness decreases for Ni / micro-SiC composite layers. The roughness is higher for pure nickel and composite layers obtained at a value of 4A/dm^2 for electrodeposition current density as compared with the values of roughness obtained at a value of electrodeposition current density of 2A/dm^2.

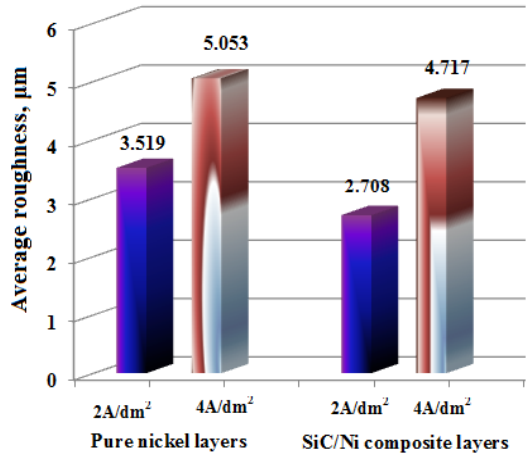

Fig. 9. *Variation of roughness surfaces of pure nickel and Ni / micro-SiC composite layers obtained at different electrodeposition current density*

The smaller values of the composite layers average roughness compared with the values of average roughness for pure nickel layers could be determined by the inhibition of nickel crystals growth induced by SiC micro particles.

The dispersed phase was uniformly distributed in the nickel matrix and the Ni / micro-SiC composite layers are more smoothed, uniform and compact surface than the pure nickel surface, that is indicated by the values of average surface roughness.

Conclusions

From the AFM images of the tested surfaces for nickel obtained at 2A/dm^2 the electrodeposited nickel was observed to consist of pyramidal crystals with pronounced crystallographic polyhedral form with equigrannular structure and for nickel layers obtained at 4 A/dm^2 a homogeneous metallic structure with regular pyramidal shape characteristical for nickel crystallites was observed.

From the AFM images of Ni / micro-SiC composite layers it could be observed that the surfaces are smooth and it could be observed the micro SiC particles embedded into Ni matrix. The particle size of SiC has an important role in the entrapment of SiC in the electrodeposited nickel coatings layers. The micro SiC particles could adsorb more nickel ions and the Coulombic force is high. Comparing the topography of the pure nickel layers with the composite layers it could be observed that the pure nickel layers have a rather regular surface and the composite coatings have a nodular disturbed surface structure. The growing of the nickel crystals was perturbed by the current density used for electrodeposition and the incorporation of SiC macro particles.

From the surface average roughness values roughness is observed to decrease for composite layers. The roughness is higher for the pure nickel and composite layers obtained at a value of 4A/dm^2 for electrodeposition current density compared with the values of roughness obtained at a value of electrodeposition current density of 2A/dm^2.

The smaller values of average roughness of the composite layers compared with the values of average roughness for pure nickel layers could be explained by the inhibition of nickel crystals growth induced by micro SiC particles.

References

[1]. J. A. Calderón, J. E. Henao, M. A. Gómez, *Erosion-corrosion resistance of Ni composite coatings with embedded SiC nanoparticles*, Electrochimica Acta, 124, p. 190-198, 2014.

[2]. E. García-Lecina, I. García-Urrutia, J. A. Díez, M. Salvo, F. Smeacetto, G. Gautier, R.Seddon, R. Martin, *Electrochemical preparation and characterization of Ni/SiC compositionally graded multilayered coatings*, Electrochimica Acta, 54, p. 2556-2562, 2009.

[3]. M. Srivastava, V. K. William Grips, K. S. Rajam, *Influence of SiC, Si_3N_4 and Al_2O_3 particles on the structure and properties of electrodeposited Ni*, Materials Letters, 62, p.3487-3489, 2008.

[4]. L. Benea, P. L. Bonora, A. Borello, S. Martelli, *Wear corrosion properties of nano-structured SiC–nickel composite coatings obtained by electroplating*, Wear, 249, p. 995-1003, 2002.

[5]. Felicia Bratu, Lidia Benea, Jean-Pierre Celis, *Tribocorrosion behaviour of Ni–SiC composite coatings under lubricated conditions*, Surface and Coatings Technology, 201, p. 6940-6946, 2007.

[6]. S. Pradeep Devaneyan, T. Senthilvelan, *Electro Co-deposition and Characterization of SiC in Nickel Metal Matrix Composite Coatings on Aluminium 7075*, Procedia Engineering, 97, p. 1496-1505, 2014.

[7]. R. V. Williams, *Electrodeposited composite coatings*, Electroplating Metal Finishing, 19, p. 92-96, 1966.

[8]. M. Musiani, *Electrodeposition of composites: an expanding subject in electrochemical materials science*, Electrochimica Acta, 45, p. 3397-3402, 2000.

[9]. Prasanna Gadharia, Prasanta Sahooa, *Influence of process parameters on multiple roughness characteristics of Ni–P–TiO_2 composite coatings*, Procedia Engineering, 97, p. 439-448, 2014.

[10]. Greg Haugstad, *Atomic Force Microscopy: Understanding Basic Modes and Advanced Applications*, John Wiley & Sons, Inc. Publications, 2012.

[11]. Camila Fernández, Chiara Pezzotta, Gijo Raj, Eric M. Gaigneaux, Patricio Ruiz, *Understanding the growth of RuO_2 colloidal nanoparticles over a solidsupport: An atomic force microscopy study*, Catalysis Today, 2015, article in press.

[12]. Hans-Jurgen Butt, Brunero Cappella, Michael Kappl, *Force measurements with the atomic force microscope: Technique, interpretation and applications*, Surface Science Reports, 59, p. 1-152, 2005.

[13]. Lidia Benea, Sorin-Bogdan Başa, Eliza Dănăilă, Nadege Caron, Olivier Raquet, Pierre Ponthiaux, Jean-Pierre Celis, *Fretting and wear behaviors of Ni/nano-WC composite coatings in dry and wet conditions*, Materials and Design, 65, p. 550-558, 2015.

[14] Mohajeri S, Dolati A, Rezagholibeiki S., *Electrodeposition of Ni/WC nanocomposite in sulfate solution*, Materials Chemistry and Physics, 129, p. 746-750, 2011.

[15]. P. Narasimman, Malathy Pushpavanam and V. M. Periasamy, *Effect of Surfactants on the Electrodepositionof Ni-SiC Composites*, Portugaliae Electrochimica Acta, 30, p. 1-14, 2012.

[16]. Abouzar Sohrabi, Abolghasem Dolati, Mohammad Ghorbani, Aidin Monfared, Pieter Stroevec, *Nanomechanical properties of functionally graded composite coatings: Electrodeposited nickel dispersions containing silicon micro- and nanoparticles*, Materials Chemistry and Physics, 121, p. 497-505, 2010.

[17]. Th. Lampke, A. Leopold, D. Dietrich, G. Alisch, B. Wielage, *Correlation between structure and corrosion behaviour of nickel dispersion coatings containing ceramic particles of different sizes*, Surface and Coatings Technology, 201, p. 3510-3517, 2006.

[18]. D. Thiemig, R. Lange, A. Bund, *Influence of pulse plating parameters on the electrocodeposition of matrix metal nanocomposites*, Electrochimica Acta, 52, p. 7362-7371, 2007.

[19]. R. R. L. De Oliveira, D. A. C. Albuquerque, T. G. S. Cruz, F. M. Yamaji, F. L. Leite, *Measurement of the Nanoscale Roughness by Atomic Force Microscopy: Basic Principles and Applications*, book edited by Victor Bellitto, 2012.

[20]. E. S. Gadelmawla, **M. M. Koura, T. M. A. Maksoud, I. M. Elewa, H. H. Soliman,** *Roughness Parameters, Journal of Materials Processing Technology*, 123, p. 133-145, 2002.

THE ANNALS OF "DUNAREA DE JOS" UNIVERSITY OF GALATI
FASCICLE IX. METALLURGY AND MATERIALS SCIENCE
Nº. 4 - 2015, ISSN 1453 – 083X

THE INFLUENCE OF THE PHYSICAL-CHEMICAL FACTORS ON THE DISTRIBUTION OF HEAVY METALS IN THE DELTA ECOSYSTEMS

Stela CONSTANTINESCU
"Dunarea de Jos" University of Galati
email: constantinescu_stela@yahoo.com

ABSTRACT

Recognized to the influence of micropollutants, heavy metals represented on the ecological status of surface waters, including delta ecosystems, the paper aims to study the impact of environmental factors (temperature, pH, electroconductivitity, total salt content, dissolved oxygen content) the presence of heavy metals in the aquatic ecosystems of the Danube Delta Biosphere Reserve.

In this paper special attention is given to the conservation of sampling and water samples, sediments, plankton and plant material, to the specific methods for the determination of heavy metals and physical-chemical indicators, and to the specific methods for quality assurance of chemical analysis.

It presents a wide range of data on the concentration levels of heavy metals, both in terms of spatial distribution, and bioaccumulation in water samples, sediments, plankton and morphological parts of species that characterize the Reservation of aquatic ecosystems of the Danube Delta Biosphere, in terms of the levels and effects of heavy metal pollution.

KEYWORDS: aquatic ecosystems, heavy metals, environmental factors, sediments

1. Introduction

Heavy metals are part of the persistent pollutants in the environment and is an additional argument for research activities dedicated surveillance levels of heavy metals in the delta ecosystems and assess the effects of these contaminants on aquatic ecosystems are exercised [1, 2].

To assess the influence of physical-chemical factors on the distribution of heavy metals in aquatic ecosystems were taken into account the following physico-chemical parameters: water temperature, water pH, electroconductivity, dissolved oxygen content and total content of salts. The heavy metals have selected cadmium, chromium, nickel, lead, manganese and zinc [3-5].

Increasing water temperature increases metal concentrations in water and sediment. The pH affects the toxicity of heavy metal salts, at a low level (at the upside value of heavy metal toxicity).

The practical value and theoretical significance of the results and conclusions arising from the work on the impact of environmental factors on heavy metals delta ecosystems [6, 7].

The physico-chemical analyses were performed in the chemistry laboratory of the National Institute for Research and Development Danube Delta, a laboratory accredited to EN ISO / IEC 17025: 2005 by the Accreditation Association of Romania, RENAR

2. Experimental procedure

The main topic addressed in this paper is related to the problems and damage to ecosystems due to heavy metals and toxic pollution effects of which are developed both directly and indirectly.

In an aquatic ecosystem metal toxicity can be influenced by variations of abiotic environmental factors such as oxygen, water hardness, pH and transparency.

The temperature, in particular, is an important factor influencing metal toxicity, because most aquatic organisms are poikilothermic.

Although hardness is widely recognized tot affect the aquatic toxicity of metals, the pH is often the biggest effect on metal toxicity.

Some studies show that low levels of pH in water reduce the toxicity of cadmium in seaweed and fish. It has also been suggested that the toxicity is low due to the competition between ions H + and metal cations free transport mechanism.

Other factors that may play a role are: the organic matter, the carbon dioxide, the metabolic activity, the period (time) of halving the metal, the suspended solids, the total organic carbon (TOC), the interaction between pollutants, the stage of development and intraspecific bodies changes of the of metals. The influence of these factors on the distribution of physical-chemical properties of metal, occurs either through direct action on the physiological activity of the body's metabolic processes changing intensity or acting on the microclimate by changing the physico-chemical or pollutant concentration.

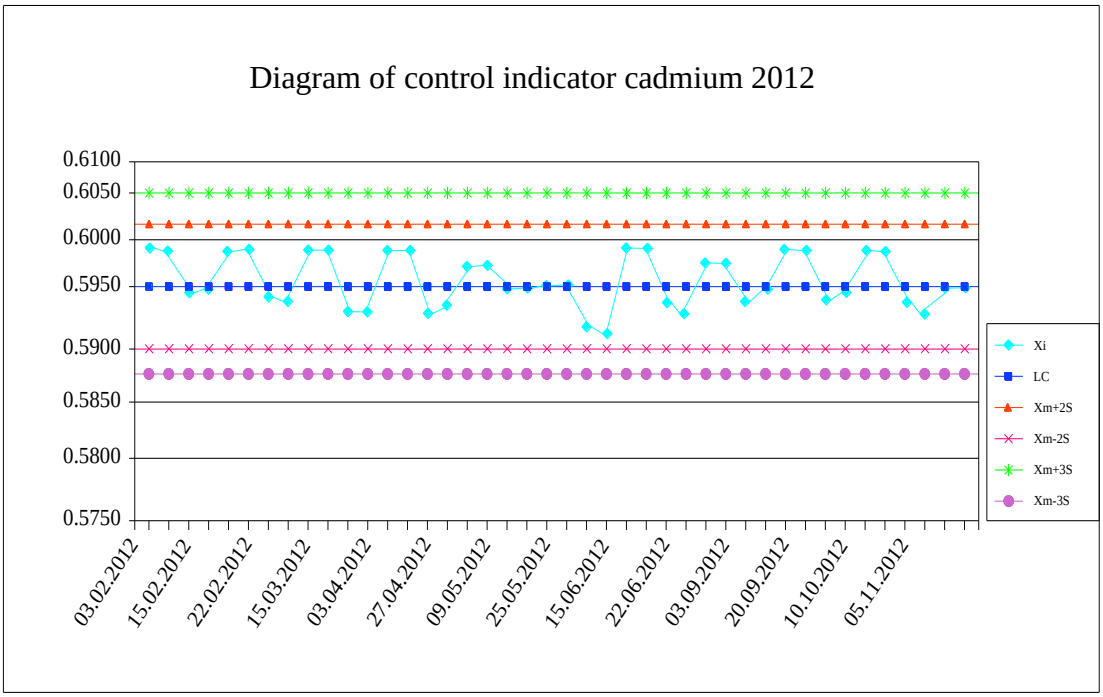

Fig. 1. *Diagram of control indicator cadmium*

Determining the pollution gradient and the degree of accumulation of inorganic pollutants on substrates (water, mineral, vegetable) and for the purposes set out in this paper, we consider the aquatic complex Razim-Sinoe as representative of the Danube Delta Biosphere Reservation.

The types of samples are: samples of surface water, sediment samples, samples of plant material (Phragmites australis (reed) Typha angustifolia (rush). Water samples were collected quarterly in 2012-2015. Sediment samples were collected annually in 2012-2015. Aquatic vegetation samples were collected quarterly in 2012-2015.

The samples were mineralized in the Anton Paar. Microwave. The step mineralization is performed differently depending on the type of sample, in compliance with applicable standards and recommendations suggested by the Anton Paar oven manufacturer.

The determination of heavy metals by atomic absorption spectrometry. Atomic absorption may be used to determine very low concentrations of ions in solution.

This method is widely applied in biological samples, metallurgical, geological or to determine pollution. Figure 1 represents the diagram of the cadmium control indicator. Values with concentrations in the control charts are determined to be valid measurements, respectively in Xm +/- 2 S, (mean +/- standard deviation of all measurements).

For comparative extraction and analysis tests of the same type of sample, two systems of extraction and analysis were established:

1. Skalar mineralizer and atomic absorption spectrometer VARIAN AA100.

2. Anton Paar microwave oven and mass spectrometer with inductively coupled plasma ICP-MS Elan DRC.

Samples of water, sediment and reed treated by both methods were taken starting from 2014 in aquatic complex Razelm-Sinoe.

3. Result and discussions

In relation to the national quality standards for lake bottom sediment, most of the samples investigated in the period 2012-2015, had levels of manganese and zinc limits. Cadmium was the item that recorded the highest percentage of exceedances of the standard for quality, as shown in Figure 2.

To assess concentrations of metals, we considered the mean concentrations of cadmium determined in 2014 the aquatic complex Razim-Sinoe.

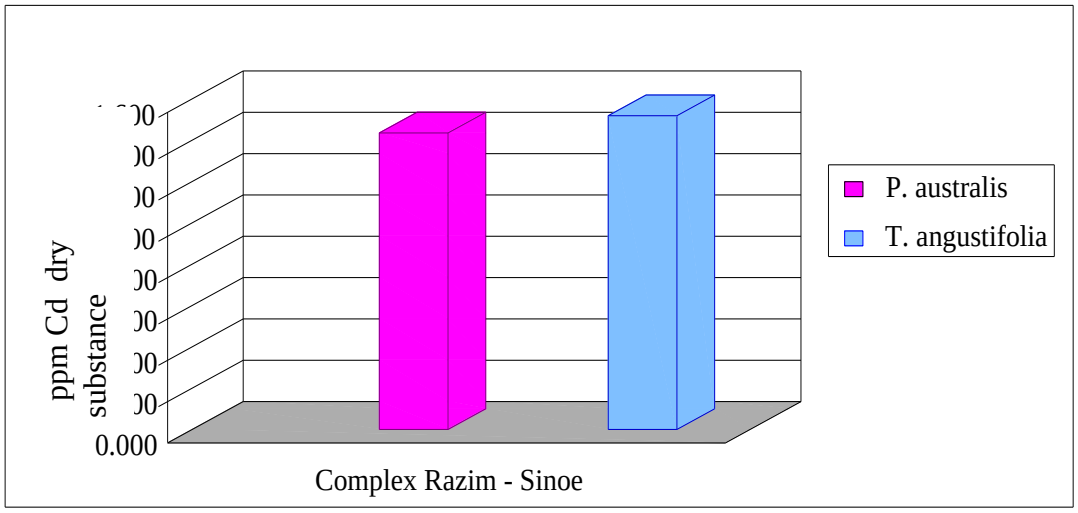

Fig. 2. *Dynamics of cadmium concentrations in samples Phragmites australis and Typha angustifolia, aquatic complex Razim-Sinoe*

Heavy metals enter into cyclic biological aquatic plants through the roots and leaves. They can directly affect plant growth, excessive intake of such elements in plants can also be dangerous for human and animal health. The chemical composition reflects the composition of the soil and plant, the plant surface contamination indicates the presence of contaminants harmful to the environment, in the air. In order to assess the accumulation of heavy metals in parts morphology of the species Phragmites australis, respectively, stalk, rhizomes and leaves, aquatic plant samples were collected at the stage of developing their most complex Razim-Sinoe water in the summer of 2014.

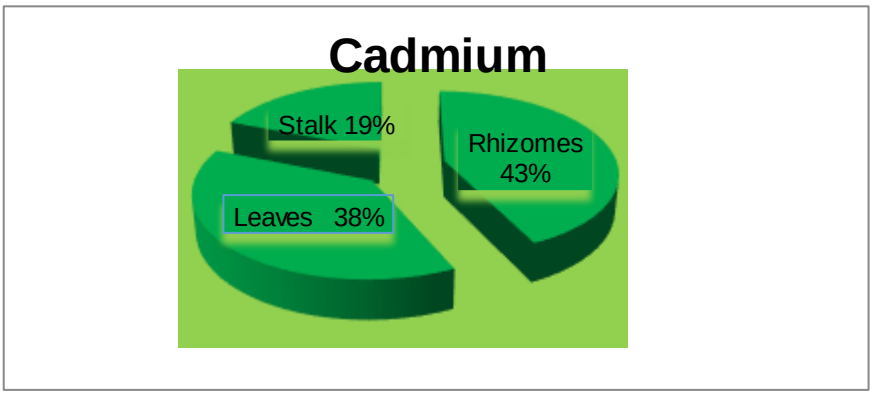

Fig. 3. *Distribution of cadmium in morphological parts Phragmites australis species of aquatic complex Razim-Sinoe*

Analysing the percentage values of the concentrations of heavy metals, we observed that all analysed metals, namely cadmium, chromium, nickel, lead, manganese and zinc, accumulate mostly in the

rhizomes samples Phragmites australis (between 37% and 75%), Figure 3.

The results show that Phragmites australis leaves have a capacity to accumulate heavy metals in comparison to the roots, the reason for this is probably short-lived; leaves renew every year, while rhizomes have a longer life, so rhizomes accumulate a larger amount of heavy metals than the leaves.

Table 1. *Values factors bioaccumulation of heavy metals in aquatic vegetation in Razim-Sinoe*

No	Complex aquatic	Vegetation aquatic	BCF Cd L/kg	BCF Cr L/kg	BCF Ni L/kg	BCF Pb L/kg	BCF Mn L/kg	BCF Zn L/kg
1.	Razim-Sinoe	P. australis	120.111	90.501	759.500	2.998	8.490	360.160
		T. angustifolia	123.180	101.622	692.401	5.900	9.998	390.100

To calculate the bioaccumulation factors, the average annual values of concentrations of heavy metals in water and helofile two species, Phragmites australis and Typha angustifolia, were taken into account Table 1.

Analyzing large amounts of bioaccumulation factors obtained for these two species studied macrophytes in the aquatic complex, we conclude that both species have shown great potential for bioaccumulation of heavy metals. In general, the order growth factors bioaccumulation of heavy metals in the two species studied helofile the pool complex is as follows:

BCF Pb <BCF Mn <BCF Cr <BCF Cd <BCF Zn <BCF Ni.

Given this abundance, the distribution of these plants must be seriously taken into consideration.

In terms of the accumulation of heavy metals, the emerged vegetation is different from the submerged vegetation in that the submerged vegetation accumulated more metal than that emerged.

Heavy metals in the two types of vegetation accumulate mostly in submerged vegetation to vegetation emerged, except cadmium and lead that accumulate the same values in both types of aquatic macrophytes, Figure 4.

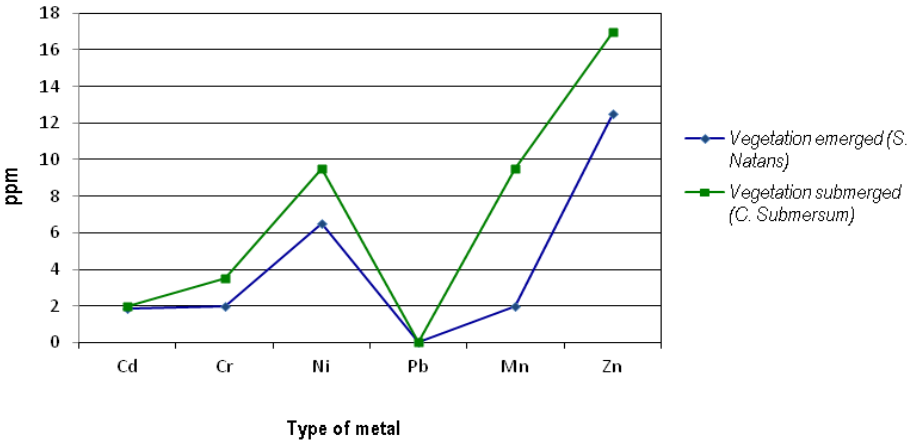

Fig. 4. *Accumulation of heavy metals in vegetation submerged and emerged*

In conclusion, the species of the selected aquatic macrophytes, i.e. Phragmites australis, Typha angustifolia, so take heavy metals from water and sediment (by-rhizome root system, highly developed) in studying aquatic complex.

Investigations on the use of the aquatic macrophytes as bioaccumulate heavy metals as well as their ability to be used in modern techniques of cleaning a water body could be very useful for environmental monitoring and health check of the water body.

To assess the influence of physical-chemical factors on the distribution of heavy metals in aquatic ecosystems were taken into account the following physico-chemical parameters: water temperature, water pH, electroconductivity, dissolved oxygen content and total content of salts. The heavy metals have selected cadmium, chromium, nickel, lead, manganese and zinc. Increasing water temperature increases metal concentrations in water and sediment. pH affects the toxicity of heavy metal salts, at a low level (at the upside of heavy metal toxicity).

Analyzing the correlations between the concentrations of metals in water samples and sediments and physico-chemical properties, we conclude that strict rules are not possible to give both positive and negative values of the indices Pearson, Table 2. This Danube Delta it is an open system that continuously circulates water so that the concentrations of metals in water and sediment undergo permanent changes.

***Table 2**. Pearson correlation index values determined for cadmium in aquatic complex Razim-Sinoe*

	Temperature (ºC)	**pH**	**Ec** (µs/cm)	**O_2 disolvation** (mg O_2/L)	**Total salts** (mg/L)	**Cd-Water** (mg/L)
Cd-Water (mg/L)	0.3500	0.1801	0.1158	0.4700	-0.3110	1
Cd-Sedim. (mg/kg)	0.5010	-0.7900	0.8051	0.7998	-0.2612	-0.1161

The Pearson correlation index values were the basis for determining the influence of physical-chemical factors on the distribution of heavy metals in the delta ecosystems.

4. Conclusions

The Chemical analyses were performed by standard methods.

Aquatic macrophytes having the ability to absorb and accumulate large amounts of heavy metals, have an important role as biofilters, bio-accumulate and bio-indicators. Similar trends in the accumulation of heavy metals in the analyzed samples show the universal importance of these aquatic macrophytes in environmental clean living.

The particular capacity of these two species, Phragmites australis and Typha angustifolia, to accumulate heavy metals and that these two macrofite produce a significant amount of organic matter, which increases the potential for accumulation of toxic substances in these two species of macrophytes, make them suitable for use in environmental monitoring of water quality where they live and their role biofilters aquatic ecosystems.

Analyzing the influence of physical-chemical factors (water temperature, water pH, electroconductivity, dissolved oxygen content and total content of salts) on the distribution of heavy metals (cadmium, chromium, nickel, lead, manganese and zinc) in the lake complex Razim-Sinoe found that the influence of these factors acting on the microclimate manifests itself by changing its physico-chemical properties.

The increase of the water temperature increases metal concentrations in water and sediment, with certain exceptions; the pH affects the toxicity of heavy metal salts, at a low level (at the upside of heavy metal toxicity microclimate manifests itself by changing its physico-chemical properties.

Cadmium aquatic vegetation has resulted from a normal distribution.

References

[1]. P. Kotze, H. H. Du Preez, J. H. J. Van Vuren, *Bioaccumulation of copper and zinc in Oreochromis mossambicus and Clarias gariepinus from the Olifants river*, Mpumalanga, South Africa. Water SA, 25(1), p. 99-110, 1999.
[2]. M. Van Der Merwe, J. H. J. Van Vuren *et al.*, *Lethal copper concentration levels for Clarias gariepinus (Burchell, 1822) - a preliminary study*, Koedoe, 36, p. 77-86, 1993.
[3]. P. D. Abel, *Water Pollution Bilogy*, ed. E. H. Poblishers, Chichester, 231. 1989.
[4]. L. Teodorof *et al.*, *Heavy metals extraction and analysis in aquatic ecosystems with automated techinques, in Advances in Electrical and Computer Engineering*, Suceava, Romania, p. 102, 2009.
[5]. D. J. Pietrzyk, C. W. Frank, *Chimie Analitica. 2 ed.*, Bucuresti, Editura Tehnica, 558, 1989.
[6]. A. Shehu *et al.*, *Assessment of Heavy Metals Accumulation by Different Spontaneous Plant Species Grown along Lana River*, Albania. Balwois, Ohrid, 2010.
[7]. G. Jamnická *et al.*, *Heavy metals content in aquatic plant species from some aquatic biotopes in Slovakia*, in Proceedings 36th International Conference of IAD, Austrian Committee Danube Research/ IAD, 2006, Vienna.

THE ANNALS OF "DUNAREA DE JOS" UNIVERSITY OF GALATI.
FASCICLE IX. METALLURGY AND MATERIALS SCIENCE
Nº. 4 - 2015, ISSN 1453 – 083X

CORROSION BEHAVIOUR AND BIOCOMPATIBILITY OF 316 STAINLESS STEEL AS BIOMATERIAL IN PHYSIOLOGICAL ENVIRONMENT

Georgeta TODERAŞCU[1], Valentin DUMITRAŞCU[1], Lidia BENEA[1,*], Alexandru CHIRIAC[2]

[1]Research (Competences) Centre: Interfaces-Tribocorrosion and Electrochemical Systems (CC-ITES), Faculty of Materials and Environmental Engineering, Dunărea de Jos University of Galati, 47 Domnească Street, RO-800008, Galati, Romania

[2]Faculty of Medicine and Pharmacy, Dunărea de Jos University of Galati, 47 Domnească Street, RO-800008, Galati, Romania

[*]Corresponding author
e-mail: Lidia.Benea@ugal.ro

ABSTRACT

Although stainless steel is a material widely used for biomedical applications, its surface properties for long term application are still a serious concern. 316L stainless steel (SS 316L) is a material commonly used in dentistry for orthodontic braces, wires and in some cases as dental crowns. The pH value of natural saliva from the oral cavity can undergo sudden modification due to food products which are rich in citric acid. The electrochemical corrosion behavior of 316L stainless steel was evaluated in two simulated body fluid solutions, Fusayama-Mayer artificial saliva with pH=5 and Fusayama-Mayer artificial saliva adjusted with citric acid to a pH=1.58 which simulates the environmental conditions of the oral cavity. The surface of SS316L was investigated by optical microscope before and after corrosion assays. The electrochemical corrosion behavior was studied by open circuit potential, potenitodynamic polarization and linear polarization. Optical microscopy was used to characterize the corrosion damage after the electrochemical assays.

KEYWORDS: biomaterials, stainless steel, corrosion, simulated body fluids

1. Introduction

Man-made materials and devices have been developed to replace diseased or damaged parts (which become non-functional) in the human body in order to prolong life, to improve and restore tissue function, and to improve quality of life [1], through production of contact lenses, dental implants, artificial skin, heart valves, breast implants, joint prostheses or bone plates. Significant developments have been taking place to provide suitable biomaterials from metals/alloys, ceramics, bioglasses, and polymers with minimal reaction and rejection by the body [1].

It is well known that a series of interactions occur between the surface of biomaterials and the biological environment after they have been implanted into the human body. Therefore, the biomaterials surface plays an extremely important role in the response of artificial medical devices to the biological environment [2]. The current research focuses on the biomaterials and the research community is aimed at understanding the fundamental processes at the interface between the implant surfaces and surrounding living tissues [2].

Table 1. shows the types, applications, and major failure mechanism of various biomaterials including metallic/alloys. However, each of these has some limitations. A single material cannot offer all desired properties; therefore, they have been used in combination with each other in the form of coatings and joints [1].

Metallic materials such as Ti, Ti-alloy, Co–Cr alloy and stainless steel–AISI (American Iron and Steel Institute) 316L are used as biomaterials due to their superior tensile and fatigue strength and fracture toughness as compared to nonmetals such as polymeric and ceramic. However, metallic materials

corrode by aggressive biofluid and release metallic ions which resulted in the reduction of their biocompatibility [1, 3]. The biocompatibility and corrosion resistance of these implants are primarily determined by their constituent material and surface micro structural properties such as roughness, grain size, etc. [3].

Table 1. *Types of biomedical materials and their applications* [1]

Biomaterials	Objectives	Degradation mechanism	Applications
Metals/alloys: SS316L, Co-Cr alloy, Ti and Ti alloys, Ni-Ti alloys	Load bearing	Corrosion and mechanical	Fracture fixation plates, screws, pins, nails, joint replacements, orthodontic wires, femoral stems, cases for pacemakers, supports for heart valves, dental implants, dental crowns, bridges, fillings, and inner ear bone replacements
Ceramics: Carbon coatings, alumina, oxides, zirconia, glass, glass ceramics, and hydroxy apatite (HAP)	High hardness, wear resistance, and better bone bonding	Corrosion and mechanical	Carbon in heart valves, dental implants, joint implants, coatings for dental and joint implants, fill bone voids/cavities by HAP, tissue scaffolds, drug delivery systems, and inner ear implants
Polymer: Ultra high molecular weight polyethylene, polyester, polytetraflouroethylene, PMMA, hydrogels, silicone rubber, PGA/ PLA, collagen, cellulose, and chitosan	Articulating surfaces	Wear, swelling, leaching, chemical	Joint replacement, vascular grafts, bone cement, orthodontic devices (e.g. plates, dentures) contact and intraocular lenses, catheters, hand and toe joints, artificial tendon and ligament, reconstructive surgery, sutures, staples, tissue scaffolds, drug delivery systems, and hemostatic bandages, pace maker leads.

The stability of the surface oxide layer is one of the most important requirements of a biomaterial. For untreated 316L SS, the stability of the surface oxide layer is not very high and the possibility of metal ions being released is greater in comparison to Co-Cr and Ti-6Al-4V alloys [4]. After electrolytic polishing, 316L stainless steel forms a very thin, of a few-nanometer, compact oxide film resistant against corrosion in the presence of physiological human body fluids environments [5].

Among the metallic materials, AISI 316L stainless steel is most commonly employed for temporary devices such as fracture plates, bone screws and hip nails due to its low cost and acceptable biocompatibility [3, 6, 7]. It also has good ductility and possesses good biocompatibility [7, 8].

However, it has been often reported to suffer from severe crevice and galvanic corrosion, primarily due to the presence of occluded sites and high chloride concentration in physiological fluids.

The corrosion of the stainless steel implant releases metal ions such as Fe, Ni and Cr, which produce local systematic effects and thereby plays a role in prosthetic loosening [3].

In the dental industry, the metallic alloys are mainly used for crown, bridges, prostheses, supra-constructions and implants. They need to fulfill important requirements such as ease and reliability of handling and treatment, toughness appropriate to the situation of application, good biocompatibility and aesthetic properties. These materials are confronted with extreme environmental conditions in the mouth, as the temperature can vary between 5 and 55 ^{o}C and the composition and the pH of the saliva varies depending on the nutrition [9]. The interactions between saliva and these foreign materials can affect the corrosion and tribocorrosion performance of 316L stainless steel prostheses [10].

The original artificial saliva solution was introduced by Takao Fusayama [10], but the chemical composition of artificial saliva has changed in time. Although saliva has a neutral acidity (pH of 7), due to the acidity of the modern western diet rich in citric acid from fruits and vegetables, saliva frequently becomes acidic (pH 5-6) during mastication. It is not uncommon for proteins, antibacterial agents and enzymes to be added to artificial organic solutions.

In recent years, there has been a significant increase in the number of studies examining the corrosion properties of 316L stainless steel used in medical/dental applications. In some recent studies the corrosion mechanisms of 316L stainless steel in various solutions, including different artificial saliva [10-13], have been examined. The aim of this study is to identify the occurring corrosion mechanisms where 316L stainless steel is exposed to an environment

with different pH values, which is similar to the oral cavity through electrochemical methods.

2. Experimental procedure

2.1. Materials

In this work it was analyzed 316L stainless steel with the chemical composition given in Table 2. Before corrosion examinations, the 316L stainless steel samples were polished with SiC #600 and diamond paste. The polish plates were degreased with alcohol and acetone and rinsed with distilled water. Afterwards the polished samples were dried with a hair dryer and inserted in corrosion holder to obtain a measurable surface of 1.76 cm^2.

2.2. Electrochemical behavior tests in bio-simulated fluid solution

In situ electrochemical measurements such as open circuit potential (OCP), linear polarization (Rp) and potentiodynamic polarization (PD) were carried out to access the anti-corrosive characteristics of 316L stainless steel in Fusayama-Mayer artificial saliva with two different pH. All electrochemical assays were performed using VoltaLab PGZ100 potentiostat/galvanostat and the data were recorded with VoltaMaster software.

The surfaces of SS 316L were investigated with an optical microscope type OPTIKA XDS-3MET before and after corrosion tests in order to confirm the results of electrochemical assays. The optical images were performed with software Vision Pro Plus, version 5.0 on computer connected to optical microscope.

Table 2. *Chemical composition of 316L stainless steel*

Element	Composition (wt.%)
C	0.02
Si	0.47
P	<0.007
S	<0.03
Cr	17.5
Mn	1.92
Cu	0.3
Ni	13.3
Mo	2.04
Nb	0.07
Fe	Balance

The electrochemical measurements were carried out in a conventional three electrodes cell shown in Fig. 1. consisting of Platinum-Rhodium grid as counter electrode (CE), Ag/AgCl (saturated solution of KCl, E=200 mV vs. Standard Hydrogen Electrode (SHE)) as reference electrode and 316L stainless steel as working electrode (WE).

The corrosion behavior of 316L stainless steel was tested in the Fusayama Mayer artificial saliva with pH=5 and respectively pH=1.58 adjusted with citric acid. Chemical compositions of these solutions are close to the natural saliva and contain different types of salts which are shown in Table 3.

The pH of Fusayama-Mayer artificial saliva was adjusted to 1.58 in order to understand the corrosion behavior of SS 316L under the worst-case conditions, although it is known that this pH value is much more aggressive than it would be normal for natural saliva.

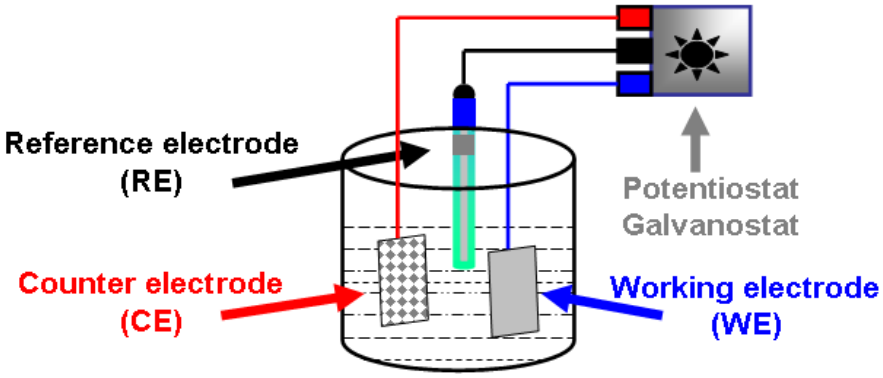

Fig. 1. *Electrochemical cell set-up for corrosion tests*

Table 3. *Chemical composition of Fusayama-Mayer artificial saliva*

Compound	Fusayama-Mayer artificial saliva
NaCl	0.4 g/L^{-1}
KCl	0.4 g/L^{-1}
$CaCl_2$	0.8 g/L^{-1}
Na_2HPO_4	0.69 g/L^{-1}
CH_4N_2O	1 g/L^{-1}
Deionized water	Balance
pH	5

3. Results and discussion

3.1. Open Circuit Potential

The open circuit potential was monitored with the exposure time of 60 minutes, in order to obtain a stable potential vs. Ag/AgCl (reference electrode). The potential-time measurements are one of the ways to study the corrosion behavior of 316L stainless steel in the Fusayama-Mayer artificial saliva with two different pH values and recorded data are presented in Fig. 2.

From Fig. 2. it can be observed that the potential of 316L stainless steel immersed in the Fusayama-Mayer artificial saliva with two different pH values shift to positive values at the end of 60 minutes. The same Fig. 2. shows that the potential of sample immersed in the Fusayama-Mayer artificial saliva with pH=5, drops down slowly in the first 2 minutes due to the slow degradation of native passive layer from the surface and after that, it increases up to -90 mV at the end of studied time period. The potential of samples immersed in the modified Fusayama-Mayer artificial saliva with pH=1.58, the potential decreases faster in the first 5 minutes due to the rapid degradation of passive film and after that increases slowly up to value of -120 mV.

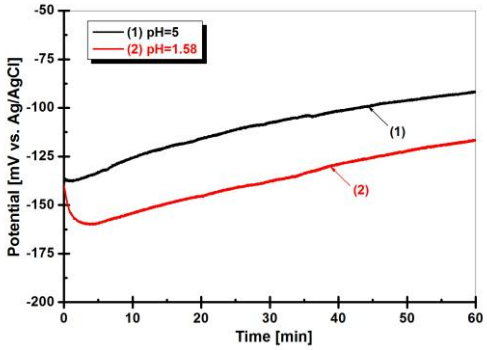

Fig. 2. *Open circuit potential plots obtained in: (1) Fusayama-Mayer artificial saliva pH=5.0 and (2) Fusayama-Mayer artificial saliva adjusted with citric acid at pH=1.58*

This increasing trend of potential has been observed by T. Hryniewicz [14] for 316L stainless steel after immersion in a Ringer solution. The increasing trend of 316L stainless steel potential reveals the formation of a stable passive oxide layer on the sample surface.

3.2. Evolution of polarization resistance (Rp) values during immersion time

The linear polarization method was used to evaluate the polarization resistance of 316L stainless steel in the Fusayama-Mayer artificial saliva with two different pH values. The evaluation of polarization resistance was measured around open circuit potential value with a very small potential amplitude (±40 mV) in order to preserve the steady state surface.

Fig. 3 (a) presents the polarization resistance diagrams of SS 316L immersed in Fusayama-Mayer artificial saliva with pH=5 and 1.58, respectively.

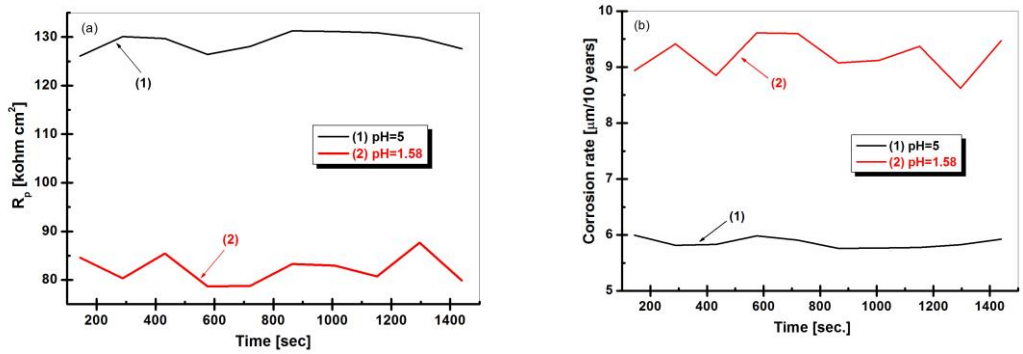

Fig. 3. *(a) The evolution of polarization resistance (Rp) and (b) the evolution of corrosion rate values during the immersion in Fusayama-Mayer artificial saliva with (1) pH=5 and (2) pH=1.58*

Fig. 3 (a). shows that the polarization resistance value of SS 316L, immersed in Fusayama-Mayer with pH=5, is equal to *130 kohm·cm²*. In comparison, the polarization resistance value of SS 316L immersed in the Fusayama-Mayer artificial saliva adjusted with citric acid to a pH value of 1.58 is equal to *80 kohm·cm²*. The increased polarization resistance value means that the formed passive film after immersion in the Fusayama-Mayer artificial saliva with pH=5 is more resistant compared with that formed in low pH value equal to 1.58. A decrease of the polarization resistance value at once with the decrease of pH value lead to the increasing of the corrosion current density and therefore to a higher corrosion rate, as noticeable in Fig. 3 (b). Fig. 3 (b) presents the corrosion rates versus the time corresponding to SS 316L surfaces immersed in the Fusayama-Mayer artificial saliva with two different pH values. According with the data plotted in Fig. 3 (b). the higher corrosion rate is shown to correspond to SS 316L immersed in the Fusayama-Mayer artificial saliva with the lowest pH value (pH=1.58) in comparison with the corrosion rate of SS 316L immersed in the Fusayama-Mayer artificial saliva with pH=5. These results show that the SS 316L has a lower corrosion resistance in the Fusayama-Mayer artificial saliva (pH=5) and are in good agreement with the evolution of open circuit potential values.

3.3. Potentiodynamic polarization

The potentiodynamic polarization studies were recorded in a range of potential starting from -1.5 V vs. Ag/AgCl to +1.5 V vs. Ag/AgCl at a scan rate of 5 mV/s. Fig. 4. shows the potentiodynamic polarization of SS 316L after immersion in the Fusayama-Mayer artificial saliva with two different pH value, 5 respectively 1.58.

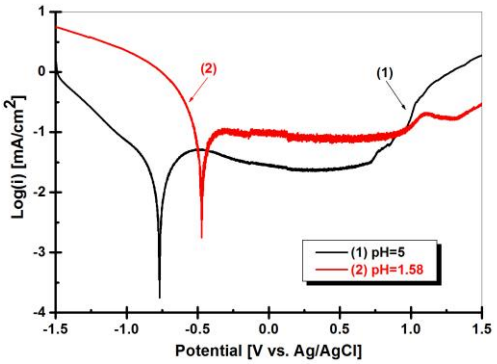

Fig. 4. *Tafel representation of potentiodynamic polarization for SS 316L immersed in Fusayama-Mayer with (1) pH=5 and (2) pH=1.58*

Table 4. *The electrochemical corrosion data extracted from the electrochemical corrosion polarization curves*

Sample/ Solution	**E_{corr} (i=0) (mV vs. Ag/AgCl)**	**R_p kohm. cm²**	**i_{corr} mA. cm²**	**b_a (mV vs. Ag/AgCl)**	**b_c (mV vs. Ag/AgCl)**
SS 316L/ Fusayama-Mayer pH=5	-770	3.25	11.21	241.4	-214.4
SS 316L/ Fusayama-Mayer with citric acid pH=1.58	-472.7	1.16	52.49	380.2	-146.8

The anodic Tafel constant *βa* and cathodic Tafel constant *βc*, as well as the corrosion current density *Icorr*, were calculated from the intersection of the anodic and cathodic Tafel lines in the polarization curves at *Ecorr* [15, 16].

The results are listed in Table 4. Fig. 4. shows that the corrosion current (i_{corr}) of SS 316L immersed in the Fusayama-Mayer artificial saliva with pH value equal to 1.58 is higher than the corrosion current of SS 316L immersed in Fusayama-Mayer artificial saliva with pH value equal to 5 which provoked the decreasing of the corrosion rate from *3.25 kohm·cm²* to *1.16 kohm·cm²* with decreasing of pH value.

3.4. Optical microscopy

The surfaces of SS 316L were investigated before and after corrosion tests in the Fusayama-Mayer artificial saliva with the pH value equal to 5 and Fusayama-Mayer artificial saliva adjusted with citric acid and the pH value equal to 1.58 in order to estimate the corrosive effects and are presented in Fig. 5.

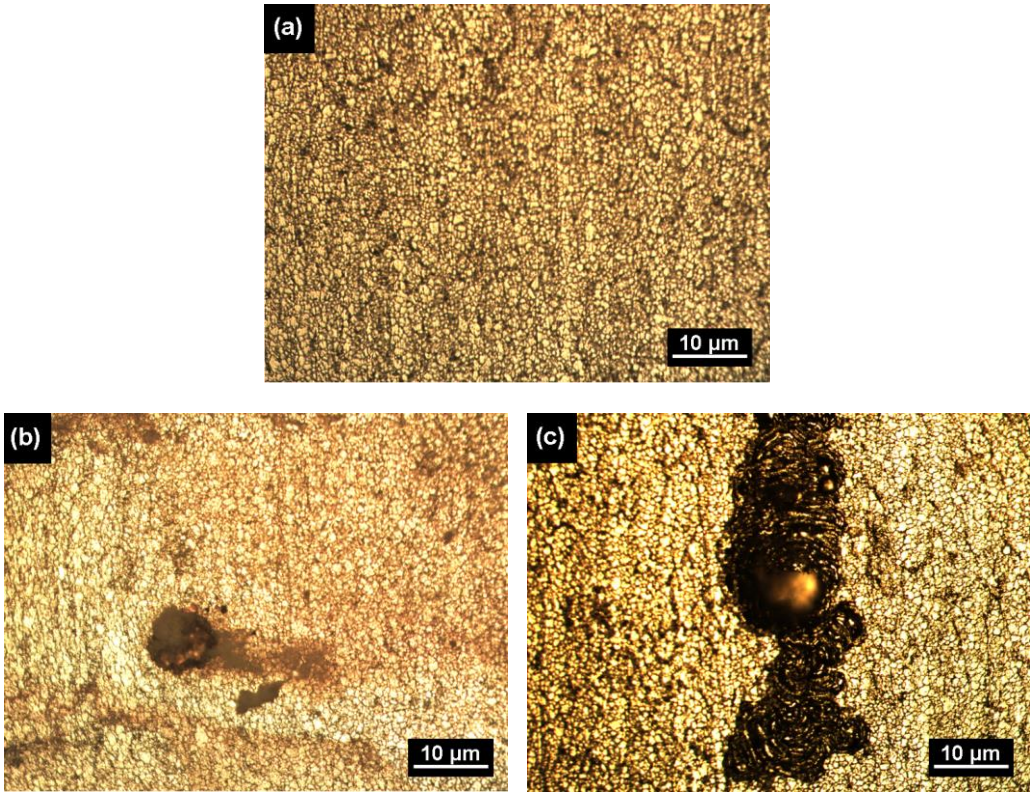

Fig. 5. *Optical microscopy of SS 316L (a) before corrosion, (b) after corrosion in Fusayama-Mayer artificial saliva with pH=5 and (c) after corrosion in modified Fusayama-Mayer artificial saliva with citric acid and pH=1.58*

Fig. 5 (a). shows that before corrosion tests the SS 316L has a uniform surface with no defects. After corrosion tests in Fusayama-Mayer artificial saliva with pH=5 (Fig. 5 (b)), the 316L stainless steel undergo small diameters pits and a few rust spots are visible in comparison with the 316L stainless steel surface (Fig. 5 (a)) before corrosion assays.

The samples of 316L stainless steel surface immersed in Fusayama-Mayer artificial saliva adjusted with citric acid and whose pH value is equal with 1.58, present severe pitting damage (Fig. 5 (c)) in comparison with the samples immersed in Fusayama-Mayer artificial saliva with the pH value equal with 5. The pitting damage covers a high surface of the 316L stainless steel samples and the pits are deeper into the substrate.

4. Conclusion

The corrosion behavior of Stainless Steel 316L was investigated in simulated body fluid – Fusayama-Mayer Artificial Saliva at different pH values.

The experimental results reveal that the SS316L present a better corrosion behavior in the Fusayama-Mayer Saliva with pH=5 in comparison with the Fusayama-Mayer Saliva modified with Citric Acid and pH=1.58.

From the linear polarization curves it can be seen that the decreasing of pH from 5 to 1.58 produce a decrease of polarization resistance (Rp) from *130 kohm·cm^2* to *80 kohm·cm^2*.

The optical microscopy images are in good agreement with electrochemical measurements.

Acknowledgements

UEFISCDI - Ministry of Education and Research is acknowledged for the financial support to Competences Centre Interfaces - Tribocorrosion and Electrochemical Systems (CC-ITES) - Dunarea de Jos University of Galati - Research Project: *HyBioElect*, contract 10 /30-08-2013 (2013 - 2016) in the frame of National Research Programme Romania - PN II PCE.

References

[1]. R. Singh, N. B. Dahotre, *Corrosion degradation and prevention by surface modification of biometallic materials*, Journal of Materials Science: Materials in Medicine, 18, p. 725-751, 2007.

[2]. X. Liu, P. K. Chu, C. Ding, *Surface nano-functionalization of biomaterials*, Materials Science and Engineering R 70, p. 275-302, 2010.

[3]. S. K. Tiwari, T. Mishra, M. K. Gunjan, A. S. Bhattacharyya, T. B. Singh, R. Sing, *Development and characterization of sol–gel silica–alumina composite coatings on AISI 316L for implant applications*, Surface & Coatings Technology, 201, p. 7582-7588, 2007.

[4]. T. P. Singh, H. Singh, H. Singh, *Characterization, corrosion resistance, and cell response of high-velocity flame-sprayed HA and HA/TiO_2coatings on 316L SS*, Journal of Thermal Spray Technology, 21, p. 917-927, 2012.

[5]. T. Hryniewicz, R. Rokicki, K. Rokosz, *Surface characterization of AISI 316L biomaterials obtained by electropolishing in a magnetic field*, Surface & Coatings Technology, 202, p. 1668-1673, 2008.

[6]. A. Mahapatro, *Bio-functional nano-coatings on metallic biomaterials*, Materials Science and Engineering C 55, p. 227-251, 2015.

[7]. A. Parsapour, S. N. Khorasani, M. H. Fathi, *Effect of surface treatment and metallic coating on corrosion behavior and biocompatibility of surgical 316L stainless steel implant*, Journal of Materials Science Technology, 28, p. 125-131, 2012.

[8]. J. Yang, F. Cui, I.S. Lee, X. Wang, *Plasma surface modification of magnesium alloy for biomedical application*, Surface & Coatings Technology, 205, p. S182-S187, 2010.

[9]. W. D. Mueller, C. Schoepf, M. L. Nascimento, A. C. Carvalho, M. Moisel, A. Schenk, F. Scholz, K. P. Lange, *Electrochemical characterization of dental alloys: its possibilities and limitations*, Analytical and Bioanalytical Chemistry, 381, p. 1520-1525, 2005.

[10]. A. Hayes, S. Sharifi, M. M. Stack, *Micro-abrasion-corrosion maps of 316L stainless steel in artificial saliva*, Journal of Bio- and Tribo-Corrosion, 1, p. 1-15, 2015.

[11]. K. Hajizadeh, H. Maleki-Ghaleh, A. Arabi, Y. Behnamiam, E. Aghaie, A. Farrokhi, M. G. Hosseini, M. H. Fathi, *Corrosion and biological behavior of nanostructured 316L stainless steel processed by severe plastic deformation*, Surface and Interface Analysis, 47, p. 978-985, 2015.

[12]. Y. Kayali, A. Buyuksagis, Y. Yalcin, *Corrosion and wear behaviors of boronized AISI 316L stainless steel*, Metals and Materials International, 19, p. 1053-1061, 2013.

[13]. B. Al-Mangour, R. Mongrain, E. Irissou, S. Yue, *Improving the strength and corrosion resistance of 316L stainless steel for biomedical applications using cold spray*, Surface & Coatings Technology, 216, p. 297-307, 2013.

[14]. T. Hryniewicz, R. Rokicki, K. Rokosz, *Electrochemical and XPS studies of AISI 316L stainless steel after electropolishing in a magnetic field*, Corrosion Science, 50, p. 2676-2681, 2008.

[15]. L. Benea, E. Mardare-Danaila, M. Mardare, J. P. Celis, *Preparation of titanium oxide and hydroxyapatite on Ti–6Al–4V alloy surface and electrochemical behavior in bio-simulated fluid solution*, Corrosion Science, 80, p. 331-338, 2014.

[16]. K. F. Khaled, S. S. Abdel-Rehim, *Electrochemical investigation of corrosion and corrosion inhibition of iron in hydrochloric acid solutions*, Arabian Journal of Chemistry, 4, p. 397-402, 2011.

THE ANNALS OF "DUNAREA DE JOS" UNIVERSITY OF GALATI
FASCICLE IX. METALLURGY AND MATERIALS SCIENCE
Nº. 4 - 2015, ISSN 1453 – 083X

MICROSTRUCTURAL CHARACTERIZATION OF THE TiMoZrTa ALLOY

Mădălina Simona BĂLȚATU[1], Ramona CIMPOEȘU[1], Petrică VIZUREANU[1,2], Dragoş Cristian ACHIȚEI[1,2], Mirabela Georgiana MINCIUNĂ[1,2]

[1]Gheorghe Asachi Technical University of Iasi, Faculty of Materials Science and Engineering, Blvd. D. Mangeron 41, 700050, Iasi, Romania

[2]Center of Excellence Geopolymer & Green Technology (CEGeoGTech), School of Materials Engineering, Universiti Malaysia Perlis, 01000 Kangar, Perlis, Malaysia

e-mail: cercel.msimona@yahoo.com

ABSTRACT

In recent years, different types of titanium alloys have been investigated with the aim of using materials in biomaterials field, and Ti-Mo system alloys are very promising materials. Alloying titanium with biocompatible elements like Mo, Zr and Ta make then possible for these alloys to be used in medical applications. Microstructures of two TiMoZrTa alloys were investigated. Obtaining of this original recipes alloys was prepared using vacuum arc re-melting method afterwards composition of this alloys were verified by quantitative qualitative analysis EDX. Aim of this study is investigating aspects of microstructures TiMoZrTa alloys using optical and scanning electron microscopes, verifying the type of grains, that will show us the most important properties.

KEYWORDS: Ti-based alloy, biomaterials, microstructure, XRD analysis

1. Introduction

Metallic biomaterials, like stainless steel or Co-based alloys, titanium and its alloys continue to be used extensively in different medical applications, therefore these are researched and improved [1, 2].

Titanium and its alloys are still widely used for implant materials, because they present an acceptable biocompatibility, relatively low elastic modulus, have an excellent corrosion resistance due superficial oxide layer and the density / resistance rapport is very good [3, 4].

Representative titanium alloys used for implant materials are Ti-6Al-4V and commercial pure titanium. These alloys of the type of α+β, in time, has been shown that V and Al are toxic for the human body. Therefore, researchers replaced V and Al with non-allergic elements like Mo, Nb, Ta, Sn and Zr. In recent years, the β-type titanium alloys composed of nontoxic elements was extensively investigated because processing variables can be controlled to produce selected results (e.g. Ti-15Mo, Ti-35.5Nb-5.1Ta-7.1Zr, Ti-24Nb-4Zr-8Sn and Ti-12Mo-6Zr-2Fe alloys) [5-8]. The β type alloys compared to α and (α+β) type Ti have advantages like lower elastic modulus, improved fatigue resistance and excellent resistance to wear and abrasion [9, 10].

Titanium has an allotropic transformation from a hexagonal close-packed (hcp) which is referred to "alpha" phase into a body-centered cubic (bcc), called "beta" phase at 882 ºC.

Depending on phase microstructure of the alloyed, titanium alloys can be classified into three main structural types: alpha alloys, alpha + beta alloys and beta alloys, but these metallographic transformations can be improved by additions of selected α or β alloying stabilizers [11-13].

The aim of this study is to characterize microstructures of a new alloy with medical applications.

2. Experimental procedure

The alloy was obtained from the melting of pure elements like Ti, Mo, Zr, Ta in an arc melting furnace, MRF vacuum ABJ 900.

Due to the big difference in the melting point of elements (Ti: 1.668 ºC, Mo: 2.623 ºC, Zr: 1.855 ºC, Ta: 3.020 ºC) and density (Ti: 4.51 g/cm^3, Mo: 10.2 g/cm^3, Zr: 6.5 g/cm^3, Ta: 16.65 g/cm^3) between the

four pure metals, the alloy was followed by re-melting of the alloy for 6 times in the same installation for refining and homogenizing its structure [11, 14].

The alloy used in this study, after melting, was characterized by chemical composition, X-ray diffraction, optical microscopy. Chemical composition of the alloy was analyzed with the EM VEGA II LSH scanning electron microscope manufactured by the TESCAN Co., the Czech Republic, coupled with an EDX QUANTAX QX2 detector manufactured by the BRUKER/ROENTEC Co., Germany.

The phases were analyzed using the X-ray diffraction, made on the diffractometer X'Pert PRO MPD PANalytical X-ray with the following parameters: continuous scan, 2θ - (10°-90°), Step size: 0.0131303, Time per step: 61.20, Scan speed: 0,05471,45 KV and 40 mA using a copper anode X-ray tube.

After the X-ray diffraction, the alloys were prepared by a standard metallographic process, by polishing alloys in SiC waterproof papers until #2000 grit and colloidal alumina suspension.

The metallographic structure of alloys was shown by the attack surface with a chemical solution having the following composition: 10 ml HF, 5 ml HNO_3, 85 ml H_2O immersed in 5-30s [12].

The device used in the microstructure analysis for Ti alloy was the metallographic microscope Leica 5000DMI.

3. Results and discutions

3.1. Chemical composition

The chemical analyses (EDX or XRF) were performed in many different areas. The results and spectrum are shown in Fig. 1.

The chemical composition of the alloy (Table 1) was homogeneous and it showed no differences between surface and core.

Figure 1 shows the spectrum and distribution map of the chemical elements of the studied alloy.

The distribution map shows that studied alloy is homogeneous all over the surface.

Table 1. *Chemical composition of alloy studied*

Element (wt.%)	
Ti	67.65
Mo	12.84
Zr	8.8
Ta	10.71

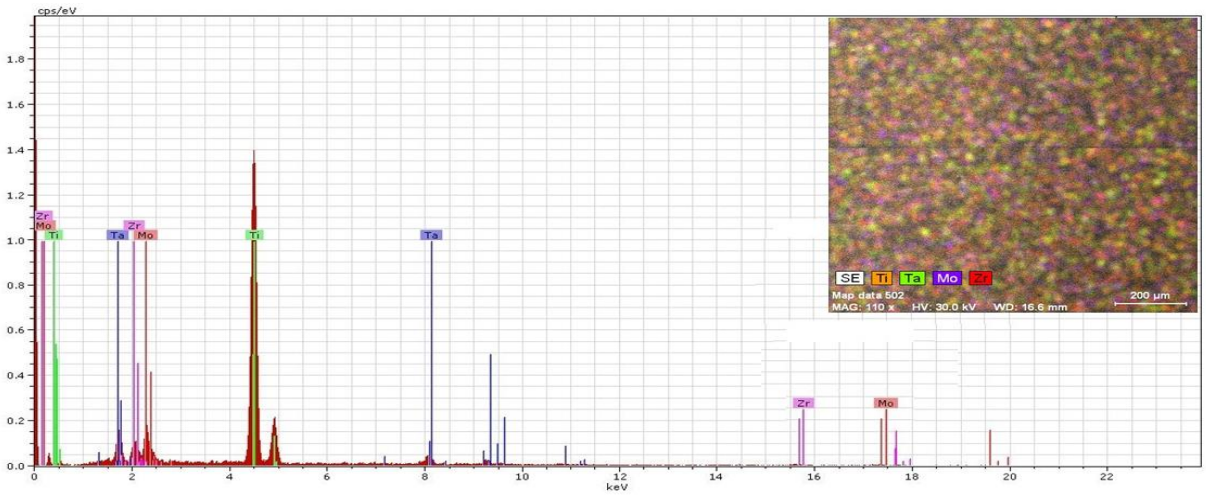

Fig. 1. *Spectrum and distribution map of the main chemical elements of the alloy studied*

3.2. X-ray diffraction

Figure 2 shows the X-ray diffraction patterns for Ti-based alloy. The patterns of alloy could be indexed in the cubic β type structure, the space group of Im-3m [10, 14].

According to Table 2, the increased amount of β stabilizing elements (Mo, Ta) alloys present in the composition was not enough to form a single phase β.

In the structure of the alloy there have been identified two main phases: β with a body-centered cubic structure and α'' with orthorhombic structure.

The adding of pure tantalum leads to the appearance emergence phase α'' as β phase is confirmed and to Y. L. Zhou [8]. According X.H. Min, by adding zirconium in conjunction with a higher percentage of 10% of Mo leads predominantly to the β phase appearance [15].

In the alloy sample β phase was found with the major peak at the angle 2θ = 38.8485 and α'' with the major peak at the angle 2θ = 37.0213.

Table 2 gives the network unit cell parameters of the alloy.

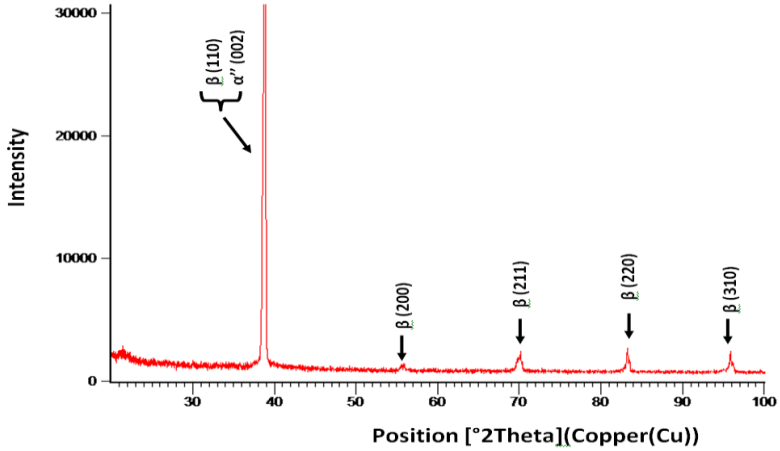

Fig. 2. *X-ray diffractograms for Ti-based alloy*

Table 2. *Compound parameters*

Elements	**Ti, Mo, Zr, Ta**
Space Group	Im-3m
Crystal system	Cubic
a(Å)	3.31
b(Å)	3.31
c(Å)	3.31
α(º)	90
β(º)	90
γ(º)	90
Cell volume (10^6 pm^3)	36.30

Its very important to know the microstructure of a metallic biomaterial, like Ti and its alloys, because of a coexistance of hexagonal α Ti and bcc β Ti.

Knowing these important aspects can control the mechanical properties and corrosion resistance, having a direct effect on their biocompatibility.

3.3. Microstructures

The microstructure of the studied alloy, as shown in the Fig. 3-4, was consistent with the XRD results.

The optical microstructure of the Ti-based studied alloy present acicular (dendritic) structure with irregular grain boundaries (Fig. 3). The microstructure of the TiMoZrTa alloy is a specific beta [16, 17].

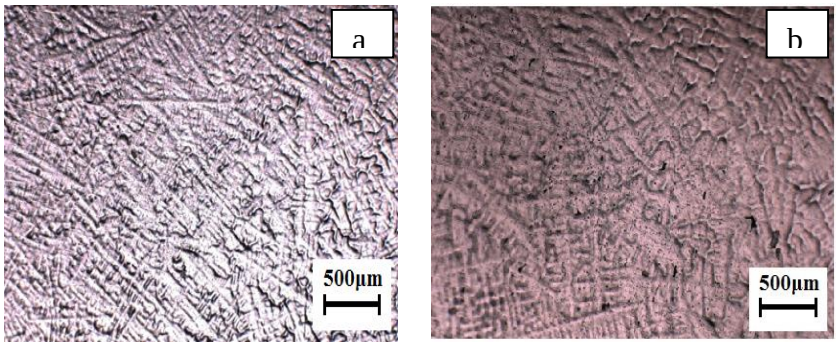

Fig. 3. *Optical microstructure of Ti-based alloy: a) 50 X, b) 100 X*

For the microstructure characterization of the studied alloy were acquired images secondary electron (SE) and backscatter (BSE) using detectors BSE (Backscattered Detector). Because metal samples were analyzed, the High Vacuum mode using a voltage of 20 kV was used.

The SEM images of the studied alloy confirm the acicular (dendritic) structure.

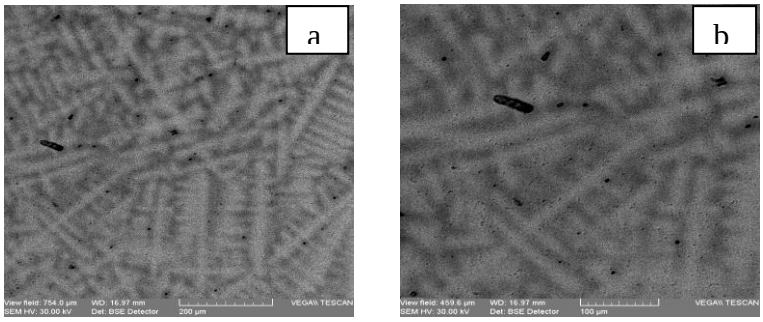

Fig. 4. *SEM image of Ti-based alloy: a) 300 X, b) 500 X*

The electron micrographs (Fig. 4) of the alloy show a biphasic structure, consisting of a high proportion of β solid solution, occurring a lamellar structures intragranulation peculiar to orthorhombic martensite α'', as shown in Fig. 3. The orthorhombic martensite α'' occurs frequently in the case of titanium base alloys which are found in β-stabilized transition metal category, in which Ta and Zr is included [15, 18].

4. Conclusions

An alloy was developed from the melting of the pure elements like Ti, Mo, Zr, Ta in an arc melting furnace.

The SEM analysis revealed surfaces without defects and the elements mapping showed a homogeneous distribution for all alloys.

Molybdenum, zirconium and tantalum alloying elements present an influence on the structure and microstructure of alloy, through the β- stabilizer action. The microstructure of the studied alloy presents an acicular structure with irregular grain boundaries, with a β phase. The XRD results present a predominant β phase and an α'' secondary phase shown in the Figure 2. Finally, we conclude that the presented alloy can be used for medical application.

References

[1]. D. M. Bombac, *et al.*, *Review of materials in medical applications*, Materials and Geoenvironment, 54, (4), p. 471-499, 2007.

[2]. M. G. Minciuna, P. Vizureanu, D. C. Achitei, N. Ghiban, A. V. Sandu, N. C. Forna, *Structural Characterization of Some CoCrMo Alloys with Medical Applications*, 65, (3), p. 335-338, 2014.

[3]. M. Niinomi, M. Nakai, J. Hieda, *Development of new metallic alloys for biomedical applications*, Acta Biomater, 8, p. 3888-3903, 2012.

[4]. C. Leyens, P. Manfred, *Titanium and titanium alloys: Fundamentals and Applications*, John Wiley & Sons, 2003.

[5]. N. T. C. Oliveira, G. Aleixo, R. Caram, A. C. Guastaldi, *Development of Ti-Mo alloys for biomedical applications: Microstructure and electrochemical characterization*, Materials Science and Engineering A, 452-453, p. 727-731, 2007.

[6]. L. C. Zhang, D. Klemm, J. Eckert, Y. L. Hao, T. B. Sercombe, *Manufacture by selective laser melting and mechanical behavior of a biomedical Ti-24Nb-4Zr-8Sn alloy*, Scr. Mater, 65, p. 21-24, 2011.

[7]. M. G. Minciuna, P. Vizureanu, V. Geanta, I. Voiculescu, A. V. Sandu, D. C. Achitei, A. M. Vitalariu, *Effect of Si on the Microstructure and Mechanical Properties of Biomedical CoCrMo Alloy*, Revista de chimie, 66(6), p. 891-894, 2015.

[8]. Y. L. Zhou, M. Niinomi, T. Akahori, *Effects of Ta content on Young's modulus and tensile properties of binary Ti-Ta alloys for biomedical applications*, Materials Science and Engineering A, 371, p. 283-290, 2004.

[9]. S. B. Gabriel, *et al.*, *Characterization of a new beta titanium alloy, Ti-12Mo-3Nb, for biomedical applications*, J. Alloys Compd., 536 (Suppl.1), p. S208-S210, 2012.

[10]. A. C. Bărbînță, R. Chelariu, M. Benchea, C. I. Crimu, S. Iacob Strugaru, C. Munteanu, *A comparative analysis of new Ti-Nb-Zr-Ta orthopedic alloys*, Advanced Materials Research, 837, p. 259-264, 2014.

[11]. ***, *ASM Handbook, Alloy Phase Diagrams*, vol. 3, p. 254.

[12]. ***, *ASM Handbook, Metallography and Microstructure*, vol. 9, p. 2157-2208.

[13]. I. C. Lupu, D. Agop-Forna, I. G. Sandu, C. Mocanu, *Microscopic Assessment of the Corrosion Resistance of some Superficially Enhanced Ti-Based Dental Alloys with Hidroxyapatite*, Revista de Chimie, 66 (6), p. 808-812, 2015.

[14]. Lutjering G., Williams J. C., *Titanium*, Springer-Verlag, Berlin, p. 289, 2003.

[15]. X. H. Min, S. Emura, L. Zhang, K. Tsuzaki, *Effect of Fe and Zr additions on ω phase formation in β-type Ti-Mo alloys*, Materials Science and Engineering A, 497, p. 74-78, 2008.

[16]. Oliveira N. T. C., Aleixo G., Caram R., Guastaldi A., *Development of Ti-Mo alloys for biomedical applications: Microstructure and electrochemical characterization*, Materials Science and Engineering A, 452-453, p. 727-731, 2007.

[17]. D. R. N. Correa, *et al.*, *Effect of substitution elements on the microstructure of the Ti-15Mo-Zr and Ti-15Zr-Mo system alloys*, J Mater Res Technol., 4(2), p. 180-185, 2015.

[18]. S. Ehteman Haghighi, H. B. Lu, C. Y. Jian, G. H. Cao, D. Habibi, L. C. Zhang, *Effect of α''martensite on the microstructure and mechanical properties of beta-type Ti-Fe-Ta alloys*, Materials and Design, 76, p. 47-54, 2015.

THE ANNALS OF "DUNAREA DE JOS" UNIVERSITY OF GALATI
FASCICLE IX. METALLURGY AND MATERIALS SCIENCE
Nº. 4 - 2015, ISSN 1453 – 083X

TREATMENT OF AMMONIA WASTEWATER BY ULTRASOUND. PART I: THE INFLUENCE OF THE ULTRASOUND ENERGY ON THE ULTRASOUND BATH TEMPERATURE

Nicoleta MATEI (CIOBOTARU)[1*], Dan SCARPETE[2]
[1]"Dunarea de Jos" University of Galati, Faculty of Engineering and Agronomy,
Calarasi Street, 29, RO-810017, Braila, Romania
[2]"Dunarea de Jos" University of Galati, Faculty of Engineering,
Domneasca Street, 47, RO-800008, Galati, Romania
[*]Corresponding author
e-mail: nicoleta.ciobotaru@ugal.ro

ABSTRACT

The industrial ammonia water decontamination depending on the sample temperature is monitored by this study. The treatment was conducted by the UP100S ultrasound generator (Hielscher Ultrasound Technology, Germany), operating at 30kHz frequency and acoustic power densities of 90 W/cm^2 and 460W/cm^2 respectively. The effect of sonication both on the bath temperature and ammonia removal, based on treatment time, is presented in this paper. Experiments were carried out according to different parameters, so as the sample temperature variation by ultrasonic treatment to be determined. Studied parameters were: the operating mode variation (continuous or intermittent), the additional aeration and the application of a cooling water serpentine. Based on the results, the ammonia removal efficiency is improved by the heating produced by the ultrasonic energy.

KEYWORDS: ultrasound, ammonia wastewater, acoustic cavitation, temperature, ammonia removal

1. Introduction

Among all the uses of power ultrasound, the treatment of wastewater containing toxic and complex pollutants, both from industrial and domestic sources, appears to be the most attractive field of study [1]. The advantages of this technology include the potential chemical-free and simultaneous oxidation, thermo-lysis, shear degradation, enhanced mass-transfer processes together [2].

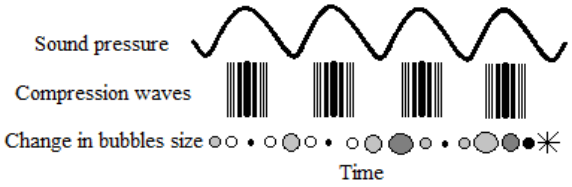

Fig. 1. *Compression and expansion cycle of ultrasound* [4]

The enhancement in the processing rates is mainly due to the fact that, when ultrasound is passed through a liquid medium, it can generate cavitation phenomena due to alternate compression and rarefaction cycles [3], as shown in Figure 1 [4]. The cavitation can be a suitable technology for the degradation of wastewater streams or, at the minimum, it can be used for lowering the toxicity levels of the effluent stream so that conventional biological oxidation can be readily applicable [5].

The ultrasonic cavitation concentrates the energy and, with the collapse of bubbles, the energy is released within a tiny area, which generates a very high local temperature (around 5000 °C) and pressure (in excess of 500 atm), forming the so-called 'hot spots', which will open up widespread new chemical reaction routes and abruptly accelerate the chemical reaction rate [6].

During the treatment process, an ultrasonic generator transforms the electrical energy into other kinds of energies, as shown in Figure 2.

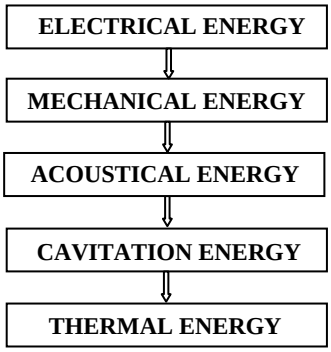

Fig. 2. *The energy transformation chain during ultrasonic treatment* [7]

In this work, the effect of the temperature rise due to the thermal energy emitted by the probe during sonication was assessed. The potential influence of the bulk phase temperature at ultrasonic treatment application and the optimum temperature range for different processes is discussed in many papers [8-15]. The thermal impact of continuously imploding cavitation bubbles on the surrounding liquid or sonicated matter itself depends on the physical properties of a sonication medium, such as vapor pressure or viscosity [16, 17], surface tension, gases dissolved and bulk temperature. According to many authors, the temperature increase of the sonicated liquid medium leads to an increase of the vapor pressure and a reduction of viscosity and surface tension [18-20]. With an increase in the vapor pressure of the liquid, the vapor content of the cavity increases thereby lowering the energy released during the cavitational collapse [18]. On the other hand, the reduction of viscosity and/or surface tension lowers the threshold intensity required to produce cavitation [19] and makes the effects temperature rise to be favorable. Increasing temperature results in reduction in acoustic cavitation threshold, meaning, the liquids cavitate at lower intensities [21]. Notwithstanding, Raman et al. explain that lower cavitation thresholds translate into the ease of cavity formation, thereby making higher temperatures more favorable for particle breakage [20].

The present study refers to the ammonia water decontamination by sonication and it is focused on the ultrasound influence on the heating occurring in the treated sample. This work is further continued by Part II, referring to the effect of ultrasound on ammonia removal. Considering that the separation of the ammonia-water mixture can be achieved by conventional distillation [22], heating appears to have a beneficial effect in ammonia removal. However, the separation performance is subject to the thermodynamic constraints of the system based on the volatility (boiling point) difference of the various substances (e.g., -33.4 °C for ammonia and 100 °C for water at atmospheric pressure) [22, 23].

2. Materials and methods

2.1. Wastewater Features

This research is conducted on ammonia water decontamination by ultrasonic treatment. Several activities generate high-strength ammonia wastewater including human waste, agricultural waste and industrial effluent [24].

The sample utilized in the current paper is generated in the ion exchangers chemical industry. By washing the ammonium gas, ammonia water results as residual water. In order to carry out experiments in normal laboratory conditions, appropriate dilutions of 1:1000 were applied to the effluent. The final concentration of the sample subjected to tests was of 72.840 mg/l ammonium and 56.597 mg/l ammonia nitrogen respectively, after dilution. The volume of the sample to be treated was set at 300 ml.

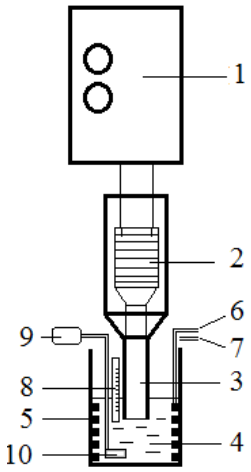

Fig. 3. *Schematic representation of experimental set-up*

The temperature increase was measured at room temperature by using a thermometer, which was immersed and held at the half height of the sonicated sample of ammonia water.

2.2. Experimental Set-Up

The schematic representation of the ultrasonic setup designed for the treatment of industrial ammonia water is shown in Figure 3, where: 1-electronic generator; 2-electromechanical transducer; 3-probe; 4-vessel containing ammonia water sample; 5-water cooling coil; 6, 7-hoses for cooling water in

and out; 8-thermometer; 9-aeration pump; 10-air stone.

The electric energy produced by the piezoelectric type generator 1 is converted to mechanical energy by transducer 2, further converted into acoustic energy in the form of ultrasonic waves transmitted through probe 3 to the ammonia water sample from vessel 4. This energy causes physical and chemical effects in the liquid medium to be treated and it is finally converted into heat.

In order to highlight both the effect of sonication and the effect of heating that occurs during the treatment process, the cooling water coil 5 was sunk in the vessel 4. The cooling water was taken from the current water source by hose 6 and the used water was directed to a sink by the drain hose 7. Experimental tests have been carried out both with and without water cooling coil. Ammonia water temperature is constantly monitored by the thermometer 8 immersed in the ammonia wastewater sample. To create the effect of bubbling, or the additional oxygen diffusion into the liquid, the aeration pump 9, fitted with air stone 10 (having the role of a fine spray air bubbles) were used.

The ultrasonic processor UP100H, Hielscher Ultrasonics GmbH, Teltow, Germany, was utilized to conduct the experiments. The generator is working at a 30 kHz fixed frequency, with the possibility to adjust the amplitude of the oscillating system. The amplitudes used in the treatment process were the maximum amplitudes working with each of the used probe (70 and 180 μm, respectively). Also, to each probe a different acoustic power density (ultrasonic intensity) corresponds, as follows:

- Probe MS 3 (3 mm diameter): 460 W/cm^2;
- Probe MS 10 (10 mm diameter): 90 W/cm^2.

The maximum depth to which the probe was immersed in the tested liquid was 30 mm.

3. Results and discussion

For both acoustic intensities of the ultrasonic piezoelectric generator, various ways of temperature variation were registered. In the following, the dynamics of the temperature during sonication is discussed depending on the working parameters (with or without additional aeration, in either continuous or intermittent operation and depending on whether the cooling water coil is applied). Temperature values were read every 5 to 5 minutes for 60 minutes by the thermometer immersed in the solution. The constant value of temperature was noted after an hour of treatment, which is explained by the dynamic thermal equilibrium conditions of permanent transfers of heat between the treated ammonia water and the ambient air.

The initial temperature at which the readings started could vary by experiment, due to the ambient temperature of the laboratory, which was constantly monitored. However, of primary interest is the dynamics of temperature rise and the registered upper limit.

3.1. Thermal effect at higher acoustic intensity

Fig. 4 shows the dynamics of temperature depending on the operating mode (continuous or intermittent) and the additional aeration at higher acoustic intensity.

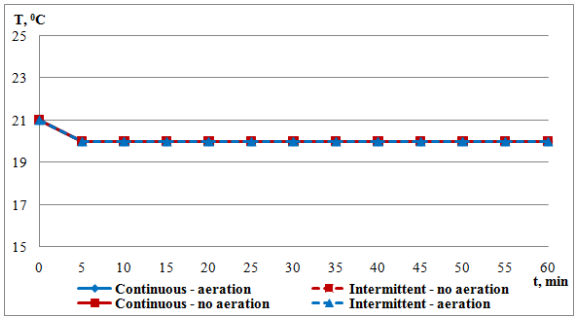

Fig. 4. *Dynamics of temperature at 460 W/cm^2 acoustic intensity*

The ultrasonic power of 460 W/cm^2 generates the temperature raise in the treated sample, up to a maximum constant at 34 °C, after 50 minutes, in continuous operation without additional aeration.

At additional aeration, the sample temperature reaches a maximum of 33 °C after 55 minutes, due to the air generated to the working vessel by the aeration pump attached to the set-up designed for the treatment of industrial ammonia water.

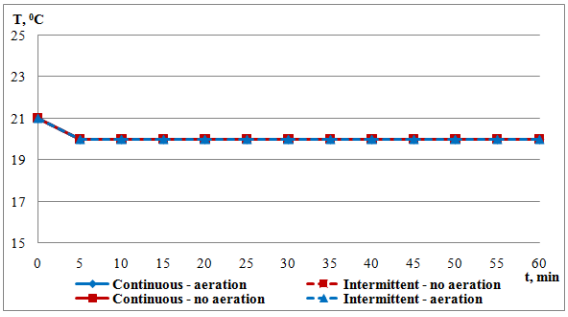

Fig. 5. *Dynamics of temperature at 460 W/cm^2 acoustic intensity by cooling water coil*

In the case of intermittent operation of 0.5 seconds, the temperature of the sample reaches 28 °C after 45 minutes, without aeration or 27 °C after 50 minutes with additional aeration.

Considering the role of maintaining the sample of treated water at a constant temperature, the applications where the cooling water coil was utilized recorded a decrease of 1 °C compared to the initial temperature of the water, according to Figure 5. This water temperature evolution was recorded when using the MS 3 probe in both continuous and intermittent operation. Additional aeration does not affect the studied water temperature.

3.2. Thermal effect at lower acoustic intensity

When the ultrasonic treatment is conducted at an acoustic power density of 90 W/cm^2, the sample heating is remarkable. The maximum constant value of 60 °C is reached after 60 minutes of continuous mode treatment, both with and without additional aeration. Intermittent operation of the ultrasonic irradiation generates a constant upper limit of 46 °C after 50 minutes without additional aeration or after 55 minutes with aeration applied (Figure 6).

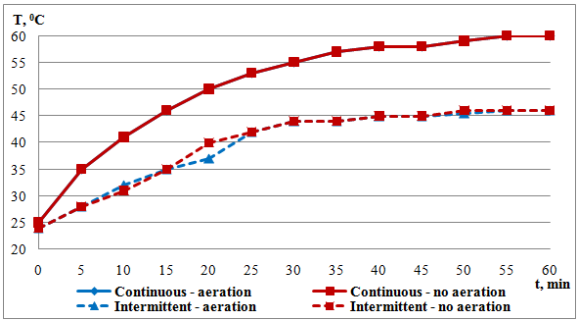

Fig. 6. *Dynamics of temperature at 90 W/cm^2 acoustic intensity*

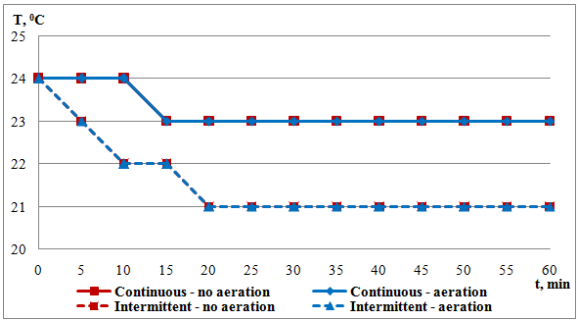

Fig. 7. *Dynamics of temperature at 90 W/cm^2 acoustic intensity by cooling water coil*

Figure 7 shows the effects on temperature when using the cooling water coil for the treatment with MS 10 probe. In intermittent operation, there is a temperature drop of 3 °C in the first 20 minutes of ultrasound treatment, followed by a temperature maintaining to the value equal to the cooling water temperature throughout the treatment period.

In the continuous mode, the temperature remains constant, but the cooling is provided only with 1 °C, due to a much higher heating trend of the sample.

Any additional aeration has no influence on the studied water temperature.

In the second part of the study, complete results obtained in the treatment of ammonia water with a detailed discussion will be presented. Some of the objectives can be summarized as follows:

- The thermal effect in ammonia removal by ultrasonic technique is intended. In order to determine both effects of ultrasonic irradiation with heating and without heating on elimination rate, the experiments will be conducted by the addition of the cooling water coil.

- The removal efficiency according to allowable discharge limits (to natural water courses or public sewerage networks) will be determined.

4. Conclusions

The entire study refers to the determination of the optimum removal of ammonia from industrial ammonia wastewaters. In this part of the study, the influence of the acoustic power density on the liquid medium temperature by sonication was determined.

At higher ultrasonic intensity (460 W/cm^2) the temperature rise is recording an upper limit of 34 °C in 60 minutes of treatment. The lower studied ultrasonic intensity (90 W/cm^2) generates higher temperature rise rates of 60 °C after 60 minutes of treatment.

The beneficial effect of heating on the elimination of ammonia from liquid mediums is already known. However, to strictly observe the effect of ultrasonic treatment without additional heating effect, a cooling water coil to maintain a constant sample temperature was applied to the treatment setup.

Acknowledgements

The work has been funded by the Sectorial Operational Programme Human Resources Development 2007-2013 of the Ministry of European Funds through the Financial Agreement POSDRU/ 159/1.5/S/132397.

References

[1]. P. R. Gogate *et al.*, *Sonochemical reactors for waste water treatment: comparison using formic acid degradation as a model reaction*, Advances in Environmental Research, 7, p. 283-299, 2003.

[2]. M. Matouq *et al.*, *The kinetic of dyes degradation resulted from food industry in wastewater using high frequency of ultrasound*, Separation and Purification Technology, 135, p. 42-47, 2014.
[3]. V. S. Sutkar *et al.*, *Theoretical prediction of cavitational activity distribution in sonochemical reactors*, Chemical Engineering Journal, 158, p. 290-295, 2010.
[4]. A. Mahvi, *Application of Ultrasonic Technology for Water and Wastewater Treatment*, Iranian J Publ Health, 38, p. 1-17, 2009.
[5]. P. R. Gogate, *Treatment of wastewater streams containing phenolic compounds using hybrid techniques based on cavitation: A review of the current status and the way forward*, Ultrasonics Sonochemistry, 15, p. 1-15, 2008.
[6]. J. Huang *et al.*, *Low-MHz frequency effect on a sonochemical reaction determined by an electrical method*, Ultrasonics Sonochemistry, 2, p. S93-S97, 1995.
[7]. Z. Kobus *et al.*, *Influence of physical properties of liquid on acoustic power of ultrasonic processor*, TEKA Kom. Mot. Energ. Roln. – OL PAN, 8a, p. 71-78, 2008.
[8]. V. A. Lemos *et al.*, *Ultrasound-assisted temperature-controlled ionic liquid microextraction for the preconcentration and determination of cadmium content in mussel samples*, Food Control, 50, p. 901-906, 2015.
[9]. S. Rochebrochard *et al.*, *Sonochemical efficiency dependence on liquid height and frequency in an improved sonochemical reactor*, Ultrasonics Sonochemistry, 19, p. 280-285, 2012.
[10]. M. Plesset, *Temperature effects in cavitation damage*, Journal of Basic Engineering, 94, p. 559-566, 1972.
[11]. S. Hattori *et al.*, *Influence of air content and vapor pressure of liquids on cavitation erosion*, Trans. JSME, 68 B, p. 130-136, 2002.
[12]. S. Hattori *et al.*, *Influence of temperature on erosion by a cavitating liquid jet*, Wear, 260, p. 1217-1223, 2006.
[13]. B. Ondruschka *et al.*, *Ultrasound in environmental engineering*, TUHH Reports on Sanitary Engineering, p. 139, 1999.
[14]. H. Destaillats *et al.*, *Applications of ultrasound in NAPL remediation: sonochemical degradation of TCE in aqueous surfactant solutions*, Environ. Sci. Technol., 35, p. 3019-3024, 2001.
[15]. L. Wenjun *et al.*, *Removal of Organic Matter and Ammonia Nitrogen in Azodicarbonamide Wastewater by a Combination of Power Ultrasound Radiation and Hydrogen Peroxide*, Chinese Journal of Chemical Engineering, 20, p. 754-759, 2012.
[16]. P. V. Cherepanov *et al.*, *Up to which temperature ultrasound can heat the particle?* Ultrasonics Sonochemistry, 26, p. 9-14, 2015.
[17]. M. Ashokkumar *et al.*, *Sonochemistry*, in: Kirk-Othmer Encyclopedia of Chemical Technology, John Wiley & Sons, 2007.
[18]. P. R. Gogate *et al.*, *Sonochemical reactors: Important design and scale up considerations with a special emphasis on heterogeneous systems*, Chemical Engineering Journal, 166, p. 1066-1082, 2011.
[19]. M. Goel *et al.*, *Sonochemical decomposition of volatile and non-volatile organic compounds-A comparative study*, Water Research, 38, p. 4247-4261, 2004.
[20]. V. Raman *et al.*, *Experimental investigations on ultrasound mediated particle breakage*, Ultrasonics Sonochemistry, 15, p. 55-64, 2008.
[21]. T. Mason *et al.*, *Applied Sonochemistry: The Uses of Power Ultrasound in Chemistry and Processing*, Wiley-VCH Verlag GmbH and Co. KGaA, 2002.
[22]. X. Yang *et al.*, *A Pervaporation Study of Ammonia Solutions Using Molecular Sieve Silica Membranes*, Membranes, 4, p. 40-54, 2014.
[23]. Y. A. Cengel *et al.*, *Thermodynamics: An Engineering Approach*, Mcgraw-Hill College: New York, USA, ISBN-13: 978-0073398174, 2011.
[24]. S. H. Mirhossaini *et al.*, *Effect of influent COD on biological ammonia removal efficiency*, International Journal of Environmental, Chemical, Ecological, Geological and Geophysical Engineering, 4, p. 86-88, 2010.

THE ANNALS OF "DUNAREA DE JOS" UNIVERSITY OF GALATI
FASCICLE IX. METALLURGY AND MATERIALS SCIENCE
Nº. 4 - 2015, ISSN 1453 – 083X

URBAN POLLUTION ISSUES GENERATED BY TRAMS TRAFFIC

Adrian LEOPA, Diana ANGHELACHE
"Dunarea de Jos" University of Galati,
Engineering and Agronomy Faculty of Braila
e-mail: adrian.leopa@ugal.ro

ABSTRACT

The modern society development involves new and diverse issues considering urban environmental pollution. Traffic generated sound and vibration are two up-to-date urban environmental pollution causes besides air and water pollution ones. Public transportation in metropolitan areas is a major and constant all levels environmental pollution cause. Electric engines as an alternative to internal combustion ones could reduce the air pollution caused by urban public transportation. The tram network is an important element of this approach even if a poor condition of tram network elements could be a major cause of sound and vibration environmental pollution. This research paper is a study of a particular case considering the vibration level transmitted to a building close to tram network in the town of Braila City.

KEYWORDS: urban, pollution, vibration, tram

In this century of speed, the tram, as a part of public transportation, generates few environmental and economic problems. For instance, it requires expensive runways and power networks, low speed and a high weight. For example, the Imperio model produced by SC Astra vagoane Arad, Romania, can be purchased for 1.7 million Euros despite the above mentioned drawbacks as well as acoustic and vibration pollution.

Having said the low maintenance costs and high exploitation durability, this type of public transportation does not pollute the environment as much as internal combustion engines do.

Due to the increase of registered vehicles, the use of trams has become a compulsory necessity regarding the pollution of the atmosphere.

In Romania, immediately after the early beginning of the 2008 financial crisis, the car park has been keeping its increasing tendency, but at a slower rate.

As a result, between 2010 and 2014, it increased by 777 547 vehicles.

The city of Braila had its auto park expanded by a number of 13079 cars, in the 2010-2014 period, reported to the 180 000 inhabitants. A natural consequence of the increased number of vehicles is the pollution emphases caused by the gases released by the internal combustion engine [1].

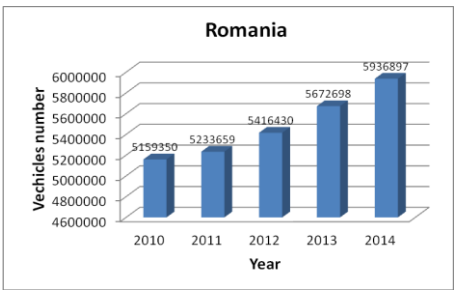

Fig. 1. *Evolution of the number of vehicles in Romania*

Even if some vehicles are provided with catalysts, they start functioning at an optimum level after a certain time, when they reach at least 400 ºC, which is equal to driving for nearly 10 km.

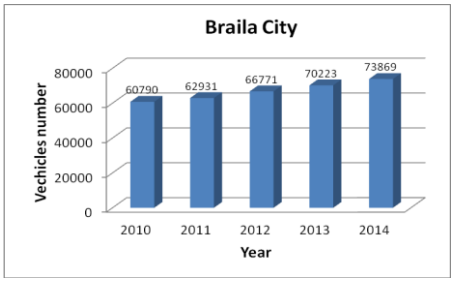

Fig. 2. *Evolution of the number of vehicles in Braila City*

2. The effects of the trams on buildings and their inhabitants

Usually, when both the driving way and the tram do not have defects of intense usage or accident, this type of transportation must not produce polluting vibrations. Otherwise, the vibrations generated by the functioning tram may have undesirable effects on nearby buildings, their tenants and technical equipment, as well. As for the buildings placed in the propagated vibration area, it can result in the defacement of the construction elements, such as unequal settlements or even a reduced level of structure stability. The same phenomenon may induce to the inhabitants of those buildings tiredness which leads to various pathologies or may have bad effects on the proper functioning of electronic equipment which require a high performance level [2, 3, 4]. There are legal notices which enforce the maximum values to vibration parameters for the nearby buildings, to avoid negative effects produced by trams' traffic.

In Romania, the laws and regulations in the field consider the SR12025-2-94 as the standard, which mention the legal limit for vibrations generated by the road traffic and transmitted to buildings or to certain parts of them.

2.1. Building presentation

For inhabited buildings or socio-cultural ones, using them properly can be reached by providing structural entirety and inside comfort. The assessment of these two desires can be achieved by predictive maintenance activities which consists of periodic checks of the vibration parameter values for buildings in imposed limits by the regulations.

Fig. 3. *The building located near tram line: 1 - residential building; 2 - road* [5]

Through the current study, the vibration parameters which are generated by the trams' traffic transmitted to a block of flats from Brăila city were quantified experimentally, with a view to examining these values in order to compare them to the permitted quota.

The building monitored throughout this experimental study is placed on the Independence Boulevard in Braila, at a 9 meters' distance from the drive way of the tram of the Radu Negru-Vidin route.

The block of flats is built on two floors, semi-basement and a story, its structure being made out of brick.

2.2. The system of measurement devices

The assessment of the vibration level originated in the trams' traffic was realized using the following equipment:

- acquisition and processing system with PCeight-channel acquisition board HARMONIE Octav - Sinus Messtechnik GmbH;
- two piezoelectric seismic accelerometers, type 393B04 - PCB;
- required connectors.

a. floor

b. semibasement

Fig. 4. *Accelerometer location on the first and second floor, on the external wall, parallel to the tram rails*

Experimental measurements were carried out with two vertically placed accelerometers, at the same time, on different building elements, as follows:

- simultaneous positioning on two levels;
- two floors simultaneous positioning on the wall, parallel to the road;
- two floors simultaneous positioning on the wall, perpendicular to the road;

a. floor

b. semibasement

Fig. 5. *Accelerometer location on the first and second floor*

a. floor b. semibasement

Fig. 6. *Accelerometer location on the first and second floor, on the external wall, perpendicular to the tram rails*

In order to determine the level of vibration absorbed by each building element, seven sets of signal acceleration were recorded and processed using the MATLAB R14, [6, 7]. A spectral analysis of the acquired acceleration signals was performed to identify the significant frequencies and to determine their parameter levels.

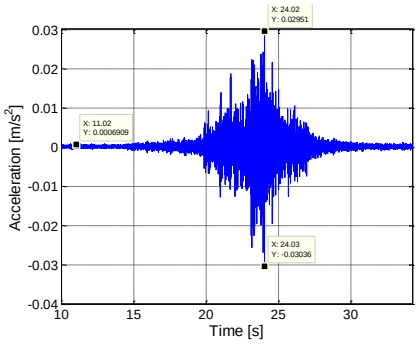

a. floor

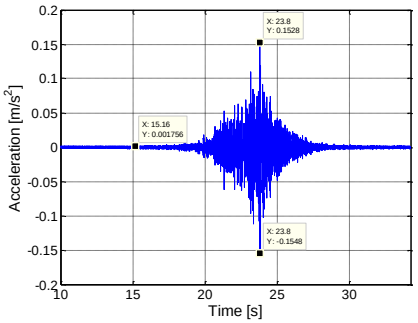

b. semibasement

Fig. 7. *Acceleration signals from exterior wall accelerometer, parallel to the tram line*

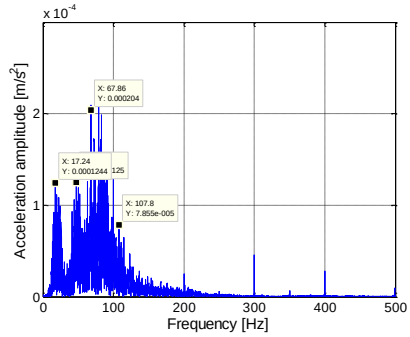

a. floor

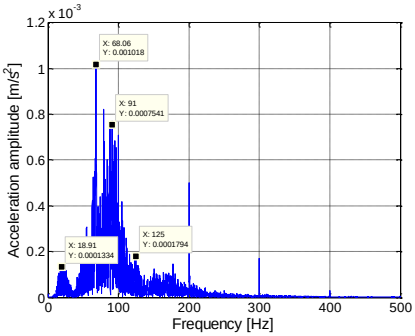

b. semibasement

Fig. 8. *Graphic presentation of the spectral accelerometer acceleration signals from exterior wall, parallel to the tram line*

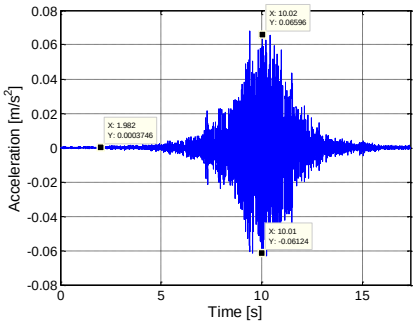

a. floor

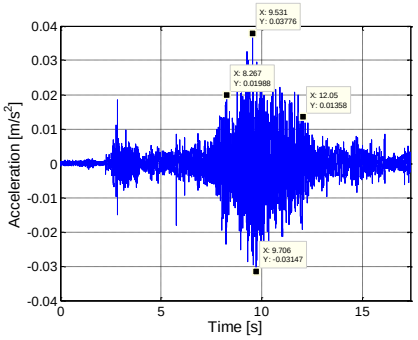

b. semibasement

Fig. 9. *Acceleration signals considering accelerometer floor location*

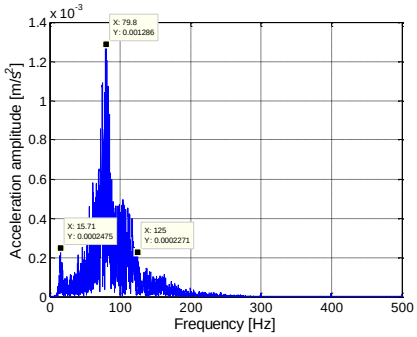

a. floor

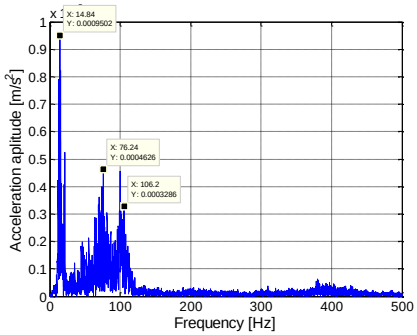

b. semibasement

Fig. 10. *Graphic presentation of the spectral acceleration for accelerometer location on floors*

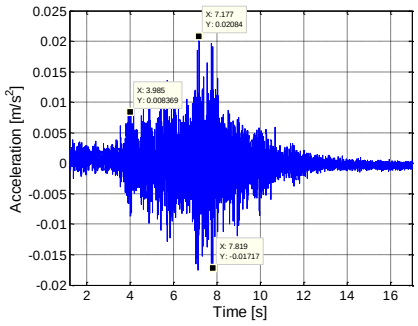

a. floor

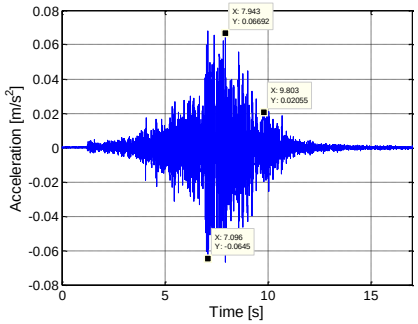

b. semibasement

Fig. 11. *Accelerometer acceleration signals from exterior wall, perpendicular to the tram line*

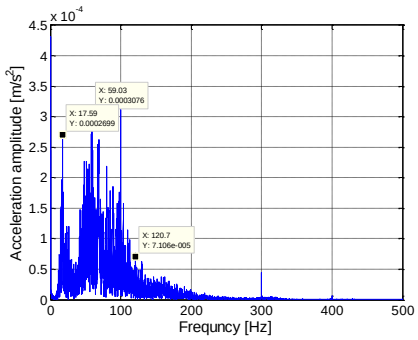

a. floor

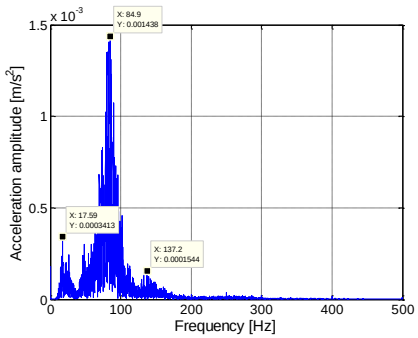

b. semibasement

Fig. 12. *Graphic presentation of the spectral acceleration signals for accelerometers on the outer wall, perpendicular to the tram line*

3.3. Final evaluation

To assess the harmfulness of the tram traffic induced vibrations, the following parameters were calculated: the vibration intensity, the acceleration level and vibration strength [3, 8, 9].

To assess the comfort of the building occupants, the vibration acceleration values (according to SR 12025/94) were used for vibration levels being reported to 80 equal curve physiologically tolerable level (A_V^Z), corresponding to residential buildings. According to Table 1, some values (red) stand out. They are located above the curve 80, especially for low frequencies vibration, but under the 92 curve, corresponding to commercial buildings.

In order to evaluate the effect of vibration on the structure of the building, the vibration strength levels were compared to allowable values recommended in the literature [2]. One single value, which is classified as a mild tremor, exceeded the vibration strength levels for the wall that paralleled the tram rails.

Table 1. *Vibration parameters on residential buildings*

Accelerometers positioned	Recording	Level	Acceleration peak [m/s^2]	Frequency [Hz]	Vibration intensity [cm^2/s^3]	Acceleration level [dB]	Vibration strength [vibrar]
A.Accelerometer location on the first and second floor, on the external wall, parallel to the tram rails	**Recording 2**	semibasement	0.016	15	0.17	84.08	2.32
		floor	0.091	81	1.02	99.18	10.09
	Recording 3	semibasement	0.029	67	0.12	89.24	0.98
		floor	0.15	66	3.40	103.52	15.32
	Recording 4	semibasement	0.02	14	0.28	86.02	4.55
		floor	0.077	66	0.89	97.72	9.53
B.Accelerometer location on the first and second floors	**Recording 5**	semibasement	0.065	79.8	0.52	96.25	7.23
		floor	0.038	14	1.03	91.59	10.13
	Recording 6	semibasement	0.044	79.7	0.24	92.86	3.85
		floor	0.03	14	0.64	89.54	8.08
C.Accelerometer location on the first and second floors, on the external wall, perpendicular to the tram rails	**Recording 7**	semibasement	0.013	16	0.10	82.27	0.23
		floor	0.029	63	0.13	89.24	1.25
	Recording 8	semibasement	0.02	17	0.23	86.02	3.71
		floor	0.066	64	0.68	96.39	8.32

4. Conclusions and outlook

The assessment of the tram traffic vibration level on residential buildings is a necessity imposed by the requirements of indoor comfort for residents and ensures the structural integrity of the building.

Experimental measurements showed an excess of vibration level that did not affect the residents. There was a single case of vibration which can be classified as a light one. We can consider that currently the vibrations are not a major stress factor for inhabitants or an imminent threat to the structural integrity of the building, due to reduced traffic (one tram at every 10 or 15 minutes).

The application of predictive maintenance has to be considered. It requires regular assessment of the level of trams traffic vibration on buildings as a method of evaluation for normal operation and tread.

Several solutions can be implemented to reduce or even eliminate the effects of vibration from trams traffic on nearby buildings:

- rehabilitation by replacing the tread rubber damping elements installed under tram tracks. The viscoelastic proprieties of the rubber vary with time. After 15 years, the rubber „is getting old", losing its initial properties;
- replacing the old trams;
- insulating the base of nearby buildings. This is an approach for new buildings (too expensive for old ones).

References

[1]. ***, http://www.drpciv.ro/.
[2]. Bratu P., *Monitorizarea în timp real a vibraţiilor transmise de sursele industriale cu efect asupra omului şi a mediului construit*, Simpozion AGIR, 2007.
[3]. Buzdugan Gh., *Izolarea antivibratorie a maşinilor*, Ed Academiei Republicii Socialiste România 1980.

[4]. Buzdugan Gh., *Izolarea antivibratorie*, Bucureşti, Editura Academiei Române, 1993.
[5]. ***, *Harta 3D a municipiului Braila*, http://www.harta3d.ro/harta-satelit-braila.html.
[6]. Ghinea M., Fireteanu V., *Matlab - Calcul numeric, grafica, aplicatii*, Teora Publishing House, Romania, 2003.
[7]. Gilat A., *MATLAB: An Introduction with Applications 2nd Edition*, Wiley edition, 2004.
[8]. Bratu P., *Vibratiile sistemelor elastice*, Editura Tehnică Bucuresti, ISBN 973-31-1418-9, 1999.
[9]. Pei Q., Tao X., Xue Z., *Study on Environmental Vibration Induced by Urban Rail Transit in Urban Area of the Near Buildings*, Proceedings of the 8th International Conference on Structural Dynamics, EURODYN 2011 Leuven, Belgium, 4-6 July 2011.

THE ANNALS OF "DUNAREA DE JOS" UNIVERSITY OF GALATI
FASCICLE IX. METALLURGY AND MATERIALS SCIENCE
Nº. 4 - 2015, ISSN 1453 – 083X

ENVIRONMENTAL RISK ASSESSMENT FOR THERMAL POWER PLANTS

Tamara RADU
"Dunarea de Jos" University of Galati, Romania
e-mail: tradu@ugal.ro

ABSTRACT

Thermal power plants still represent an important source of energy both in Romania and in Europe. Risks on the environment are primarily generated by the noxae generated from combustion of fossil fuels, namely: noxious gases (CO_2, CO, NO_x, SO_x), particulate, heavy metals (As, Cd, Cr, Cu, Ni, Pb), CH_4, polycyclic aromatic hydrocarbons (PAHs), dioxins and furans. All these pollutants plus the slag and the ash resulting from the combustion of fuels have, in time, a significant environmental impact. The environmental hazards caused by these emissions are analyzed in this paper depending on the gravity of the consequences and likelihood of occurrence. It shows the risk analysis, the risk matrix and treating and monitoring to identified risks.

KEYWORDS: hazards, risk analysis, risk matrix, management

1. Introduction

After a several-decade descendant trend, the use of coal for energy is rising again. Coal is still an important energy source in Europe, covering about a quarter of the electricity production [1].

Thermal Power Plants (TPP) are producing electricity by converting thermal energy resulting from the combustion of fossil fuels such as coal, fuel, oil and natural gas. The combustion of fossil fuel in large combustion plants such as those for TPP generate CO_2, present in variable proportions and SO_2, SO_3, NO_X and in smaller quantities heavy metals, halogenated compounds, dioxins and furans [2]. All these pollutants plus the slag and the ash resulting out of fuels combustion have a significant environmental impact in time.

Romania, the same as Germany are on second place in the top of pollution generated by thermal power plants on coal. To reduce the environmental impact, both at European and national level, series of regulations to limit emissions of certain pollutants from these large combustion installations were adopted.

The main pollutants emitted in the air by TPPs are those resulting from the combustion of fuels: huila /lignite and natural gas or fuel oil [3, 4]. The pollutants specific of the combustion in boilers are: noxious gases (CO_2, CO, NO_x, SO_x), particulate matter, heavy metals (As, Cd, Cr, Cu, Ni, Pb), CH_4, polycyclic aromatic hydrocarbons (PAHs), dioxins and furans [5].

The most likely way of transfer of the pollutants to receptors is through air, an environmental factor that favors a fast transport and direct contamination by inhalation. In this manner, employees are affected by pollutants present in the atmosphere of the workplace, from diffuse sources and in high concentrations. Also in this way, the population and ecosystems in the vicinity of TPP come in contact with gaseous and particulate pollutants specific to the processes, resulting out of controlled sources and diffuse sources, but in smaller concentrations, after having undergone a prior dilution in the atmosphere.

The main sources of *air pollution* are:

- emissions of SO_2, NO_x, particulates and CO_2;
- coal dust originated from the deposits solid fuel (coal), which has an action zonal;
- dust arising from deposits (dumps) of ash and slag through deflation, when these particles are shattered by the wind and entrained into the atmosphere.

The pollutants emissions (E) are influenced by the quality of fuels (coal, fuel oil, natural gas).

The methodology for calculating the quantity of those emissions is based on fuel consumption (B), caloric power of the fuel (C) and emission factors (e) [2]:

$$E[Kg] = B \times C \times e \quad (1)$$

The water required for the technological steam production in thermal circuit of the TPP and for fires extinguishing is collected and treated (softened, demineralized and deferrized).

The rainwater polluted with oil products resulting from the site of the fuel oil deposit are collected through the sewage system and transported to an oil separator then discharged in the pluvial and technological drainage system.

The soil can be affected by deposition of particulates and action of heavy metals resulting out of combustion of coal. The main waste materials derived from the combustion of fuels solid (coal) at the TPPs are the slag (15%) and the ash (85%) [5].

The slag-ash mixture, coming from electrofilters and water is called hydro-mixture and it is discharged into specially designed storage (dump).

Slag-ash dumps cause pollution of the atmosphere and soil through slag-ash drifting. Soil monitoring is performed periodically (usually annually).

2. Environmental risk assessment

2.1. Analysis of the impact on the environment

Water pollution [6], air pollution and disposal of wastes have a significant impact on biotic factors. The dispersion in atmosphere of CO_2, SO_2, of particulates [7] and toxic VOCs and the dissolving in water and passing in soil of pollutants is a permanent source of risk to living organisms.

The particulate matter resulted from the coal deposit and into processes or the dust shattered on the slag dump may reduce the intensity of the chlorophyll assimilation by reducing light radiation. Depositions of suspensions on leaves is causing the stomata blockage affecting photosynthesis and plant regime of gas exchange with effects such as: reducing the rate of development, lower production and decreased quality of production. Dusts with content of heavy metals can indirectly affect plants growth by depositing on soil which modifies the nutrients transformation processes of the plants.

Sulfur oxides emitted to the atmosphere come in contact with rain water resulting in acid rain (dilute solution of sulfuric acid and sulfur dioxide) that cause adverse effects [2, 5] on the environment, such as:

- vegetation damage, especially of the coniferous forests, through direct destruction of chlorophyll;
- acidification of soils and deficiencies in plant nutrition by dissolving the salts of calcium and magnesium in the soil;
- dissolving of the waxy protective layer of the leaves, the plants becoming less resistant to pests;
- over-fertilizing the soil resulting in premature accelerated of plants growth;
- acidification of lakes and damage ichtyofauna.

Depending on the degree of exposure, SO_2 can lead to physiological and biochemical effects such as: reducing photosynthesis, chlorophyll degradation, changes in the metabolism of proteins, lipids and enzyme balance activity. These effects translate into necrosis, plant growth reduction, increased susceptibility to various pathogens and at the severe climatic conditions.

Sulphur oxides have negative effects on human health, causing irritation or respiratory problems [8].

Polycyclic aromatic hydrocarbons (PAHs) are carcinogenic at long exposure time, even at very low concentrations. Short-term exposures to PAHs may cause skin and upper respiratory tract irritation, dizziness, nausea, headaches, weakness. Very high doses can lead to respiratory collapse and liver damage, damage of lungs, kidneys and blood system. Long-term exposure can also lead to cancer and damage of the liver, kidneys, lungs and blood and lymph systems. The simultaneous presence of SO_2 exacerbates these effects.

The forming of nitrogen oxides the fuels combustion and in function of combustion conditions NO or NO_2 may result. NO quickly turns into NO_2 in the atmosphere, a gas with irritating smell and strong oxidant. NO_2 is a precursor to ozone forming. By reaction with the water in the atmosphere, a portion of the NO_2 is converted into nitric acid (HNO_2 and HNO_3). In urban areas these acids are combined with ammonia to form ammonium nitrate (NH_4NO_3). Ammonium nitrate is found as aerosols contributed significantly to pollution of urban areas with particulate matter (having dimensions of 2.5-10 μm).

Human health is affected directly by nitrogen oxides through exposure to NO_x and indirectly through the formation of secondary pollutants such as ozone and the atmospheric aerosols contributing to photochemical mist and particulate matter [8, 9]. Nitrogen oxides (NO_x) have a beneficial effect on the plants up to a certain concentrations contributing to plants growth. Over toxic thresholds NO_x has a clear phytotoxic action, such as reducing photosynthesis and transpiration, chlorosis and necrosis. NO_x and SO_2 have a synergistic effect on the plants, only these two pollutants or in combination with the ozone. The effects of acidic rainwater containing NO_x and SO_2 may affect plants and ecosystems situated at a great distance from the emission source.

Ozone (O_3) is formed in the atmosphere by photochemical reaction of NO_x and solar radiation, favored by a wide spectrum of volatile organic compounds (VOCs) into the atmosphere. Both

pollutants, NO_x and VOCs, are specific of combustion processes, so it is expected that ozone to be present in the atmosphere in the vicinity and inside thermal power plants. Ozone is a strong oxidant and therefore can react with each class of biological substances. Long-term exposure leads to chronic diseases of the upper respiratory tract and ischemic heart disease [10]. Ozone affects crop plants and trees, especially species that have a long growth / development cycle, causing visible alterations as defoliation and foliage changes. It can have effects both on plant species and on biodiversity of ecosystems natural.

Volatile organic compounds (VOC) are pollutants commonly found in any combustion process, as a result of incomplete combustion. The effects of these compounds on human health are related to their presence in the atmosphere in natural state or transformed. These are substances with high toxicity and potential risk of cancer.

Dioxins and furans - PCDD / F are organic compounds unintentionally produced in very low concentrations in emissions or in products of some processes. They have very high and variable toxicity with a potential hazard to the environment and people. Main emission source is represented by the combustion processes. To evaluate the toxicity of these substances the European reference standards recommended the toxic equivalent (TEQ) [11, 12]. This value is used to evaluate the health risk of those exposed to these emissions. Numerous harmful effects of dioxins and furans on human health have been demonstrated. These are characterized as destructive substances for the endocrine system, causing fertility problems, pregnancy problems and even infertility.

Water pollutants (phenols, ammonia, heavy metals, petroleum products) can affect the life and activity of aquatic ecosystems, having the effect of a quantitative reduction [13].

Radioactivity. The main source of radioactivity is coal, which may contain: U-238, Th-232 and K-40 [6]. By the burning of coals, the natural radioactive substances present in their composition are concentrating in slag and ash, and radioactivity increases. Even if the amount of radioactive elements is large, considering that the distribution in the slag dump is homogeneous, the effect of irradiation "in situ" is not usually higher than the allowable limits. The radiological risk should not be ignored; the cumulative effects can be adverse on biotic factors.

The noise. In relation to the frequency, duration, moment of production of the different noises and propagation conditions (wind direction) employees and neighboring populations may be affected. Among the frequent manifestations due to noise exposure, hearing fatigue, hearing loss and professional deafness are included.

2.2. Analysis of identified environmental hazards

The flammable materials used or resulted from processes, the toxic or corrosive materials, handled, used or generated in processes, diffuse emissions, action cumulative and synergistic of the pollutants and the noise of installations and of the aggregates, can create problems for the personnel safety and environment.

In a thermal power plant, places with high pollution potential (risk) are:

- the chemical treatment station;
- the boilers-steam power station;
- the solid fuel station.

Principal risk factors are:

- chemical risk factors (CO, CO_2, SO_2, VOC, dioxins and furans);
- physical risk factors: noise, microclimate, radioactivity, electric and magnetic fields;
- physico-chemical pollutants: diverse particulate (coal dust, slag, ash).

The usage of fuels (coal, gas, fuel oil, diesel, coal dust) has a high potential risk of fire and explosion, and poisoning with CO.

Potential hazards for environmental factors are:

P1 - the emission, transport and dispersion of SO_2 in the air over the accepted norms;

P2 - the emergence of acid rain caused by SO_2, SO_3 by reaction with rainwater;

P3 - CO_2 emissions with major influence on climate change;

P4 - NO_x emissions over the accepted norms;

P5 - formation, due to NO_2, of the nitric acid and the ammonium nitrate aerosols;

P6 - formation of the ozone; having as precursor of NO_2;

P7 - emissions diffuse / fugitive of CO;

P8 - emissions diffuse / fugitive of dioxins and furans;

P9 - soil pollution in the slag dump;

P10 - Soil pollution by coal dust in the storage of raw materials;

P11 - Soil pollution by oil products;

P12 - pollution of groundwater;

P13 - pollution by wastewater;

P14 - fly ash;

P15 - slag and ash particles shattered of the air currents;

P16 - radioactive slag and ash;

P17 - transfer and dispersion of pollutants in aquatic environments;

P18 - noise pollution;

P19 - production of the fires;

P20 - production of the explosions.

2.3. Risk Analysis

Considering the high impact of the pollutants on the environment, a matrix of the type shown in Table 1 was chosen for the environmental risk assessment.

As shown in the risk matrix, there is a large number of hazards, with medium and high risk, requiring reduction measures. The low risks will be monitored so that they remain in this class of risk.

Table 1. *Risk Matrix*

Likelihood	Low impact	Medium impact	High impact
Not very likely (<10%)	-	-	risk less (P17)
Less likely (<35%)	-	-	risk medium (P7, P8, P12, P13, P20, P19)
Can or not can happen (35%-65%)	-	risk medium (P5, P6, P11)	risk high (P2)
Fairly likely (>65%)	risk less (P4)	-	risk high (P1, P14, P15)
Very likely (>90%)		risk medium / high (P3, P9, P10, P18)	risk high (P16)

2.4. Treatment and monitoring of the risks

In order to ensure adequate health and safety conditions of work in the energy system and to improve the environmental performance, it is necessary to take organizational and technological measures. Management measures will be implemented for labor discipline and measures that lead to the operation of installations under appropriate conditions, especially the sealing of the possibly pollutant-generating equipment. Taking some technical measures will be equally important, i.e. by introducing facilities or equipment that lead to reducing emissions under a maximum admissible or that would create the possibility of conducting activities outside the noxious environment.

To reduce the environmental impact of the identified risks, many measures starting from the management ones to the technical and technological solutions should be considered, such as:

•control of combustion processes that are the main generating sources of pollutants;

• improvement of ventilation in all indoor spaces;

• modernization of the electro filters;

• use of the desulphurization installations of the latest generation;

• burning fuel with low content of ash, sulfur etc.;

• use of facilities for monitoring of gaseous emissions;

• wetting the dry areas of the dumps.

Monitoring emissions can be done through a system of monitoring and measuring of the gaseous components at the chimney exit to determine the concentrations of SO2, NOx and dust. It is also necessary to measure the relevant process parameters of the fuel burning respectively: % O_2, temperature, pressure, humidity and flue gas flow to the chimney.

3. Conclusions

- Fossil fuel combustion in thermal power plants generates large amounts of CO_2 and in varying proportions SO_2, SO_3, NO_x, heavy metals, halogenated compounds, dioxins and furans, slag and ash, that have a significant impact on the environment.
- Most of the identified dangers in the risk analysis are included in medium and high risk classes.
- The below have an impact with high risk on the environment:

- CO_2 emissions with major influence on climate change;

- the slag and ash particles shattered of the air currents from the dump and depositing them on soil and vegetation or inhaled by humans and animals;

- radioactive slag and ash;

- formation of the nitric acid and the ammonium nitrate aerosols due to NO_2;

- the emergence of acid rain caused by SO_2, SO_3 by reaction with rainwater;

- formation of the ozone; having as precursor of NO_2;

- To reduce the environmental impact of the identified risks, measures can be taken from managerial to technical measures and even closing these plants through larger scale usage of renewable energies.

References

[1]. Adrian Ioana, *Analiza impactului termocentralelor asupra mediului inconjurator Revista Tehnica Instalatiilor* ISSN 1582-6244, Targu Mures, ianuarie 2014.

[2]. Traian Vasiu, Victor Marian Bucaleț, *Aportul combustibililor solizi utilizaţi, în termocentrala Mintia–Deva, la impactul asupra mediului*, Buletinul AGIR nr. 3/2006.

[3]. Alexander Leyzerovich, *Turbine cu abur de mare putere*, Editura AGIR, București, 2003.

[4]. C. Moțoiu, *Centrale termo și hidroelectrice*, Editura Didactică și Pedagogică, București, 1974.

[5]. Victor Vaida, *Calitatea cărbunelui, factor determinant la impactul termocentralei Mintia asupra mediului înconjurător*, Buletinul AGIR, nr. 3/2006.

[6] Balint Lucica., Minodora Rîpă, Petre Stelian Niță, Balint Simion., Radu Tamara, *Air quality monitoring in Galati. Case study*, Analele Universităţii "Dunărea de Jos" din Galaţi, Fascicola IV, Frigotehnie motoare cu ardere internă cazane și turbine, 2005, p. 299-305, ISSN 1221-4558.

[7]. Radu T., Ciocan A., Balint L., *Distribution of accumulation particles in the urban atmosphere*, TEHNOMUS Journal, P - ISSN-1224-029X. E - ISSN-2247-6016, p. 9, 2013.

[8]. ***, *Studiu de evaluare a riscului la ISPAT-SIDEX Galaţi,* ICEM S.A. București - Laborator Protecţia Mediului, 2006.

[9]. Radu T., Vlad M., Dragan V., Basliu V., Istrate G. G., *Occupational Risk Management in Industry,* The Anals of "Dunărea de Jos" University of Galati, Fascicula IX ISSN 1453-083X, vol. 3, p. 34-39, sept 2013.

[10]. Radu T., Ciocan A., *Evaluation of the Occupational Risk associated to Work Environment in Ferrous Metallurgy,* The Anals of "Dunărea de Jos" University of Galati, Fascicula IX ISSN 1453-083X**,** vol. 4, p. 90-96, 2013.

[11]. Radu T., Ciocan A., Balint S. I., Balint L., *Dioxins and furans emissions in the primary steel sector,* Proceedings of the 13th International Multidisciplinary Scientific Geoconference, SGEM 2013, p. 609.

[12]. Ciocan Anișoara, *Generarea si controlul poluantilor industriali*, Ed. GUP 2013, ISBN 978-606-8348-74-2.

[13]. Lucica Balint, Doru Matei, Simion Ioan Balint, *Environmental Risk at Urban Wastewater treatment***,** The annals of "Dunarea de Jos" University of Galati, fascicle IX Metallurgy and Materials Science, ISSN 1453 – 083X, p. 293.

THE ANNALS OF "DUNAREA DE JOS" UNIVERSITY OF GALATI
FASCICLE IX. METALLURGY AND MATERIALS SCIENCE
Nº. 4 - 2015, ISSN 1453 – 083X

EMISSIONS OF HYDROCHLORIC ACID VAPORS GENERATED BY PICKLING PROCESS FROM COLD ROLLING MILL OF STEEL STRIPS

Anisoara CIOCAN
"Dunarea de Jos" University of Galati, 111, Domnească Street, 800201, Galaţi, Romania
e-mail: aciocan@ugal.ro

ABSTRACT

The most important pollutant emitted in the sector of pickling within a cold strip mill in an integrated steel mill are the hydrochloric acid vapors. This work presents the chemical reactions between the hydrochloric acid and iron oxides layers formed on the surface of the steel strip after the hot rolling process and it analyzes different areas of the pickling line as generators of acid vapors. The measurement values of hydrochloric acid vapors concentrations in the working atmosphere are correlated with the operational regimes and with occupational exposure limit values according to national legislation. Finally, solutions that can be applied to reduce emissions of hydrochloric acid vapor in the sector of analysis are presented.

KEYWORDS: steel strip, cold rolling, pickling, hydrochloric acid, pollution

1. Introduction

Cold rolling mill within an integrated steel mill is a complex technological line which is specialized in the manufacturing of low carbon steel bands or sheets. A cold-rolled sheet is a hot-rolled sheet that has been further processed through a pickle line, which is an acid bath that removes scaling from the surface of steel strips. Then it is successively passed through a rolling mill without reheating until the desired gauge, or the thickness and other physical properties have been achieved. Cold-rolling reduces gauge and hardens the steel and, when further processed through an annealing furnace and a temper mill, it improves uniformity, ductility and formability [1, 2].

The main operations related to cold rolling of steel bands are: pre-treatment to surface preparation (pickling) for improved the quality of cold rolled bands; trimming and oiling; cold rolling for reduction in thickness of steel products; degreasing and heat treatment (annealing) to get particular metallic, chemical or mechanical performances, required by customers.

All of these sub-processes are sources of pollutant emissions: hydrocarbons and decomposition products of lubricant oil; acid aerosols and fumes; nitrogen oxides and carbon monoxide, polycyclic aromatic hydrocarbons etc. [3, 4]. This paper analyses the pickling process and acid vapors emissions. The common pickling processes are operated at temperatures that usually give rise to acid aerosols and fumes. Also Emissions of acid vapors may arise also from acid regeneration processes [5].

2. Generation of hydrochloric acid vapors at pickling of the hot rolled steel strips

Emissions of hydrochloric acid vapors from pickling of the hot rolled steel strips of an integrated steel mill come from multiple sources.

During the hot rolling of steel, oxygen from the atmosphere reacts with the iron in the surface of the steel to form an iron oxides crust. There is a mixture of iron oxides, practically disposed as three kinds of scale which differ in the temporal and local evolution. The primary, secondary, and tertiary scale is formed on the steel band surface within the hot rolling process.

The share of three layers in the crust is different for different temperatures, oxidation times and steel composition (Figure 1).

The presence of oxides or scale on the surface of the steel is harmful when the hot rolled steel strip is subjected to cold rolling process. To remove iron oxides or scale from the surface of strip steel in order

to obtain a clean surface are required mechanically and chemically treatments. Firstly, is applied the de-scaling of the hot strip material into scale breaker (placed downstream to pickling installation).

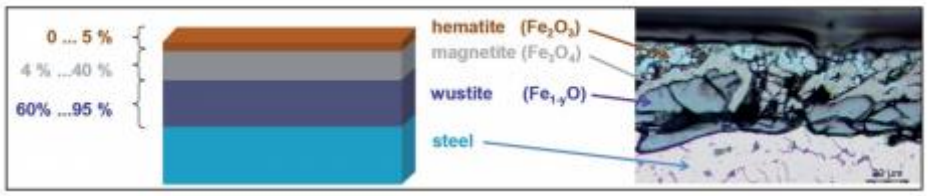

Fig. 1. *Cross section of the three-layer steel oxide scale formed during the hot rolling stage on surface of the steel strip* [6]

To increase the value of steel strip products it is essential to follow the second treatment. This involves the removing of oxides layers by the steel chemical pickling bath method (named pickling) [7, 8]. The steel strip is dipped in an acid bath (H_2SO_4 or HCl solutions). Such this is pickled for the removal of oxides and other residues from the surface. To dissolve iron oxides from the surface of a metal without any significant attack on the steel itself is used the HCl acid solution as pickle liquor. Hydrochloric acid pickling is widely used because has more advantages: high pickling efficiency; less pickling time; lower investments required; lower risk of embrittlement (hydrogen diffusion in the material), the process taking place at low temperatures; lower acid consumption per ton of pickled strip. However, sulphuric acid has a low vapor pressure and thus it requires less intensive ventilation. This is reflected in the cost-recycling regenerative technologies [1].

The HCl concentrations in a batch pickling process are 16.5 % for a fresh solution and 3.5 wt. % before acid replenishment. The rate of pickling increases with concentration of HCl and temperature.

The pickling line linked to tandem cold rolling mill is composed of several sections where take place specific technological operations: pickling in acid tanks with different concentrations, rinsing and dryer of steel strip.

In the acid tanks the iron oxides and metallic iron react with hydrochloric acid and ferrous chloride, water, and hydrogen gas are formed according to the following reactions [9]:

$$FeO(s) + 2HCl(aq) \rightarrow FeCl_2(aq) + H_2O(l)$$
$$Fe_3O_4(s) + Fe(s) + 8HCl(aq) \rightarrow 4FeCl_2(aq) + 4H_2O(l)$$
$$Fe_2O_3(s) + Fe(s) + 6HCl(aq) \rightarrow 3FeCl_2(aq) + 3H_2O(l)$$
$$Fe(s) + 2HCl(aq) \rightarrow FeCl_2(aq) + H_2(g)$$

The hydrochloric acid pickling is carried out in heated bath. Usually the range of temperature recommended is 65...85 ºC. Depending on the temperature of the pickling baths, the speed of passage of the strip through pickling baths is a maximum of 4 m/s. In these conditions HCl vapors are produced and released into the atmosphere during the pickling process (Figure 2).

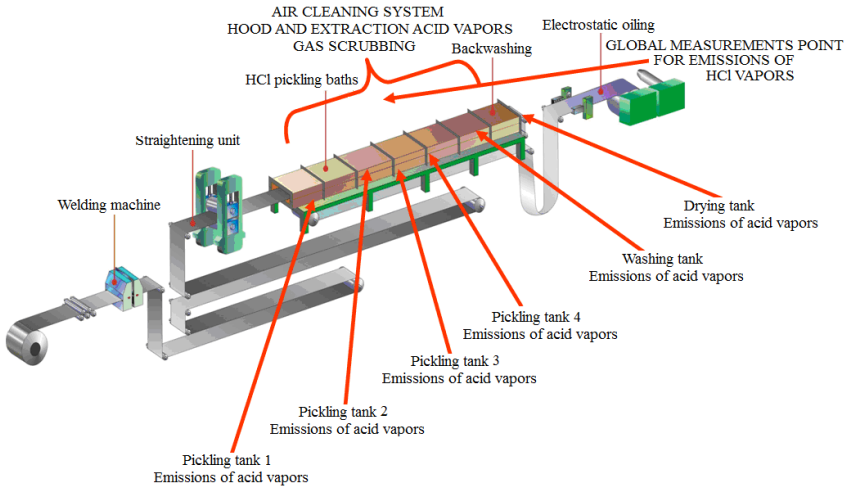

Fig. 2. *Pickling line and hot points for producing and releasing of HCl vapours emissions*

The HCl volatilized, together with steam and hydrogen gas, is released as acid fumes. It is present at the surface of the pickling tank and the pickled material. From here it is transferred to the rinse tank. Also it is present in chemical area of pumps and routes of acid.

In normal functioning and operation conditions of facilities from pickling sector hydrochloric acid vapors (as venting or fugitive emissions) are generally collected and treated in the air pollution control system to remove HCl.

There are some situations when emissions from many batch operations are uncontrolledly released as a hazardous air pollutant. Potential sources of HCl vapors are the loading and unloading operations (planned for maintenance or accidental stops). In this case the emissions of hydrochloric acid vapors are produced and released into atmosphere of the working hall as acid fumes. The natural circulation of air currents can get them up to tandem mill sector.

More emissions are released in the working space, damaging systems and equipment that handle and transport acid (pipelines, storage tanks, acid pumps etc.). In this case, emitted acid fumes in the, will be moved by the natural circulation of air currents.

The United States Environmental Protection Agency (EPA) specifies that for each million tons of steel processed at continuous coil or pushpull coil model facilities, storage tank losses are estimated to amount to 0.39 tpy. For other types of pickling facilities, storage tank losses are estimated to be about 11.19 tpy of HCl per million tons of steel processed [10].

The recovery process of HCl from the waste pickling liquid in the acid regeneration process also can be a potential source of emitting significant amounts of hydrochloric acid vapors.

HCl emissions from processes of cleaning and acid regeneration depend on the pickling process used. A range of 1 – 145 mg/Nm³ maximum (up to 16 g/t) were reported; with the range reported by industry being 10 – < 30 mg/Nm³ (~ 0.26 g/t) [3].

3. Level of hydrochloric acid vapors in atmosphere of pickling sector

The concentration of hydrochloric acid vapors is periodically controlled in the hot points of the pickling line and in the area of the tandem mill. The Ministry of Health, the Institute of Public Health and the Medical Sciences Academy Bucharest specified procedures for the determination of hydrogen chloride emissions from stationary sources. A spectrophotometric method is used. The data collection frequency is once a quarter. The conditions of the data collection are: the pickling plant in operation; the pickling plant in stationary regime; with the pickling plant off (for maintenance works).

Table 1. gives the average annual values of measured concentration for HCl vapors.

Table 1. *Average annual values of concentration of hydrochloric acid vapors for main sector of steel bands pickling lines and tandem mill, [ppm]*

Measuring point	**Year**		
	2013	**2014**	**2015**
Tandem mill: rolling stands 1…5	0.20	0.22	0.20
Pickling sector: at steel strip dipping in the pickling bath	0.21	0.23	0.20
Pickling sector: acid tanks; dryer	5.90	6.20	5.80
Pickling sector: at steel strip extraction from pickling bath	0.61	0.62	0.60

The occupational exposure limit values for hydrochloric acid vapors generated in areas of steel pickling lines imposed by Annex 1 from HG 1218/06.09.2006 are shown in Table 2 [11].

Table 2. *Occupational exposure limit values for hydrochloric acid vapors generated by process steel pickling lines according to national legislation HG 1218/06.09.2006*

Hazardous Air Pollutant	**CAS**	**EINECS**	**Occupational exposure limit values**			
			8 hours		**short time duration (15 minutes)**	
			mg/m^3	ppm	mg/m^3	ppm
HCl	7647-01-0	231-595-7	8	5	15	10

The level of measured concentrations in some areas of the pickling installation presented in Table 1 are compared with the occupational exposure limit values presented in Table 2. The results are given in Figure 3.

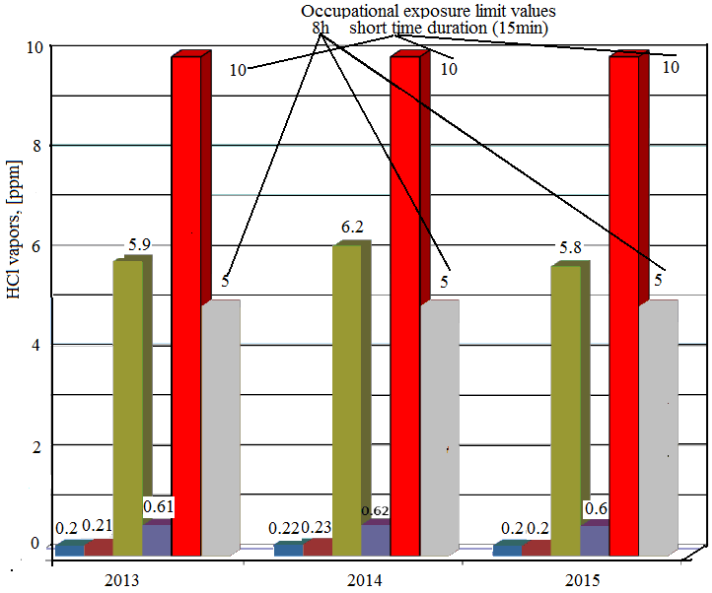

Fig. 3. *Comparison between measured values and limits allowed by legislation for hydrochloric acid vapors in the working atmosphere*

It is observed that the higher values of HCl vapors concentration were observed at the pickling tanks area. Also these are present in the area of the rinse tanks where are generated by the surface of the pickled steel band. Lower values were found at dipping and at the take out of steel strip. All measured values were below the limits stipulated by legislation for hazardous pollutants. This demonstrates that the conditions of safety are respected.

The emissions from pickling line are collected and efficient treated. The cleaning of exhaust gas and the ensuring of hydrochloric acid recuperation are imperatively used. The scrubber system to remove the hydrochloric acid vapors is shown in Figure 4.

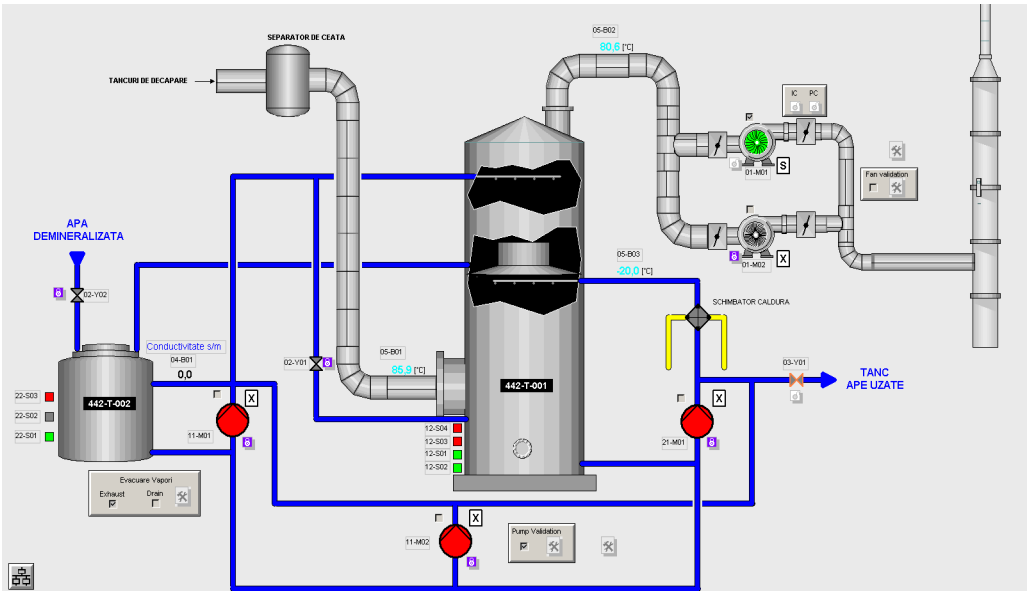

Fig. 4. *Treatment facility for HCl vapors emissions*

4. Conclusions

The acid emissions to air from cold rolling may arise from pickling and acid regeneration processes. With open pre-treatment systems, it is inevitable to eliminate the content of HCl vapor emissions in the air around the pickling facilities, especially when the material is taken out of the bath.

Generally, for all types of pickling sectors the emission control measures can be taken. The best solution for minimization of air emissions are: optimization of temperature, composition of pickle solution; covering of tanks; enclose pickling bath operations or install hoods and extraction systems; reduction of pickling emissions with gas scrubbing; pickling tank fume control [5].

To optimize operation of regeneration plant and the pickling section is necessary to minimize the acid losses as vapors. The measures to prevent emissions include a reduction of the waste gas volume and the contaminant load of the waste gas, which is exhausted from the pickling tanks.

Acknowledgements

The author wishes to thank of the student Monica Basoc, who has contributed to make this study.

References

[1]. R. Saban, C. Dumitrescu s.a., *Tratat de stiinta si ingineria materialelor metalice. Vol.5. Tehnologii de procesare finala a materialelor metalice*., Ed.AGIR, 2012.
[2]. ***, *arcelormittal - 20-f - 20080319 - company_information*, http://google.brand.edgar-online.com/.
[3]. ***, *Integrated Pollution Prevention and Control (IPPC) Reference Document on Best Available Techniques in the Ferrous Metals Processing Industry*, December 2001.
[4]. ***, *Iron and steel production, EMEP/EEA emission inventory guidebook, 2013*.
[5]. ***, *EPA, Final Draft BAT Guidance Note on Best Available Techniques for Ferrous Metal Processing and the Pressing, Drawing and Stamping of Large Castings where the Production Area exceeds 500 Square Metres*, September 2012.
[6]. M. Graf, R. Kawalla, *Scrap development on steel hot strip rolling*, La Metallurgia Italiana, No. 2/2014, p. 43-49.
[7]. R. M. Hudson, Pickling of hot rolled strip: an overview, Iron and Steelmaker (USA), 1991, 18(9), p. 31-39.
[8]. D. Wolfgang, F. Kladnig, *A review of steel pickling and acid regeneration: an environmental contribution*, International Journal of Materials and Product Technology, 19(6), p. 550-561, 2003.
[9]. Y. Jatuphaksamphan, N. Phinichka, K. Prapakorn, M. Supradist, *Pickling Kinetics of Tertiary Oxide Scale Formed on Hot-Rolled Steel Strip*, Journal of Metals, Materials and Minerals, vol. 20 No.1 p. 33-39, 2010.
[10]. ***, *EPA, Emergency planning and community right-to-know act - section 313 Guidance for Reporting Hydrochloric Acid (acid aerosols including mists, vapors, gas, fog, and other airborne forms of any particle size)*.
[11]. ***, *HG 1218/06.09.2006, Hotararea de Guvern nr. 1218 din 6 septembrie 2006 privind stabilirea cerintelor minime de securitate si sanatate in munca pentru asigurarea protectiei lucratorilor impotriva riscurilor legate de prezenta agentilor chimici*.

THE ANNALS OF "DUNAREA DE JOS" UNIVERSITY OF GALATI
FASCICLE IX. METALLURGY AND MATERIALS SCIENCE
Nº. 4 - 2015, ISSN 1453 – 083X

THE CHEMICAL AND METALLURGICAL ANALYSIS OF COOPER-BASED SHAPE MEMORY ALLOYS

Dragoş Cristian ACHIŢEI[1,2], Mirabela Georgiana MINCIUNĂ[1,2], Petrică VIZUREANU[1,2]

[1]Gheorghe Asachi Technical University of Iasi, Faculty of Materials Science and Engineering, Blvd. D. Mangeron 41, 700050, Iasi, Romania

[2]Center of Excellence Geopolymer & Green Technology (CEGeoGTech), School of Materials Engineering, Universiti Malaysia Perlis, 01000 Kangar, Perlis, Malaysia

e-mails: dragos_adc@tuiasi.ro, mirabela.minciuna@yahoo.ro, peviz2002@yahoo.com

ABSTRACT

The paper presents some aspects on the thermo-mechanical fatigue of shape memory alloy, a documentary synthesis of their industrial applications and chemical aspects concerning the use of these alloys in biomedical applications.

KEYWORDS: shape memory alloys; biomaterials; thermal fatigue; corrosion

1. Introduction

The fatigue of metals is the phenomenon which provides the cracks in different applications, in the conditions of temperature and work parameters variations. The thermal tensions are induced when the dimensions vary for a part due to the temperature change [1, 2].

In the case of equipments which work at high temperatures, the conditions to appear the cracks due to thermal fatigue are created. The behaviour of materials at thermal fatigue is influenced by the structural transformation effects and the mechanical properties.

The mechanism of defects accumulation in the crystalline network and inside the grain, due to thermal fatigue lead to creating the tension local zone, where a crack may appear. The cracks due to thermal cycles is sometimes associated to network tension by blocking the dislocation, which are moving inside the grain matrix, specially, due to mechanical or thermo-mechanical tensions which appear. The cracks by thermal fatigue are initiated along the surface. Because the cracks are initiated from the exterior, the corrosion process and oxidation along the surface of thermal fatigue cracks, it is inversely proportional with the crack depth [3, 4].

For producing a crack by fatigue three base factors are necessary:

- A maximum normal tension with a high value;
- A large enough variation of applied tensions;
- A large number of cycles for applied tension.

The cracking process develops slowly; the cracks propagation speed is progressively increased, reaching the moment of crack. The process takes place so fast, like in the case of static cracks for fragile materials, without producing a visible plastic deformation.

The cracked surface presents two zones: the old crack and the new crack. The old crack has a smooth and sometime shiny aspect. The new crack is characterized by irregular aspects, with high granulation, that proves a breakable character of cracks.

2. Results
Thermo-mechanical fatigue of shape memory alloys

In the case of metallic parts made of shape memory alloys, the possibility for the thermal or thermo-mechanical fatigue to appear does exist.

The mechanical fatigue involves the crack production in four stages: the accumulation of defects, the crack formation, crack propagation in stationary and un-stationary regime and respectively final break.

The main method to increase the resistance of mechanical fatigue for shape memory alloys is the granulation finishing, which may be realized by alloying, energy quenching and powder metallurgy.

The thermal fatigue is related to the irreversible formation of defects, which lead to a considerable hardening, in the case of binary bi-phase brasses, like (Cu-40%Zn).

In the case of shape memory alloys, Cu-Zn-Al type, should be noted that the mechanical cycling affects the critical temperatures of transformation, but much more reduced than thermal cycling.

Figure 1 presents the surface of Cu-Zn-Al alloys, with fatigue cracks.

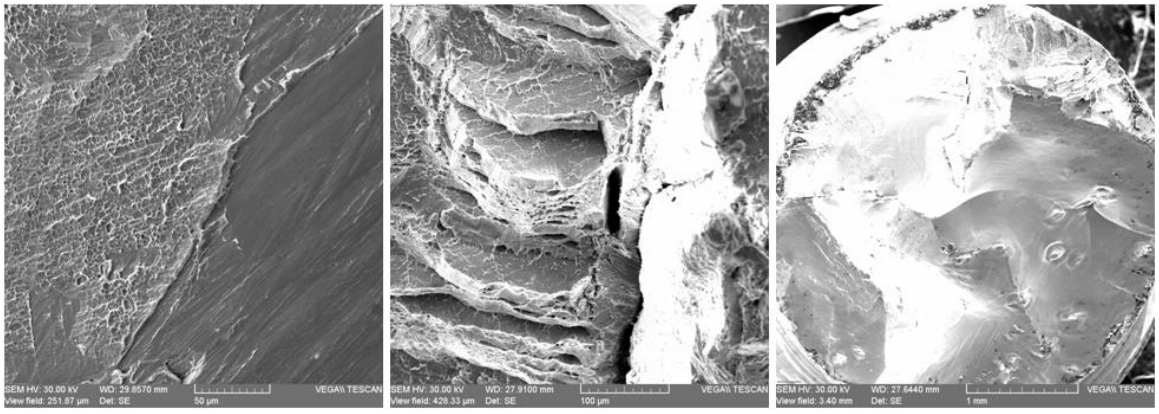

Fig. 1. *The aspects of cracks for a shape memory alloy, Cu-Zn-Al type, by thermo – mechanical fatigue on different magnifications 1000X, 500X and 100X*

The cracking by fatigue is the phenomenon which leads to break under repetitive tension or fluctuating, which are lower than the elastic tension of material.

The cracks at fatigue are progressive, with little cracks at the beginning, which increase under the action of fluctuating tension. The shape memory alloys are sensitive at fatigue.

Much more than that, the phenomenon for the classic crystalline materials, the shape memory alloys have some additional mechanism of linking at the change of phase which characterizes them.

It is found that the observed type of crack depends on the applying mode for mechanical fatigue.

The improving of life duration for these materials imposed the decrease of level for internal tension at grains limits and the increase of cracking resistance.

For obtaining these results, we can realize:

- the increase of grains measurements, decrease the measurements for martensite plates;
- the generation of laminated texture, which can reduce the differences of orientation between the grains, for reduction of the incompatibility for deformation;
- the possibility to obtain the plastic deformation at the level of grains limits appropriate also by the deformation efficiency.

Medical applications for shape memory alloys

Many types of shape memory alloys are known, but most of them are expansive due to the noble and rare metals use, also due to the complex obtaining technologies. The most interest is represented by the alloys like: Ni-Ti, Cu-Zn-Al and Cu-Al-Ni, which may be used in medical practice applications [4-9].

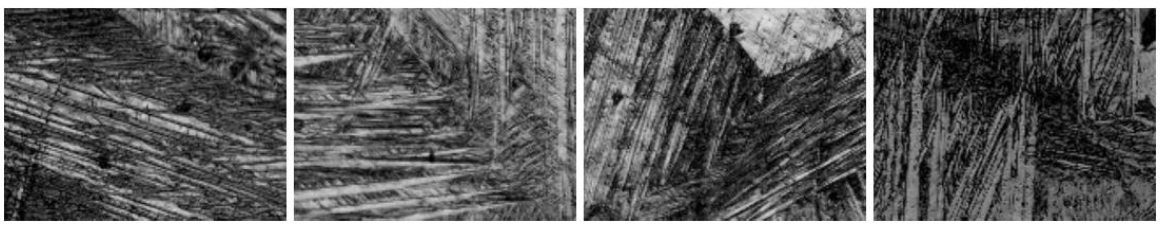

Fig. 2. *Optical microstructures for Cu-Zn-Al shape memory alloy; martensite structure (200X)*

The study of shape memory alloys has determined a development of the research in different activity domains, in the order to find the corresponding applications. At present, these alloys are used in the industry of aeronautics, aerospace, mechanical, electronic and medical technique. These materials are obtained in laboratory conditions, in order to certify the characteristics necessary in exploitation. In each of these cases, the parts made of shape memory alloys should be thermally treated

(heating and cooling), to realize the proposed objective. Between the heat shape and cold shape an energy difference exists. The reversibility of the changes for the two shapes is the base for multiple applications. In this case, of great importance is the exact reproductivity of the two shapes. After some cycles of function, this is affected and so are affected the properties of shape memory.

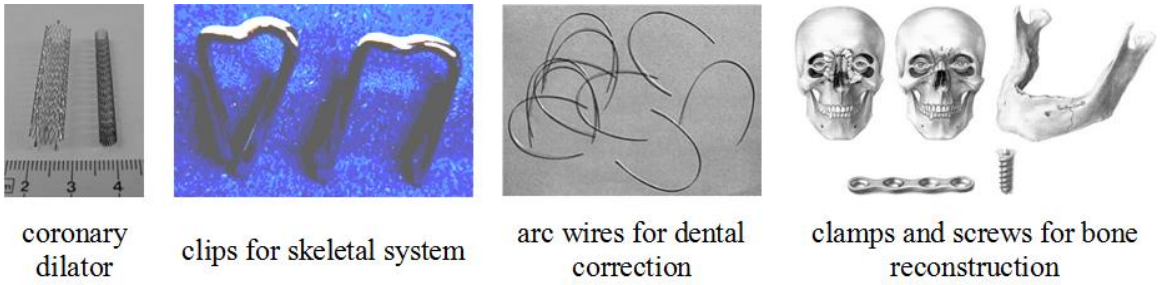

Fig. 3. *The medical applications for the shape memory alloys* [14]

Porous materials made from shape memory alloys, are also important, and they are used in various medical fields to replace some bone parts.

In time, these parts will be embedded by the human body, by the development inside the pores of the organic cells characteristics to bone system. In this way, the micro-prostheses make common body with the body cells and it is integrated in bone system, where adverse reactions should be limited.

The porous materials used in the medical field for prostheses present a good biocompatibility and elasticity, imitating the behavior of the bone part which is substituted.

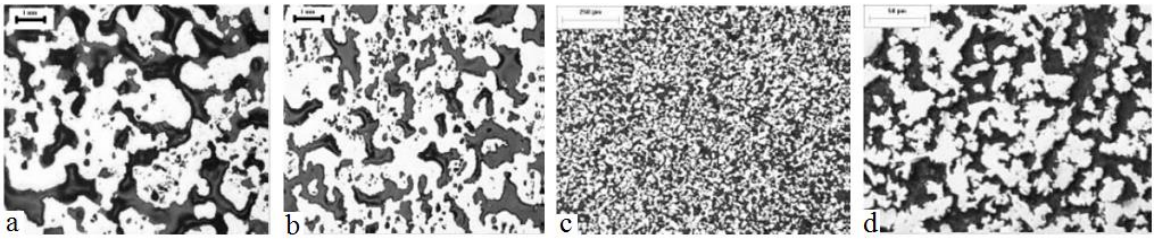

Fig. 4*. Optical micrographs on porosity of materials: a and b - large pores: porosity 42% (250X); c and d - big pores: porosity 50% (100X, 500X)* [15]

For the dental materials used to fabricate the prosthetics devices, a high diversity of metallic alloys is distinguished. The diversity was made in the direction of developing new materials with superior properties, but with lower obtaining costs. The cooper based alloys, were promoted like dental materials, for economic reasons, due to the increase of noble metals costs. In some countries of Europe, the alloys based on cooper are consider incompatible with the qualities of biomaterials used in prosthetics and are presented as materials with allergic risks and low resistance at corrosion [10-11].

Cooper and its alloys are recognized like materials with a good corrosion resistance and are used in many activity domains.

The good resistance of these materials is related to the formation of a uniform and adherent film on surface, which protect the substrate to the environment.

The appearance of the corrosion phenomenon is related to the formation and stability of this film; if the film is not formed or it is destroyed, the metal is corroded, either the entire surface, either locally.

The copper is an essential metal for living organisms, but too much cooper may be harmful. From this reason, the toxic effects of cooper alloys may be confirmed when these alloys were implanted subcutaneously or intramuscularly.

The date analysis shows clearly that these materials lead to modifications of tissues, like necrosis and inflammation. The cooper may have a chemically modifying role, inducing the carcinogen activity much more than nickel.

Chronic poisoning with cooper is a controversial problem and it frequently is related to muscle pain, hypertension, various neuro-psychological phenomena or hair loss. However, the World Health Organization considers the cooper to be a non-toxic metal.

3. Conclusions

The approach presents the correlation between the technological parameters which influenced the appearance of thermal fatigue phenomenon and the properties specific to metallic material with shape memory.

The copper-based shape memory alloys, may be used like biocompatible materials for the human body, just after the corrosion tests in different mediums which simulated the liquids from the human body.

Also the manufacturing of parts from the shape memory alloys must take into account the fact that the fatigue phenomenon may appear in the exploitation time, concretized by the degradation of shape memory effect.

These characteristics for shape memory alloys permit their use in smart structures, micro-actuators, some advanced composites, medical components and dental implants.

References

[1]. D. C. Achiţei, M. M. Al Bakri Abdullah, A. V. Sandu, P. Vizureanu, A. Abdullah, *On the Fatigue of Shape Memory Alloys*, Key Engineering Materials, 594-595, p. 133-139, 2014.

[2]. D. C. Achiţei, A. V. Sandu, M. M. Al Bakri Abdullah, P. Vizureanu, A. Abdullah, *On the Structure of Shape Memory Alloys*, Key Engineering Materials, 594-595, p. 140-145, 2014.

[3]. N. Cimpoeşu, A. D. Ursanu, S. Stanciu, R. Cimpoeşu, B. Constantin, C. Paraschiv, S. O. Gurlui, *Preliminary Results of Copper Based Shape Memory Alloys Analyze Used for MEMS Applications*, Applied Mechanics and Materials, 371, p. 368-372, 2013.

[4]. M. G. Minciuna, P. Vizureanu, D. C. Achitei, N. Ghiban, A. V. Sandu, N. C. Forna, *Structural Characterization of Some CoCrMo Alloys with Medical Application*, Revista de Chimie (Bucharest), 65, p. 335-338, 2014.

[5]. G. Ungureanu, D. Mareci, D. Aelenei, G. Nemtoi, J. Mirza Rosca, *The Gaudent – a biocompatible material?* Al V-lea Simpozion Naţional de Biomateriale – Biomateriale şi Aplicaţii Medico - Chirurgicale, Iaşi, 2005.

[6]. Y. Setiyorini, S. Pintowantoro, *Biocompatibility Improvement of NiTi Orthodontic Wire from Various Coatings*, Advanced Materials Research, 789, p. 225-231, 2013.

[7]. M. G. Minciună, P. Vizureanu, *Cobalt alloys research used in medical applications*, Metalurgia International, Special Issue 6, p. 123-126, 2013.

[8]. A. V. Traleski, S. Vurobi, O. M. Cintho, *Processing of Cu-Al-Ni and Cu-Zn-Al alloys by mechanical alloying*, Materials Science Forum, 727-728, p. 200-205, 2012.

[9]. V. Agafonov, B. Legendre, A. Kahn, G. Guénin, B. Dubois, *Study of Strain-Induced Martensites Obtained in the β-Cu-Zn-Al System*, Materials Science Forum, 56-58, p. 447-449, 1990.

[10]. A. V. Sandu, C. Bejinariu, G. Nemtoi, I. G. Sandu, P. Vizureanu, I. Ionita, C. Baciu, New anticorrosion layers obtained by chemical phosphatation, Revista de Chimie (Bucharest), 64, 8, p. 825-827, 2013.

THE ANNALS OF "DUNAREA DE JOS" UNIVERSITY OF GALATI
FASCICLE IX. METALLURGY AND MATERIALS SCIENCE
Nº. 4 - 2015, ISSN 1453 – 083X

RESEARCH ON CHEMICAL DEPOSITION OF SILVER WITH ANTIBACTERIAL ROLE IN IMPLANTOLOGY

Elisabeta VASILESCU[1], Vlad Gabriel VASILESCU[2], Dumitru DIMA[1]
[1]Dunărea de Jos University of Galați
[2]Carol Davila UMF București
e-mail: elisabeta.vasilescu@yahoo.com

ABSTRACT

The paper presents a synthesis of the laboratory research on the conditions of achieving chemical deposition of silver on oral implants made of Ti base alloy (bioalloy $Ti_{10}Zr$). There were used several chemical deposition regimes in which were modified deposition parameters (temperature, stirring time) for two types of implants (different screw thread geometry). Study of the influence of deposition conditions was performed through analysis at scanning electron microscope (SEM) with EDX analyzer. The results revealed the presence of silver, microdispersed particles with morphologies and degrees of dispersion dependent on the factors and technological conditions of obtaining the chemical deposition.

KEYWORDS: silver, $Ti_{10}Zr$ bioalloy, implant, chemical deposition, electron microscope SEM

1. Introduction

Properties and role of antibiotic, antioxidant and disinfectant of silver are known in the world for many centuries. Laboratory tests confirm today conclusively that silver ions have a bactericidal effect and constitute an effective disinfectant by destroying more than 600 viruses and harmful germs [1, 2]. Antibacterial efficacy of different metals has been established since 1893 and this property has been called oligodynamic effect, but later it was found that of all metals with antimicrobial properties, silver has the most effective antibacterial action and is less toxic to animal cells (Guggenbichler *et al.*, 1999).

Although known for centuries, only recently have there been understood the mechanisms through which silver antimicrobial properties inhibit the bacterial growth.

The evolution of modern ways of investigation and analysis, such as radioactive isotopes and electron microscopy has allowed explaining the antibacterial mechanism of silver (Modak and Fox, 1974; Feng *et al.*, 2000). One of these is based on the consideration that silver atoms bind to thiol groups (-SH) of enzymes and subsequently determine their inactivation. Forms of silver with S-Ag stable compounds contain in the cell membrane thiol that is involved in trans membrane energy production and transport of ions (Klueh *et al.*, 2000).

It is also believed that silver ions can take part in catalytic oxidation reactions which have as result the formation of disulfide bonds (RSSR). Silver does this by catalyzing the reaction between oxygen molecules from the cells and the hydrogen atoms of the thiol groups: water is released as a product and two thiol groups become covalently linked together by a disulfide bond (Davies and Etris, 1997).

Disulfide bond formation catalyzed by silver changes cellular enzyme form and subsequently affect their function. Disulfide bond formation catalyzed by silver can lead to changes in protein structure and inactivation of key enzymes such as those required for the "breath" of the cell (Davies and Etris, 1997), or may even lead to the death of cells (Yamanaka *et al.*, 2005).

Another mechanism which explains the antimicrobial activity of the silver has been proposed by Klueh *et al.* (2000), which shows that the Ag + enters the cell and cause its disruption.

It has been demonstrated that silver ions associate with the DNA once they enter the cell (Fox and Modak, 1974).

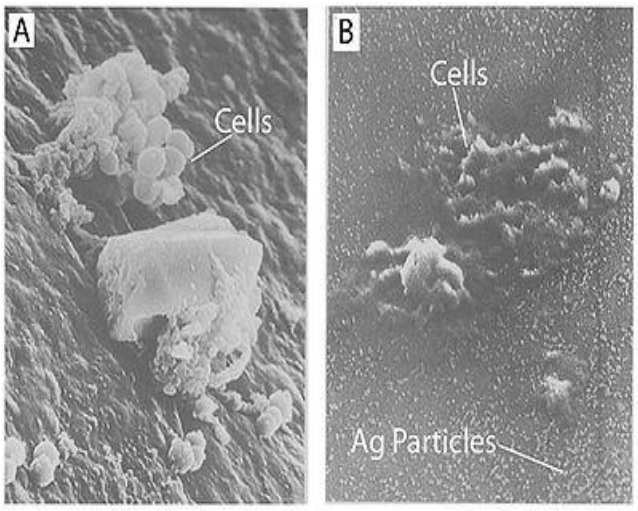

Fig. 1. *Treatment of cells with Ag^+results in DNA condensation, cell wall damage, and silver granule formation. (A) E. coli and (B) S. aureuscells with and without Ag^+treatment were observed with transmission electron microscopy (Fenget* et al.*, 2000)*

In order to have anti-microbial properties, silver has to be in its ionized shape (Lok *et al.*, 2007; Rai *et al.*, 2009). Silver in its non-ionised form is inert (Guggenbichler *et al.*, 1999), but in contact with a moist environment leads to the release of silver ions (Radheshkumar and Munstedt, 2005). Therefore, all forms of silver or silver as compounds with anti-microbial properties are in one way or another the source of silver ions (Ag +); these silver ions can be incorporated and released slowly. Feng *et al.* (2000) conducted a study to see the effects of ions of silver per gram-positive and gram-negative bacteria, such as Staphylococcus aureus and Escherichia coli. They treated cells with $AgNO_3$ which is a source of Ag + in aqueous medium, and they observed structural and morphological effects of these ions of silver on cells. Cells were exposed to $AgNO_3$ for 4-12 hours before being prepared for microscopy (TEM). There was some deterioration of the cell wall and outer dense particles, and in some cases within the cell (Figure 3). Dense particles which were formed inside and outside the cell were extracted and subjected to the X-ray microanalysis for the determination of their composition. It was found that the particles were made of silver and sulfur. This finding supports the idea that silver inactivate binding proteins to compounds that contain sulfur (Klueh *et al.*, 2000). It was also observed that when treated with Ag +, E. coli, a gram-negative bacterium causes more sustained structural damage than gram-positive S. aureus (Feng *et al.*, 2000). It was also shown that treating cells with silver leads to dehydration and contraction of the cell (Guggenbichler *et al.*, 1999). TEM images from Feng at. al. (2000) show that cells which underwent extensive damage, finally will end with the deterioration of the cell membrane. Cells membrane damage leads to the elimination of the cytoplasm, such as dehydrated and wrinkled cells are shown in the SEM images from Guggenbichler *et al.* (1999). Silver can be managed in different ways. The various effective forms of silver that contribute to the inhibition of microbial are silver salts. One of these is the silver nitrate ($AgNO_3$) and is effective because it can provide a large amount of silver ions at once. It turned out that prolonged antimicrobial activity of silver is best achieved through the continuous release of moderate amounts of silver ions. In addition, the size and shape of the nanoparticles play also an important role in the antibacterial activity (Pal *et al.*, 2007). Smaller nanoparticles require less time for penetrating through the cell membrane and cell wall in relation to larger nanoparticles that have a higher surface-volume ratio (Martinez-Castanon *et al.*, 2008). This means that per mass unit, smaller nanoparticles provide more silver atoms in contact with the solution than do large nanoparticles, meaning there are more silver atoms able to take part in the processes of cell destruction. Regarding the form of nanoparticles with a role in the antibacterial activity, Pal *et al.* (2007) had experienced three types of silver nanoparticles (spherical in the form of rods and triangular tested on E. coli.). It was found that the order in which the antibacterial effect manifested was the triangular, spherical shape and the rod-shaped form. This order of antibacterial activity is explained by the different types of veneers on nanoparticles. Triangular nanoparticles have more active facets (electrons dense facets) than spherical nanoparticles. Spherical nanoparticles, which were not perfectly spherical, have more active facets than the nanoparticles in the form of rods (Pal *et al.*, 2007).

2. Experimental conditions

For the chemical coating with metallic silver there were used solutions prepared with pure chemical reagents, double distilled water and two types of dental implants made from $Ti_{10}Zr$ alloy (developed at SC TEHNOMED Bucharest). The research was conducted in the Laboratory of Chemistry of the Faculty of Science and Environment of "Dunarea de Jos" University of Galati.

Chemical staining was performed as follows: 100 ml of a 2% $AgNO_3$ was treated with 50 ml of 5% NaOH, and then the resulting precipitate was dissolved by adding 50 ml 2% NH_3 solution. The implants (pins) were inserted in a 250 mL container in Tollens reagent obtained according to the recipe above. Also, a magnetic stirrer was inserted to achieve the homogenization of the system. Under stirring at 500 rpm, 2 ml of formaldehyde 30% were added.

The first pivot was extracted from the solution with tweezers after 5 minutes and the second pivot after 10 minutes. The two pins were rinsed in double distilled water and placed for drying in an oven at 105 ºC for 4 hours.

2.1. Method Principle Chemical reactions in metallic Ag deposition:

$(Ag^+ + NO^{3-}) + (Na^+ + HO^-) = Ag(OH)$ (white pp.)$\downarrow + (Na^+ + NO^{3-})$ (1)

$2\,AgOH \rightarrow Ag_2O$ (black pp.)$\downarrow + H_2O$ (2)

$Ag_2O + NH_3 + H_2O \rightarrow ([Ag(NH_3)_2] + HO^-)$ (complexcolorless combination) (3)

$H-C(=O)-H + 2([Ag(NH_3)_2] + HO^-) \rightarrow 2\,Ag + H\text{-}C(=O)OH + 4NH_3$ (4)

The second regime of chemical deposition using the same pivots, however, the solution heated at a temperature of 50 ºC with hold for 5 min and dripping formaldehyde from 30 to 30 seconds. The regime was repeated in the same conditions for the temperature of 70 ºC. Experimental samples were analyzed by the electron scanning electronic microscopy (SEM) with the EDX analyzer. In the next paragraphs the results obtained are presented, which revealed the presence of silver, microdispersed particles having morphologies and degrees of dispersion according to the factors and technological conditions of obtaining the chemical deposition.

3. Experimental results

The SEM microstructural aspects and EDX analysis of pivots (dental implants made at SC Tehnomed Bucuresti SA from $Ti_{10}Zr$ bioalloy).

- Regime 1 (5 min. maintaining in solution with stirring, without heating)

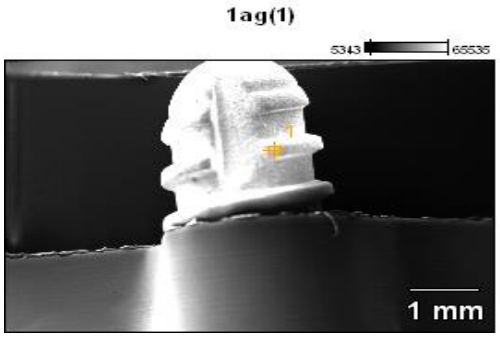

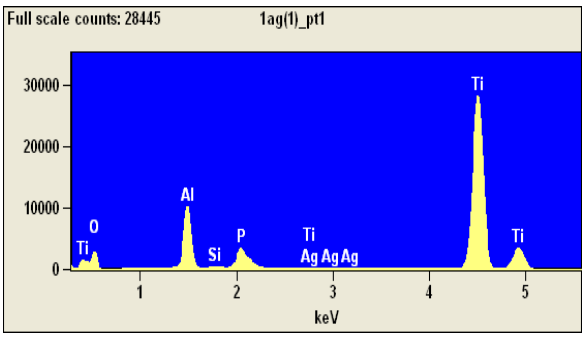

Weight %

	C-K	O-K	Al-K	Si-K	P-K	Ti-K	Ag-L
1ag(1)_pt1	2.78	26.15	8.68	0.16	2.34	59.47	0.42

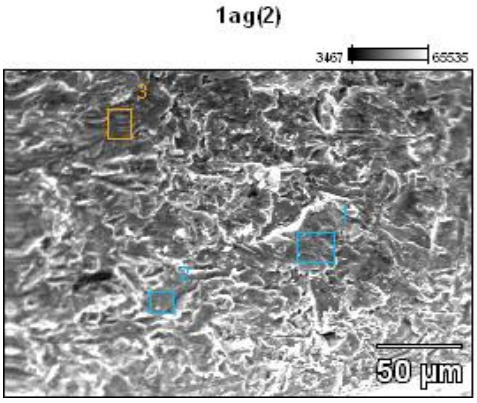

Image Name: 1ag(2)

Accelerating Voltage: 20.0 kV

Magnification: 1128

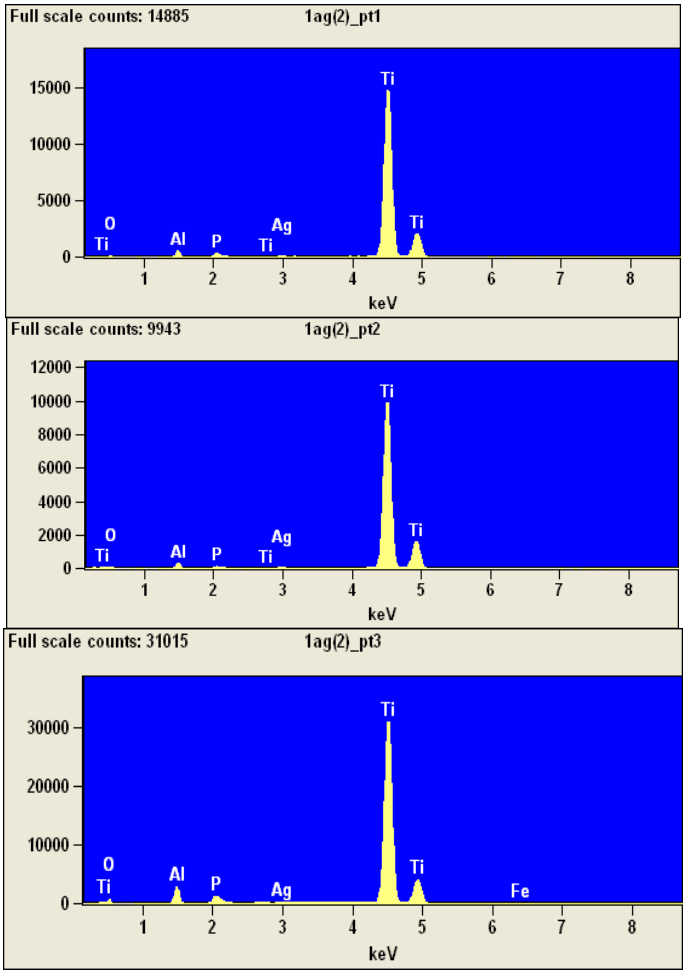

	O-K	Al-K	P-K	Ti-K	Fe-K	Ag-L
1ag(2)_pt1	5.52	1.60	0.89	91.19		0.81
1ag(2)_pt2	9.13	1.46	0.55	88.10		0.76
1ag(2)_pt3	11.90	3.53	1.26	82.35	0.45	0.51

- Regime 2 (10 min. maintaining in solution with stirring and heating at 50 ºC)

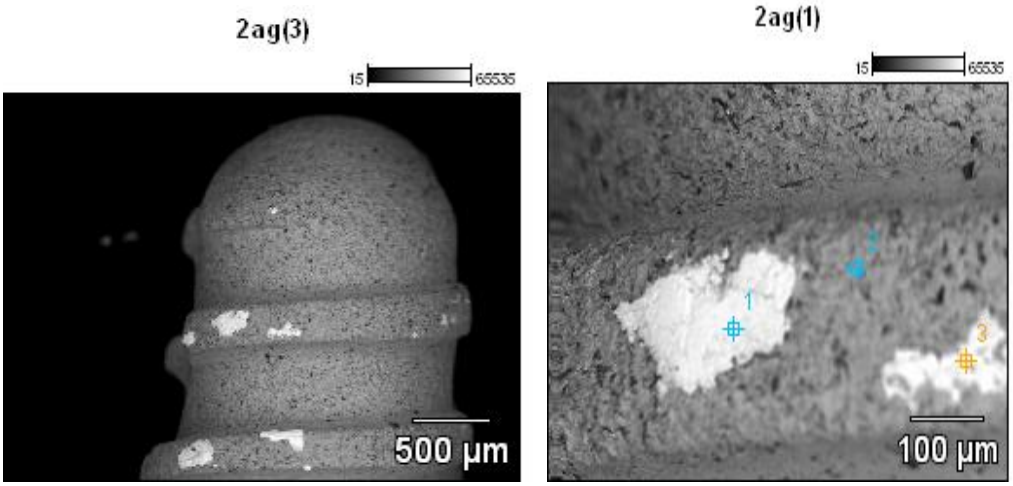

Magnification: 489

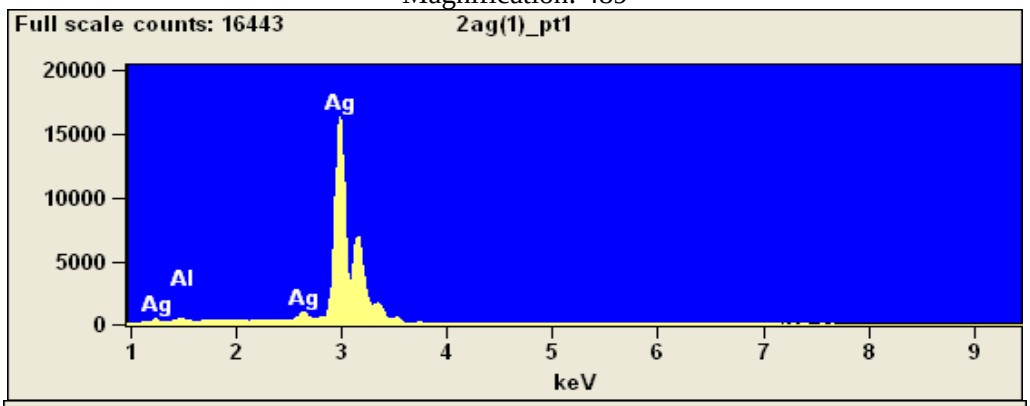

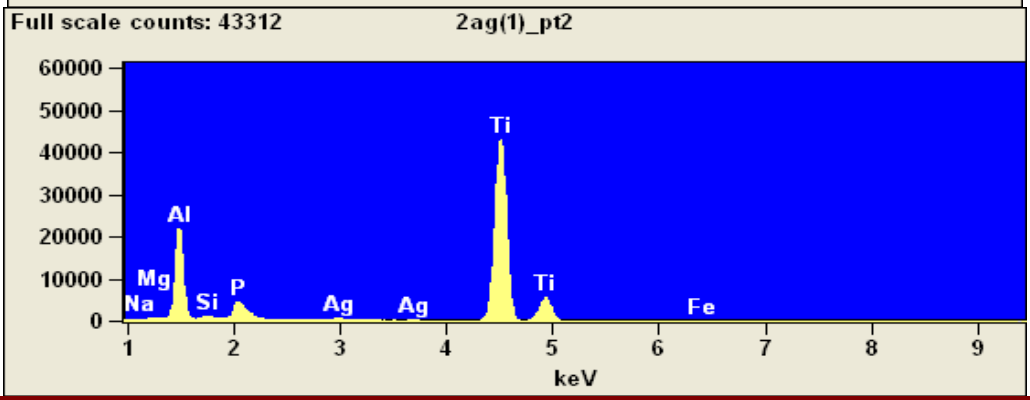

	O-K	Na-K	Mg-K	Al-K	Si-K	P-K	Ti-K	Fe-K	Ag-L
2ag(1)_pt1				0.49					99.51
2ag(1)_pt2	**40.40**	**0.04**	**0.11**	**10.19**	**0.23**	**1.66**	**46.77**	**0.28**	**0.33**

4. Conclusions

The experimental results on the chemical deposition of metallic silver on the implant built form $Ti_{10}Zr$ alloy confirm the presence of particles both in regimes of deposition without heating but also in those which were made by heating the solution at 50 ºC respectively 70 ºC and added formaldehyde drop by drop. It was noted, however, that at shorter maintenance periods (5 minutes) the silver particles have small dimensions and a low degree of dispersion. Also, heating the solution at 70 ºC does not change size, shape or degree of dispersion of metallic silver particles deposited at 50 ºC solution temperature. Electronic microscopy analysis with electron scanning (SEM) and energy dispersive spectroscopic analysis (EDX) revealed the presence of silver particles microdispersed having

morphologies and degrees of dispersion dependent on the technology of obtaining the chemical deposition and enables formulating a conclusion regarding the optimum regime. Particles with a high compactness and dispersion degree are obtained by heating the solution at temperatures of about 50 ºC, maintaining about 10 minutes with shaking and additions of formaldehyde drop by drop.

References

[1]. ***, *Wikipedia: Silver*.
[2]. ***, http://www.ziare.com/articole/proprietati+antibacteriene+argint.
[3]. Feng Q. L., Wu J., Chen G. Q., Cui F. Z., Kim T. N., Kim J. O. *A mechanistic study of the antibacterial effect of silver ions on Escherichia coli and Staphylococcusaureus*, Journal of Biomedical Materials Research Part A. vol. 52, issue 4, p. 662-668, 2000.
[4]. Kawahara K., Tsuruda K., Morishita M., Uchida M., *Antibacterial effect of silver-zeolite on oral bacteria under anaerobic conditions*, Dental Materials, vol. 16, issue 6, p. 452-455, 2000.
[5]. Martinez-Castanon G. A., Nino-Martinez N., Martines-Gutierrez F., Martinez-Mendoza J. R., Ruiz F., *Synthesis and antibacterial activity of silver nanoparticles with different sizes*, vol. 10, no. 8, p. 1343-1348, 2008.
[6]. Pal S., Tak Y. K., Song J. M., *Does the Antibacterial Activity of Silver Nanoparticles Depend on the Shape of the Nanoparticle? A Study of the Gram-Negative Bacterium Escherichia coli*, Applied and Environmental Microbiology, vol. 73, no. 6, p. 1712-1720, 2007.
[7]. ***, *The antibacterial effects of silver and its compounds*, Salt Lake Metals, November, http://www.saltlakemetals.com/Silver_Antibacterial.htm, 2008.

THE ANNALS OF "DUNAREA DE JOS" UNIVERSITY OF GALATI
FASCICLE IX. METALLURGY AND MATERIALS SCIENCE
Nº. 4 - 2015, ISSN 1453 – 083X

NOISE LEVELS IN WORKPLACES OF COLD ROLLING MILL PLANT

Beatrice TUDOR, Anisoara CIOCAN
"Dunarea de Jos" University of Galati, 111, Domnească Street, 800201, Galaţi, Romania
e-mail: btudor@ugal.ro

ABSTRACT

The excessive noise exposure is one of numerous physical hazards present in the steel industry. Considerable noise develops the steel strips rolling process. In this study are presented and discussed the noise levels at different working areas of a cold rolling mill plant. The average of annual values of noise levels is given. The annual overall values of equivalent sound levels were calculated. These are discussed in relation with the noise exposure level normalized to a normal 8hr working day allowed by standards. The results revealed that workers at numerous roll milling plant areas are exposed to noise levels higher than 87 dB(A) 8 - hour standard. As a result, at the end of the paper some specific measures to diminish noise levels are proposed.

KEYWORDS: steel strips, cold rolling mill, working areas, occupational noise

1. Introduction

A typical major source of noise in the steel industry is the hot or cold rolling processes. The sub-processes related to cold rolling mill within an integrated steel mill includes the surface preparation (pickling), trimming and oiling, cold rolling, degreasing and heating processes (annealing) [1, 2]. Many of these processes are noisy and may cause disturbance to the workplaces. Consequently, the noise is a typical environmental issue for rolling mill plants and requires continuous monitoring [3].

For this reason, noise pollution for workers in the steel industry is a great concern in world. The industrial noise from steel rolling mills induces to workers' deafness and hearing impairments [4, 5]. The European Union has established a common policy aimed at controlling the risks due to the exposure of workers to noise. EU has introduced specific legislation that provides the measures to minimize and even reduce it (Directive 2002/49/EC of the European Parliament and of the Council of 25 June 2002 relating to the assessment and management of environmental noise with successive amendments and corrections that have been incorporated into the original text (http://eur-lex.europa.eu/). Its Romanian national transposition is achieved through the adoption of various legislative acts.

The limits of exposure time for continuous noise for occupational health issues are related by International Standards. The terms used for Occupational Exposure Levels in the European Union are following: daily personal noise exposure of a worker - $L_{EP,d}$ (noise exposure level normalized to a normal 8hr working day); weekly average of the daily values $L_{EP,w}$. If the hearing damage is proportional to the acoustic energy received by the ear, then an exposure to a particular noise level for one hour will result in the same damage as an exposure for two hours to a noise level which is 3 dB lower than the original level. This is referred to the 3 dB(A) trading rule and is generally accepted in many parts of the world. However, 4 dB(A) and 5 dB(A) rules exist in the USA and the purpose of this section is to discuss the relative merits of the various trading rules in current use [6].

Several European countries followed limits adopted by the ISO standard. These are known as ″the 3 dB(A) rule″ [7]. USA respect the levels imposed by Occupational Safety and Health Administration – OSHA, so-called ″the 5 dB(A) rule″ [8, 9]. The OHS Noise Regulations set exposure levels commonly referred to as 85 dB(A)Leq for an averaged over an eight-hour period and a maximum or peak noise level of 140 dB(C) [7, 10].

In addition to the European nations, most other nations around the world have adopted the 3-dBA ER. Table 2 shows the PEL and ER used by various nations, along with the date of their standards or regulations, when available.

Table 1. *Permissible exposure limits (PEL) and exchange rates used by various nations* [11]

Nation, date	PEL (8-hour-average) dBA	Exchange rate dBA	Level dBA engineering controls	Level dBA audio tests, and other HC practices
Argentina, 2003	85	3	85	85
Australia, 2000	85	3	85	85
Brasil, 1992	85	5	85	
Canada, 1991	87	3	87	84
Chile, 2000	85	3		
China, 1985	85	3	85	
Colombia, 1990	85	5		
EU, 2003	87	3	85	85
Finland, 1982	85	3	85	
France, 1990	85	3		85
Germany, 1990	85	3	90	85
Hungary	85	3	90	
India, 1989	90			
Israel, 1984	85	5		
Italy, 1990	85	3	90	85
Mexico, 2001	85	3	90	80
Netherlands, 1987	80	3	85	85
New Zealand, 1995	85	3		80
Norway, 1982	85	3		80
Spain, 1989	85	3	90	80
Sweden, 1992	85	3	85	85
United Kingdom, 1989	85	3	90	85
United States, 1983	90	5	90	85
Uruguay, 1988	85	3	85	85
Venezuela	85	3		

The typical noise levels associated with the individual process at steel plants range between 59 and 84 dBA, while the combined noise levels for entire steel complexes range between 90 and 92 dBA [12]. The effective noise level generated by hot and cold rolling mill is 95-110 dB(A) [13].

Other studies give the general level of operating noises around 84-90dBA and peaks to 115 dBA [14].

This study presents and discusses the noise levels at different working areas of a cold rolling mill plant. The average of annual values of noise levels is given. with the discussion is related to the noise exposure level normalized to a normal 8hr working day allowed by standards.

2. Experimental method

The noise levels in workplaces of cold rolling plant were measured with the noise dosimeter with measuring range of 20-140 dB (Cirrus Research plc). The annual overall values of equivalent sound levels were calculated and compared with the regulatory limit from the Romanian Noise Regulations (HG 493/12.04.2006 about occupational safety and health regarding the exposure of workers to the risks arising from noise). This regulation establishes the exposure limit values and exposure values which trigger the action of employer on safety and health protection in relation to daily noise exposure levels and peak sound pressure. These values are as follow:

- Noise exposure limit level: L(EX, 8hr) = 87dB(A) and sound pressure p(peak) = 200 Pa (140 dB(C) at reference sound pressure in air 20 µPa), respectively;
- Maximum exposure level which triggers the action: L(EX, 8hr) = 85 dB(A) and respectively sound pressure p(peak) = 140 Pa (137 dB(C) at reference sound pressure in air 20 µPa);
- Minimum exposure level which triggers the action: L(EX, 8hr) = 80 dB(A) and the sound pressure

p(peak) = 140 Pa (135 dB(C) at reference sound pressure in air 20 μPa), respectively.

3. Results and Discussion

In the entire rolling zone develop noise. The principal sources of noise are the gearbox of the rolls and straightening machines, the pressure water pumps, the shears and saws, the throwing of the finished products into a pit and the stopping movements of the material with metal plates [14].

In respect to these aspects, the levels of noise from different working areas are presented. This is compared with the daily permissible exposure limit - L(EX, 8hr) considered for working spaces of roll milling plants (87dB). In addition, the values from other sectors of the cold rolling mill plant are presented. The average of annual values of noise levels for pickling sector are given in Table 2 and Figure 1.

Table 2. *Annual overall values of equivalent sound level inside pickling sector*

Source of noise		NAEC dB(A)		
		2013	2014	2015
Pickling line	areas of pickling tanks and drying tank	84.2	85	83.7
	area of steel band output	91.5	92.1	91.8

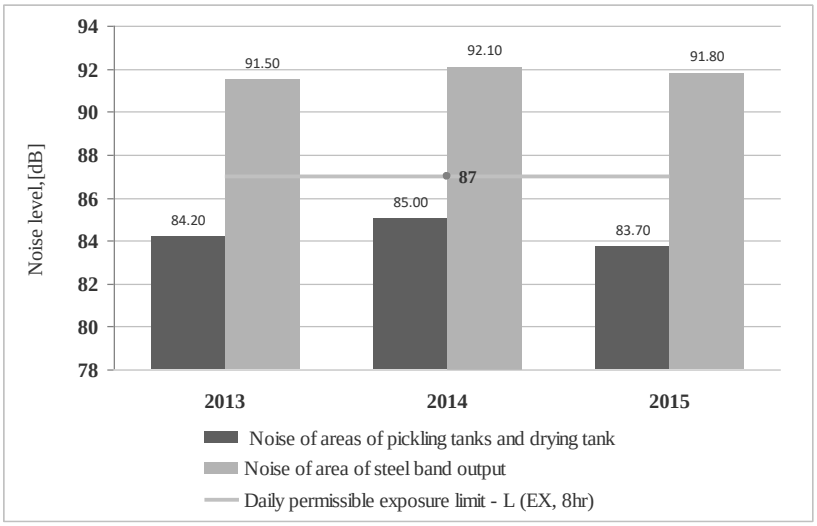

Fig. 1. *Overall values of equivalent sound level for surface preparation sector from cold rolling mill plant*

The exceedances of noise limit values are recorded in the output of the sheet strips from the pickling operation. These have been observed all along the years.

In the tandem rolling mill stands for all vertically stacked rolls, the average levels of noise exposure level normalized to a normal 8hr working day are higher than the permissible exposure limit (Table 3 and Figure 2). The maximum exposure level which triggers the action is exceeded. The steel strip that moves quickly over steel rollers produces noise.

Table 3. *Annual overall values of equivalent sound level for tandem mill sector*

Source of noise		NAEC dB(A)		
		2013	2014	2015
Stands of tandem mill	1	90.5	90.3	90.7
	2	93.8	92.4	93.2
	3	94.5	93.3	94.8
	4	97.8	96.6	97.7
	5	100.8	98.5	101.2

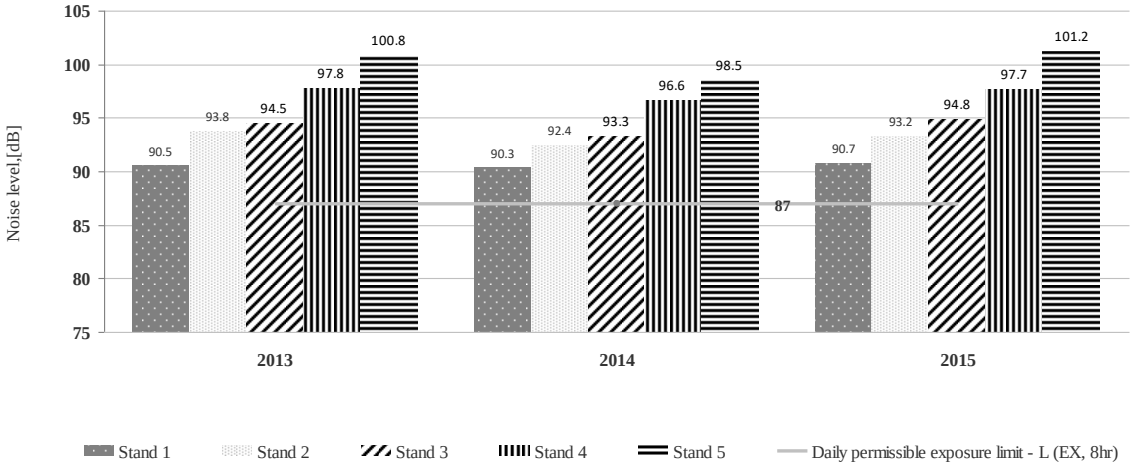

Fig. 2. *Sound level for tandem mill*

In the temper pas rolling sector the noise exceeds the permissible level developed (Table 4 and Figure 3). It has been observed that the sector of rolls machining is not so noisy. Near to straightening machines the noise levels were below standard limits. These were slightly above the permissible level for the area around the blast cleaning machine (Table 5, Figure 4).

Also inside the pumps room from water household the noise level is higher (Table 6 and Figure 5).

Table 4. *Annual overall values of equivalent sound level into area of temper pas rolling sector*

Source of noise		NAEC dB(A)		
		2013	2014	2015
Milling stand of temper pas rolling operation	open door	102.3	102.6	101.7
	door closed	100.5	100.8	98.3

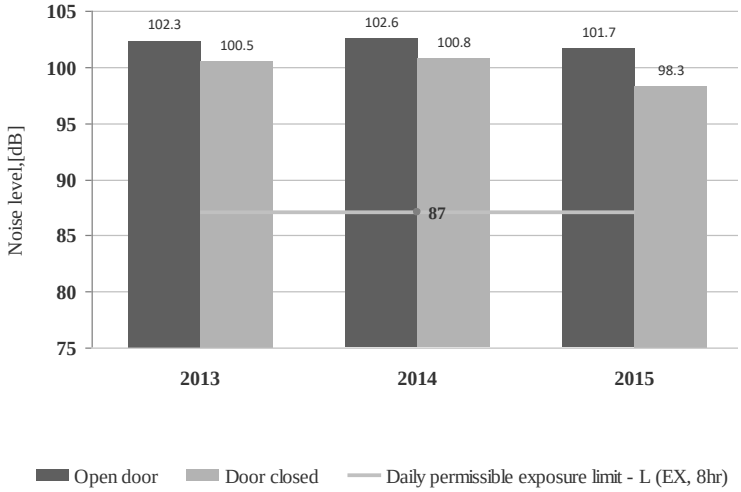

Fig. 3. *Noise level inside of temper-pas rolling sector*

Table 5. *Annual overall values of equivalent sound level for sector of machining of rolls*

Source of noise		NAEC dB(A)		
		2013	2014	2015
Machining sector of rolls	area of straightening machines	76.5	75.8	76.5
	area around blast cleaning machines	87.2	87.8	87.6

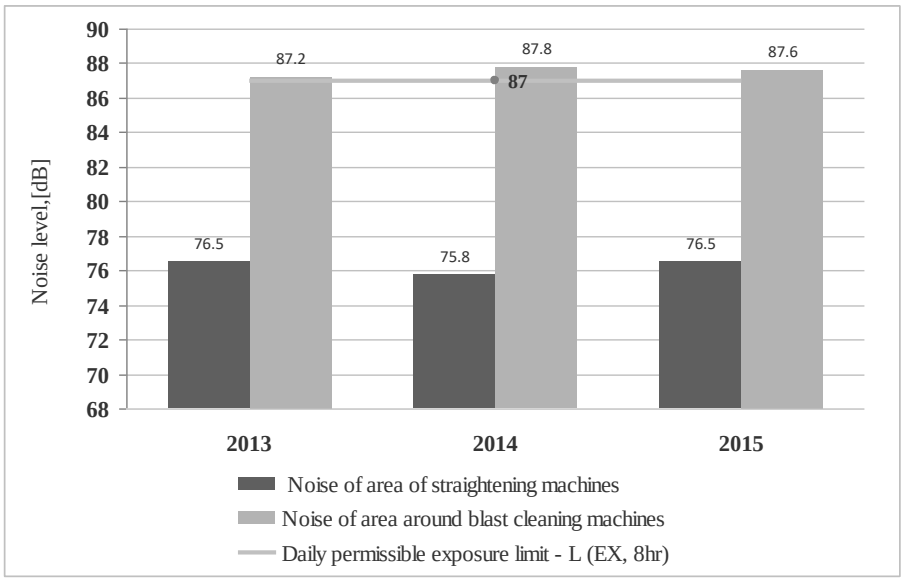

Fig. 4. *Sound level for machining sector of rolls*

Table 6. *Annual overall values of equivalent sound level for sector of pumps room from water household which serves the rolling mill plant*

Source of noise	NAEC dB(A)		
	2013	2014	2015
Pumps room	95.8	96.1	95.5

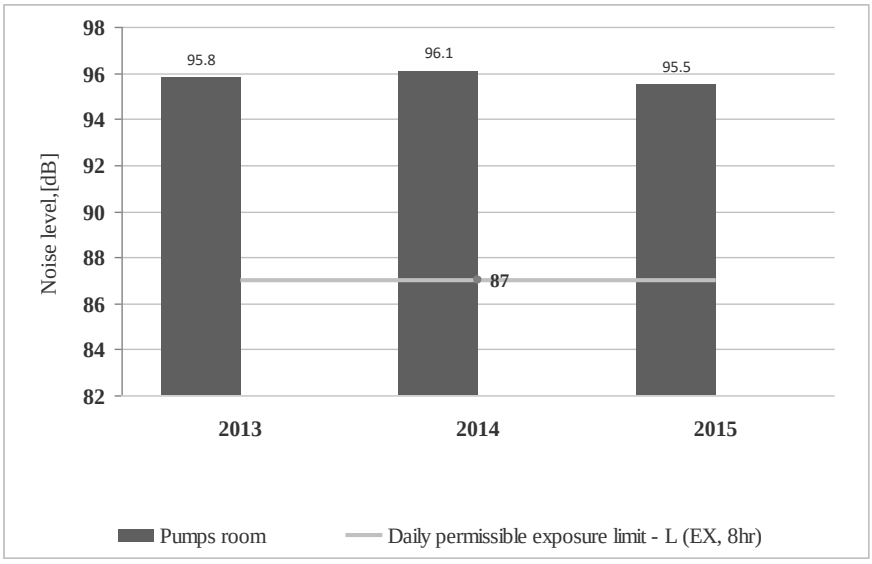

Fig. 5. *Noise level inside pumps room from water household*

Also inside the area from the hydraulic operating sector and from the sector of oiling tandem rolls the noise level recorded was higher with 10 and 15 dB over the daily permissible exposure limit (Table 7 and Figure 6).

Table 7. *Annual overall values of equivalent sound level for hydraulic operating sector and oiling tandem rolls of mill*

Source of noise	NAEC dB(A)		
	2013	2014	2015
Hydraulic operating sector and Oiling tandem rolls sector	97.8	98.2	97.5
	98.4	98.6	98.8
	102.5	102.1	102.1

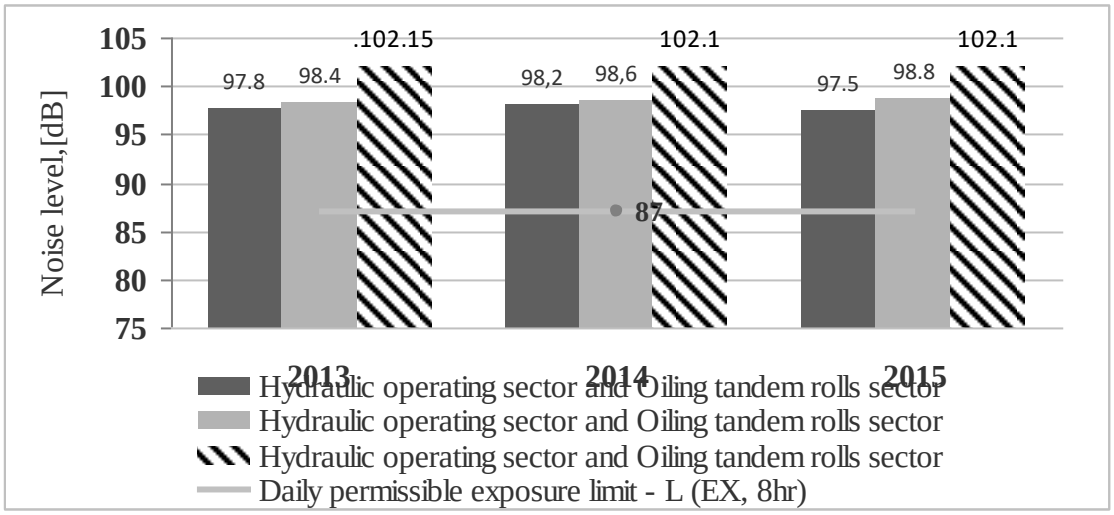

Fig. 6. *Noise level inside of hydraulic operating sector and in area of oiling tandem rolls*

Even in the intermediate rolls deposit the noise level was exceeded (Table 8 and Figure 7). The product movement in stockyards, loading vehicles and vehicle movements are sources of noises. The noise level was slightly exceeded inside the steel strips adjustment area (Table 9 and Figure 8).

Table 8. *Annual overall values of equivalent sound level for intermediate rolls deposit*

Source of noise	NAEC dB(A)		
	2013	2014	2015
Intermediate rolls deposit	91.2	90.8	91.33

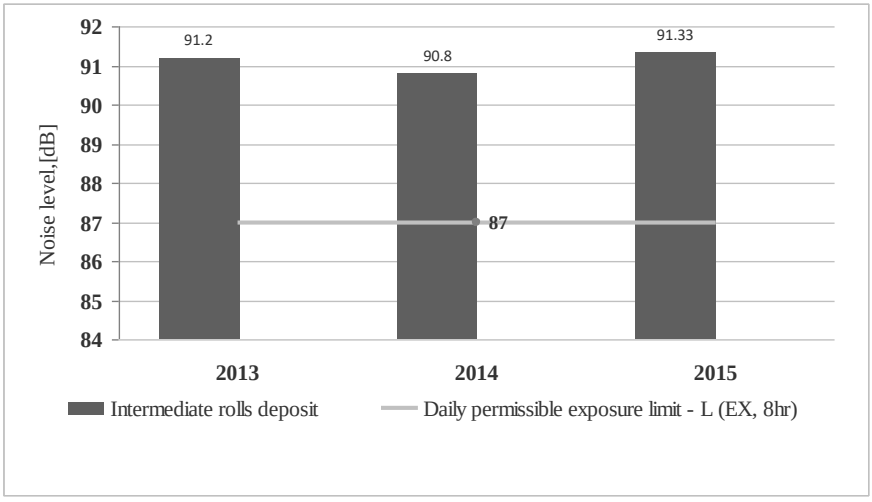

Fig. 7. *Noise level inside of intermediate deposit for steel strips rolls*

Table 9. *Noise level inside adjustment area*

Source of noise	NAEC dB(A)		
	2013	2014	2015
Sector of steel strips adjustment	88.8	87.6	88.3
	90.5	90.2	89.4

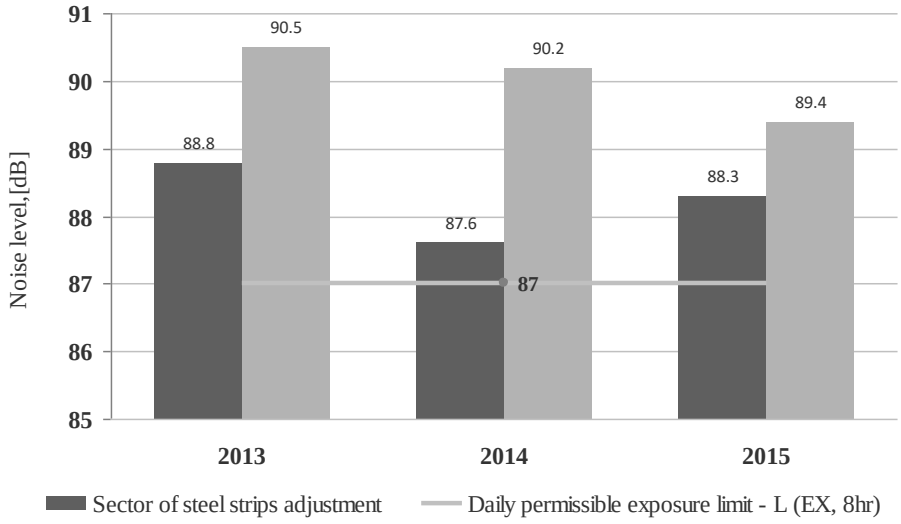

Fig. 8. *Noise level inside adjustment area*

4. Conclusions

The average noise exposure levels inside many sectors of cold steel-rolling mill were significantly higher. The results revealed that workers at numerous roll milling plat areas are exposed to noise levels higher than 87 dB(A) 8 - hour standard. To protect the workplaces from noise the effective anti-noise measures can be accordingly formulated and implemented. There is a need for employee training on noise exposure hazards and enforcement of the use of protective devices. The plant should be extensively automated. The machines and equipment demand maintenance and, the workers need personal protection. Particular attention should be paid to rollers and handling, cutting and grinding activities.

Acknowledgements

The authors wish to thank the student Basoc Monica who helped us in this study.

References

[1]. R. Saban, C. Dumitrescu s.a., *Tratat de stiinta si ingineria materialelor metalice*. vol.5. Tehnologii de procesare finala a materialelor metalice., Ed.AGIR, 2012.
[2]. ***, *Arcelor Mittal - 20-f - 20080319 - company_information*, http://google.brand.edgar-online.com/.
[3]. ***, *United Nations Environment Programme (UNEP) and Steel Institute (IISI)*, Steel Industry and the Environment: Technical and Management Issues. Technical Report no. 38. Paris and Brussels: UNEP and IISI, 1997.
[4]. F. E. Ologe, T. M. Akande, T. G. Olajide, *Occupational noise exposure and sensorineural hearing loss among workers of a steel rolling mill*, Otology, European Archives of Oto-Rhino-Laryngology and Head & Neck, vol. 263, issue 7, p 618-621, 2006.
[5]. G. H. Pandya, D. M. Dharmadhikari, *A Comprehensive Investigation of Noise Exposure in and Around an Integrated Iron and Steel Works***,** AIHA Journal, vol. 63, issue 2, p. 72-84, 2002.
[6]. D. L. Johnson, P. Papadopoulos, N. Watfa, J. Takala, *Exposure criteria, occupational exposure levels*, http://www.who.int/occupational_health/publications/noise4.pdf.
[7]. S. Kumar Nanda, *Noise Impact Assessment and Prediction in Mines Using Soft Computing Techniques*, Thesis for the award of the degree of Doctor of Philosophy in Engineering, http://ethesis.nitrkl.ac.in/4560/1/PhD50405001revised.pdf.
[8]. ***, *OSHA Technical Manual (OTM)*, Section III: Chapter 5 - Noise, https://www.osha.gov/dts/osta/otm/new_noise/.
[9]. ***, *Occupational Safety and Health Administration (OSHA).* Guidelines for Identification and Control of Safety and Health Hazards in Metal Recycling, p. 4-48, www.osha.gov, 2008.
[10]. ***, *Criteria for a recommended standard*, Occupational Noise Exposure, Revised Criteria, U.S. Department of health and human services, http://www.nonoise.org/hearing/criteria/criteria.htm, 1998.
[11]. T. K. Madison, *Recommended Changes to OSHA Noise Exposure Dose Calculation*, 3M JobHealth Highlights, vol. 25. No. 8 December 2007.
[12]. S. Kerketta, P. K. Dash, L. T. P. Narayan, *Work zone noise levels at Aarti steel plant, Orissa and its attenuation in far field*, Journal of Environmental Biology, September, 30(5), 903-908, p. 903-908, 2009.

[13]. ***, *Environmental Handbook: Volume II: Documentation on monitoring and evaluating environmental impacts*, vol. II, Agriculture, mining/energy, trade/industry. by Germany. Bundesministerium für Wirtschaftliche Zusammenarbeit und Entwicklung, http://www.worldcat.org/.

[14]. J. Masaitis, *Enciclopaedia of Occupational Health and Safety. Chapter 73. Iron and Steel*, http://www.ilocis.org/documents/chpt73e.htm.

MANUSCRISELE, CĂRŢILE ŞI REVISTELE PENTRU SCHIMB, PRECUM ŞI ORICE CORESPONDENŢE SE VOR TRIMITE PE ADRESA:

MANUSCRIPTS, REVIEWS AND BOOKS FOR EXCHANGE COOPERATION, AS WELL AS ANY CORRESPONDANCE WILL BE MAILED TO:

LES MANUSCRIPTS, LES REVUES ET LES LIVRES POUR L'ECHANGE, TOUT AUSSI QUE LA CORRESPONDANCE SERONT ENVOYES A L'ADRESSE:

MANUSCKRIPTEN, ZIETSCHRITFTEN UND BUCHER FUR AUSTAUCH SOWIE DIE KORRESPONDENZ SID AN FOLGENDE ANSCHRIFT ZU SEDEN:

After the latest evaluation of the journals achieved by National Center for the Science and Scientometry Politics (**CENAPOSS**), as recognition of its quality and impact at national level, the journal is included in B^+ category, 215 code (http://cncsis.gov.ro/userfiles/file/CENAPOSS/Bplus_2011.pdf).

The journal is indexed in:

EBSCO: http://www.ebscohost.com/titleLists/a9h-journals.pdf

Copernicus: http://journals.indexcopernicus.com/karta.php

The papers published in this journal can be visualized on the "Dunarea de Jos" University of Galati site, the Faculty of Engineering, pages: http://www.sim.ugal.ro/Annals.htm, http://www.imsi.ugal.ro/Annals.html.

Publisher's Name and Address:
Contact person: Antoaneta CĂPRARU
Galati University Press - GUP
47 Domneasca St., 800008 - Galati, Romania
Phone: +40 336 130139, Fax: +40 236 461353
Email: gup@ugal.ro

Editor's Name and Address:
Prof. Dr. Eng. Marian BORDEI
Dunarea de Jos University of Galati, Faculty of Engineering

111 Domneasca St., 800201 - Galati, Romania
Phone: +40 336 130208
Phone/Fax: +40 336 130283
Email: mbordei@ugal.ro

AFFILIATED WITH:

- **ROMANIAN SOCIETY FOR METALLURGY**
- **ROMANIAN SOCIETY FOR CHEMISTRY**
- **ROMANIAN SOCIETY FOR BIOMATERIALS**
- **ROMANIAN TECHNICAL FOUNDRY SOCIETY**
- **THE MATERIALS INFORMATION SOCIETY (ASM INTERNATIONAL)**

Edited under the care of
FACULTY OF ENGINEERING

Annual subscription (4 issues per year)

Edited date: 15.12.2015
Issues number: 200
Printed by Galati University Press
accredited CNCSIS
47 Domneasca Street, 800008, Galati
Romania